PhD degree in System Medicine
Molecular Oncology curriculum
European School of Molecular Medicine (SEMM)
University of Milan and University of Naples “Federico II”

Immunogenic cell death as a new mechanism of action of the chemotherapeutic drug mitomycin C in bladder cancer

Bianca Oresta

Supervisor: Professor Maria Rescigno
Laboratory of Mucosal Immunology and Microbiota

Academic year 2018/2019

Table of content

Index figures and tables

Abbreviations

7-AAD 7-aminoactinomycin

AGER Advanced glycosylation end product-specific receptor

APC Antigen-presenting cell

ATF Activating transcription factor

ATG Autophagy-related gene

ATP Adenosine triphosphate

BCG Bacillus Calmette-Guérin

CHOP CCAAT-enhancer-binding protein homologous protein

CIS Carcinoma in situ

CLRT Calreticulin

CRC Colorectal cancer

CTL Cytotoxic T lymphocyte

DAMP Damage associated molecular pattern

DC Dendritic cells

DEG Differentially expressed gene

EAU European Association of Urology

EGFR Epidermal growth factor receptor

eIF2α Eukaryotic translation initiation factor

ER Endoplasmic reticulum

ERAD ER-associated degradation

ERK Extracellular signal regulated kinase

EtBr Ethidium bromide

ERN1 Endoplasmic reticulum to nucleus signaling 1

Erp57 ER-protein 57

FFPE Formalin-fixed paraffin embedded

GSEA Gene set enrichment analysis

HK2 Hexokinase 2

HMGB1 High-mobility-group box 1

HR Homologous recombination

HSPA5 Heat-shock protein family A member 5

ICD Immunogenic cell death

IFN Interferon

Ig immunoglobulin

IL interleukin

IRE1-α Inositol-requiring kinase 1-α

XBP1 X-box binding protein 1

sXBP1 Spliced X-box binding protein 1

LRP1 LDL-related protein 1

MFI Mean Fluorescence Intensity

MIBC Muscle invasive bladder cancer

MHCI Major histocompatibility complex class I

MHCII Major histocompatibility complex class II

MMC Mitomycin C

moDC Monocyte-derived dendritic cell

mt Mitochondrial

mPTP Mitochondrial permeability transition pore

NDUFB8 NADH dehydrogenase 1 beta subcomplex subunit 8

NER Nucleotide excision repair

NK Natural killer

NLRP3 Leucine-rich repeat pyrin domain containing 3

NMIBC Non-muscle invasive bladder cancer

NT Untreated

OXPHOS oxidative phosphorylation

PAMP Pathogen-associated molecular pattern

PD1 Programmed cell Death protein 1

PD-L1 Programmed cell Death ligand 1

PDT Photodynamic therapy

POLG DNA Polymerase Gamma

PRR Pattern recognition receptor

PS Phospholipid phosphatidylserine

PUMA P53-Upregulated Modulator of Apoptosis

rRNA ribosomal RNA

tRNA transfer RNA

ROS Reactive oxygen species

SCC Squamous cell carcinoma

STING cGAS/stimulator of interferon genes

TAA Tumor-associated antigen

TCA tricarboxylic acid cycle

TLR Toll-like receptor

TNF Tumor necrosis factor

TOMM20 Translocase of Outer Mitochondrial Membrane 20

TURBT Transurethral resection of bladder tumor

UPR Unfolded protein response

UTI Urinary tract infection

Abstract

Despite having been used for more than a century, the exact mechanisms of action, of resistance and the best treatment schedule of most chemotherapeutic agents remain elusive. Mitomycin C (MMC) is the gold standard adjuvant treatment for bladder cancer. However, it is effective only in a proportion of patients, suggesting that, aside from cytotoxicity, other mechanisms could be involved in mediating the success or failure of treatment. We hypothesized that MMC might induce immunogenic cell death (ICD), leading to an antitumor immune response. Here, we describe that MMC fosters ICD via the exposure of damage signals, increased phagocytosis by dendritic cells (DCs) and *in vivo* tumor protection. MMC-induced ICD relies on the cytoplasmic release of mitochondrial DNA that activates the inflammasome for efficient IL-1β secretion that promotes DC maturation. We found the ICD resistant cancer cells fail to generate an inflammatory microenvironment and display mitochondria dysfunction related to low expression of mitochondrial Complex I of the respiratory chain, which is associated with drug resistance in bladder cancer patients. The identification of ICD as a novel immune-related mechanism of action of MMC provides opportunities to optimize bladder cancer management and identify ICD-related biomarkers of treatment efficacy.

1. Introduction

Bladder cancer: etiology, staging and disease management

Bladder cancer is the ninth most common malignancy worldwide and the most common malignancy of the urinary tract[1]. Most cases of bladder cancer are urothelial carcinomas (90- 95%) originating from the urothelium, the cell layer that covers the inner surface of the bladder. Others few variant histologies have been described, including squamous cell carcinoma (SCC; 2-5%), small-cell carcinoma (<1%), and adenocarcinoma (0.5- 2%)[2]. Bladder cancer incidence and mortality rates increase with age and vary across countries due to differences in risk factors, diagnostic practices and availability of treatments. In Europe, Denmark, Greece, the Netherlands, Belgium, Italy, and Germany have the highest rates of bladder cancer (21.2 to 15.8 age-standardized rate per 100,000/year)[3]. Tobacco smoking is the most well established factor for bladder cancer, causing 65% of male cases and 30% of female cases[4,5]. Occupation exposure to dyes, rubbers, textiles, paints, leathers, and chemicals is the second most important risk factor for bladder cancer[6,7]. Also bladder schistosomiasis (bilharzia) infection, a common parasite in Africa, Asia, and South America, increases the risk of developing bladder cancer, in particular SCC[8]. Similarly, invasive SCC has been linked to the presence of chronic urinary tract infection (UTI) distinct form schitosomiasis[9]. Moreover, increased rates of secondary bladder malignancies have been reported after radiotherapy for the treatment of prostate and gynecological tumors[10]. Men are about four times more likely than women to develop bladder cancer and the worldwide age-standardized incidence rate (per 100,000/year) is 9.0 for men and 2.2 for women, making bladder cancer the fourth most common cancer in the male population[11]. Differences in gender prevalence of bladder cancer may be due to other factors besides tobacco and chemical exposure. In a large prospective cohort study, post-menopausal status was associated with an increase in bladder cancer, suggesting that the differences in estrogen and androgen levels between man and women

may be responsible for some of the difference in the gender prevalence of bladder cancer[12]. There is growing evidence that genetic susceptibility factors and family association may influence the incidence of this tumor. A recent population-based study of cancer risk in relatives and spouses of patients showed an increased risk for first- and second-degree relatives, and suggested genetic or environmental roots independent of smoking-related behavior[13]. Recent studies detected genetic susceptibility with independent loci, which are associated with bladder cancer risk[14].

About 75% of newly diagnosed bladder cancer patients have non-muscle invasive bladder cancer (NMIBC)[15], with papillary tumors confined to the mucosa and invading the lamina propria as stage Ta and T1, respectively[2] (Fig 1.1). In addition, *carcinoma in situ* (CIS), which are flat, high-grade tumors, are classified as NMIBC[2]. The remaining 25% of tumors are muscle invasive bladder cancers (MIBC) that progressively invade the muscle layers (stage T2), perivesical tissue (stage T3) or metastasize to adjacent organs, like the prostate stroma, seminal vesicles, uterus, and abdominal wall (stage T4)[2] (Fig 1.1).

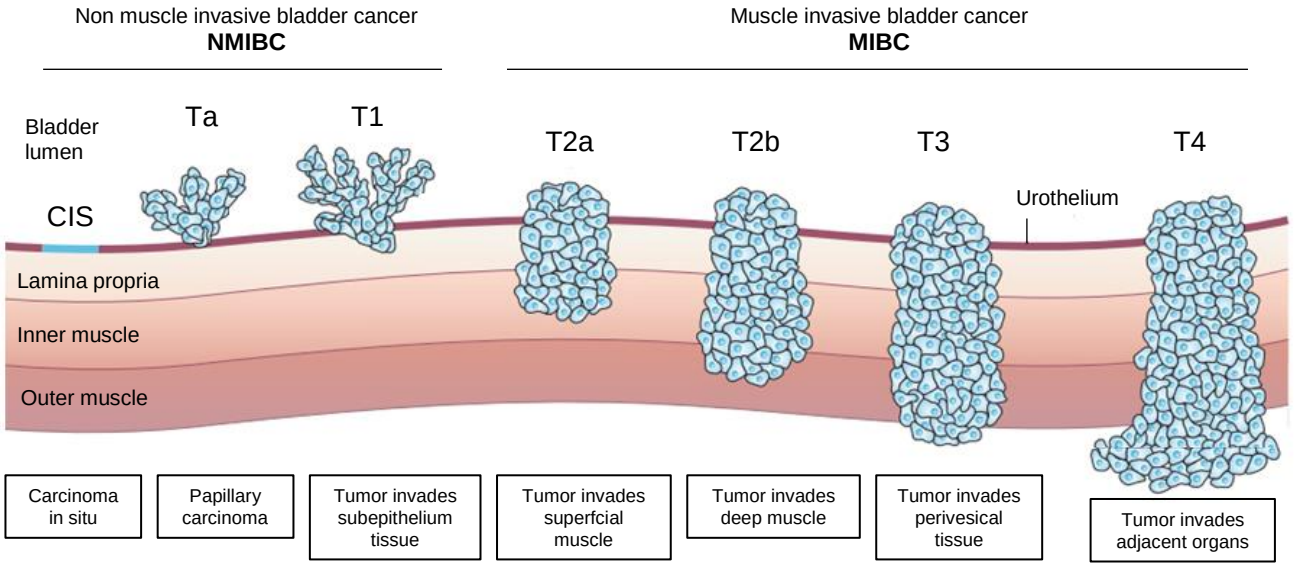

Figure 1.1. Bladder cancer stages. Around 75% of newly diagnosed bladder cancer patients have non-muscle invasive bladder cancer (NMIBC). Of these 90% consist of papillary tumors restricted to the urothelium (Ta) or invading the lamina propria (T1); the rest are *carcinoma in situ* (CIS), which are more aggressive. Once tumors have entered the muscle (T2a, T2b), they might spread to the perivascular tissue (T3) or beyond (T4). Adapted from Knowles et al., Nature Reviews Cancer (2015).

MIBCs are all high grade cancers associated with poor prognosis. The 3-year survival is nearly 60% in patients with primary T2 tumors and decreases to 30% in patients with T3 tumors or progressive disease (patients with a history of superficial carcinomas). The 3-year survival rate drops to 15% in patients with T4 tumors[16]. Therefore, standard treatment for MIBC is neoadjuvant chemotherapy with cisplatin or radiotherapy followed by radical cystectomy, i.e. removal of the entire bladder[17]. NMIBC patients instead have a better prognosis, with a 3-year survival of 80-90%[18]. Standard care for these patients foresees a transurethral resection of bladder tumor (TURBT), a minimally invasive surgery during which superficial tumors are removed endoscopically with an electrical cauterizing loop, called resectoscope. However, these tumors commonly recur, even multiple times, and can progress to MIBC, indicating that TURBT is often incomplete and not sufficient to cure the disease[18]. Therefore, intravesical adjuvant therapy is considered in all patients. In particular, patients diagnosed with TaT1 low grade tumors are treated with the chemotherapeutic drug mitomycin C (MMC)[19], whereas patients with high grade T1 tumors (big, multifocal and recurrent lesions) are treated with bacillus Calmette-Guérin (BCG)[20], a live, attenuated stain of *Mycobacterium bovis* that produces antitumor effects by infecting tumor cells and activating the host's immune response[21]. Despite having been used in the clinic for decades, intravesical treatments based on MMC or BCG instillations show efficacy only in a proportion of patients. Indeed, even after intravesical treatment the recurrence rate of NMIBC at 1 year can span from 15% to 60% and up to 17% of these recurrent tumors will progress to a higher stage[18]. At the moment, disease management is based only on histological staging and it is not possible to predict which NMIBC patients will benefit from intravesical treatments, since neither resistance mechanisms nor predictive markers have been identified. This has implications in the trial and error process of patient treatment, delaying the finding of the correct cure, and strongly affecting patient's quality of life.

The chemotherapeutic drug mitomycin C

DNA crosslinking activity

MMC is an antibiotic discovered in the 1950s in fermentation cultures of *Streptomyces caespitosus*. MMC crosslinks the complementary strands of the DNA double helix with an absolute specificity for the CpG sequence, thereby inducing inhibition of DNA synthesis, cell-cycle arrest and apoptosis[22]. Given its cytotoxic effects in mammalian cells, MMC is also an important antitumor drug that has been widely used in the clinic against bladder, anal, stomach, pancreas, liver, and breast carcinomas. MMC crosslinking activity is initiated by a reduction that converts MMC into an alkylating agent that can react with DNA[21]. The fact that MMC is activated by reduction is important in the selectivity of its antitumor reactivity, since many tumors grow in low-oxygen environments compared to normal tissues. Therefore, MMC is highly active in these hypoxic solid tumors and suppresses their growth. MMC crosslinking activity induces various types of DNA damages and, accordingly, repair of MMC-induced damages involves multiple repair pathways, such as nucleotide excision repair (NER) and homologous recombination (HR)[23]. However, persistent DNA damage and impaired DNA replication cause significant cytotoxicity to cells, resulting in cell death.

Mitomycin C administration in NMIBC

Given its low association with side effects upon instillation in the bladder, MMC has been widely used to treat NMIBC[24]. Following TURBT, MMC is instilled intravesically with a catheter and is retained in the bladder for around 1-2 hours, during which it gets diluted with the urine, and then drained[24]. Intravesical chemotherapy with MMC is known to prevent bladder cancer recurrence by killing remaining tumor cells at resection sites and prevent implantation of the postoperative tumor cells[25]. Four meta-analysis have consistently shown that after TURBT an early single instillation with MMC significantly

reduces the recurrence rate of NMIBC compared to TURBT alone, since MMC prevents tumor cell implantation that occurs in the first few hours after surgery[19,26,27,28]. For the majority of the patients further intravesical MMC administrations are needed to reduce the likelihood of recurrence and progression[29]. Independent randomized trials showed a 38% reduction in one year recurrence among patients treated with intravesical chemotherapy versus TURBT alone[24]. The length and frequency of MMC administration is still controversial. Current evidence does not support treatment longer than one year. Despite the popularity of MMC in the treatment of NMIBCs, many questions regarding the optimal approach to MMC therapy remain unanswered and a large proportion of NMIBCs recur[25,30], suggesting that, aside from cytotoxicity, other mechanisms could be involved in mediating the success or failure of the treatment.

Immunogenic cell death

Features of immunogenic cell death

In the healthy human body several millions of cells die every day as a result of the turn-over necessary for the preservation of the whole body homeostasis. This type of cell death goes unrecognized by the immune system or is considered tolerogenic[31]. However, the death of cells due to infectious pathogens can trigger a robust antigen-specific immune response and the establishment of long-term immunological memory. In the past years this modality of immunogenic cell death (ICD), that does stimulate an immune response against dead cell antigens, has been proved to be induced not only by infectious pathogens, but also by certain anti-cancer agents[32]. In particular, treatments with anthracyclines (e.g., doxorubicin, mitoxantrone), oxaliplatin, radiation therapy, photodynamic therapy (PDT), and some targeted therapies were shown to render tumor cells "visible" to the immune system and mediate the stimulation of *de novo* or pre-existing tumor-specific immune responses in different cancer types[33–37]. Efficient ICD

induction relies on the combination of antigenicity and adjuvanticity[32]. Similarly to infected cell expressing exogenous antigens, tumor cells express neoantigens as a result of somatic mutations that originate during oncogenesis and cancer progression[38]. Moreover, tumor cells express proteins that are normally expressed only during embryonic development or in immunologically privileged tissues, like cancer-testis antigens[39]. The mutational load and amount of tumor-associated antigens (TAAs) determine the antigenicity of cancer cells and their propensity to stimulate ICD and respond to immunostimulatory therapies, like checkpoint inhibitors[38]. Adjuvanticity during ICD is conferred by the release specific damage associated molecular pattern molecules (DAMPs) that favor the uptake of dying tumor cells by innate immune cells and the priming of adaptive immune responses[40].

Danger signaling in ICD

Several DAMPs that are specifically expressed during ICD have been characterized. During the early phases of ICD, DAMPs are displayed as a consequence of endoplasmic-reticulum (ER) stress induced by anti-cancer treatments[41]. ER stress elicits signaling pathways that lead to the translocation to the outer surface of the plasma membrane of proteins that are normally located in the ER lumen, like chaperones and heat shock proteins. Of these proteins, calreticulin (CLRT), a Ca^{2+}-binding chaperone, was identified in the first systemic screening of cytotoxic compounds as a marker of ICD induction[42]. Surface exposure of CLRT is an active pre-apoptotic process that relies on ER-stress response initiated by the activation of the eukaryotic translation initiation factor eIF2α[43]. On the plasma membrane, CLRT has been shown to bind the transmembrane receptor LDL-related protein 1 (LRP1; also known as CD91), mostly expressed by antigen-presenting cells (APCs)[44]. CLRT-LRP1 interaction acts as ‘eat me’ signal, thereby promoting the uptake of dying cell and debris, and stimulates the production of the pro-

inflammatory cytokines, interleukin (IL)-6 and tumor necrosis factor (TNF)-α by activation of NFkB signaling pathway (Fig 1.2)[45]. Concomitantly with CLRT exposure, during the early phases of apoptosis the membrane phospholipid phosphatidylserine (PS) translocates from the inner to the outer leaflet of the plasma membrane stimulating the removal of dying cells, but without activating an inflammatory response[46].

In the mid- and late mortem stages, ICD is associated with the release of endogenous Toll-like receptor (TLR) agonists. In particular, secretion of the non-histonic chromatin-binding protein high-mobility-group box 1 (HMGB1) operates as a potent proinflammatory stimulus. HMGB1 can be actively secreted by innate immune cells in response to pathogenic products or passively released by injured cells[47,48]. The molecular mechanism responsible for the release of HMGB1 from cells undergoing ICD remains to be elucidated. Extracellular HMGB1 mediates robust adjuvant effects by binding various distinct pattern recognition receptors (PRRs), like TLR2, TLR4 and advanced glycosylation end product-specific receptor (AGER; also known as RAGE) on APCs[49] (Fig 1.2). In particular, strong immune responses against cancer cells treated with ICD inducers require binding of HMGB1 to TLR4, as well as its adaptor protein MYD88[50]. Indeed, tumors established in *Tlr4*$^{-/-}$ or *Myd88* $^{-/-}$ mice respond less efficiently to anti-cancer therapies with ICD inducers, like anthracyclines or oxaliplatin, compared to the same tumors growing in immunocompetent wild type mice[50]. TLR4 activation in dendritic cells (DCs) is essential for cell maturation and optimal cross-presentation of engulfed neoantigens and TAA[51].

Other important molecules that contribute to the formation of a robust immunostimulatory environment are released nucleotides, like adenosine triphosphate (ATP), and cytokines[52]. ICD-associated release of ATP depends on the induction of autophagy and depletion of several autophagy-related gene (ATG) products (*ATG5*, *ATG7*, *ATG10*, *Beclin-1*) significantly decreases the accumulation of autophagosomes

and ATP release in tumor cells treated with ICD-inducers, without affecting CLRT exposure and HMGB1 release[53]. Extracellular ATP interacts with the purinergic receptors P2Y2 and P2X7 (P2RY2, P2RX7) on APCs to promote inflammasome activation[54]. Altogether the described DAMPs favor the recruitment of innate immune cells, like DCs, macrophages, neutrophils and natural killer (NK) cells, and the engulfment of dying cells by APCs. In turn, immune cells secrete different cytokines at the site of damage, such as IL-12, IL-6 and IL-1β, that shape T cells and NK cells responses[52]. Neoantigens and TAA captured by DCs are processed and presented on major histocompatibility complex class I and II (MHCI and MHCII) molecules to T cells, resulting in the priming and activation of effector T cell responses against the cancer-specific antigens (Fig 1.2). Anti-tumor lymphocytes expand and produce effector cytokines, such as interferon (IFN)-γ, granzymes and IL-17, that mediate tumor cells lysis. ICD is not only associated with a first anti-tumor immune response, but it has also the potential to establish immunological memory, that ensures immune surveillance[55].

Evasion of ICD

ICD may not be efficiently triggered, even by well-characterized ICD-inducers, due to low antigenicity of cancer cells or host characteristics, such as immunodeficiencies or inability to sense DAMPs. Moreover, tumors efficiently control immunogenicity by various mechanisms operating on adjuvanticity, which can impair the efficacy of ICD induction. Different mechanism of resistance to ICD have been described, including both defective DAMPs emission or suppression of upstream adaptive mechanisms.

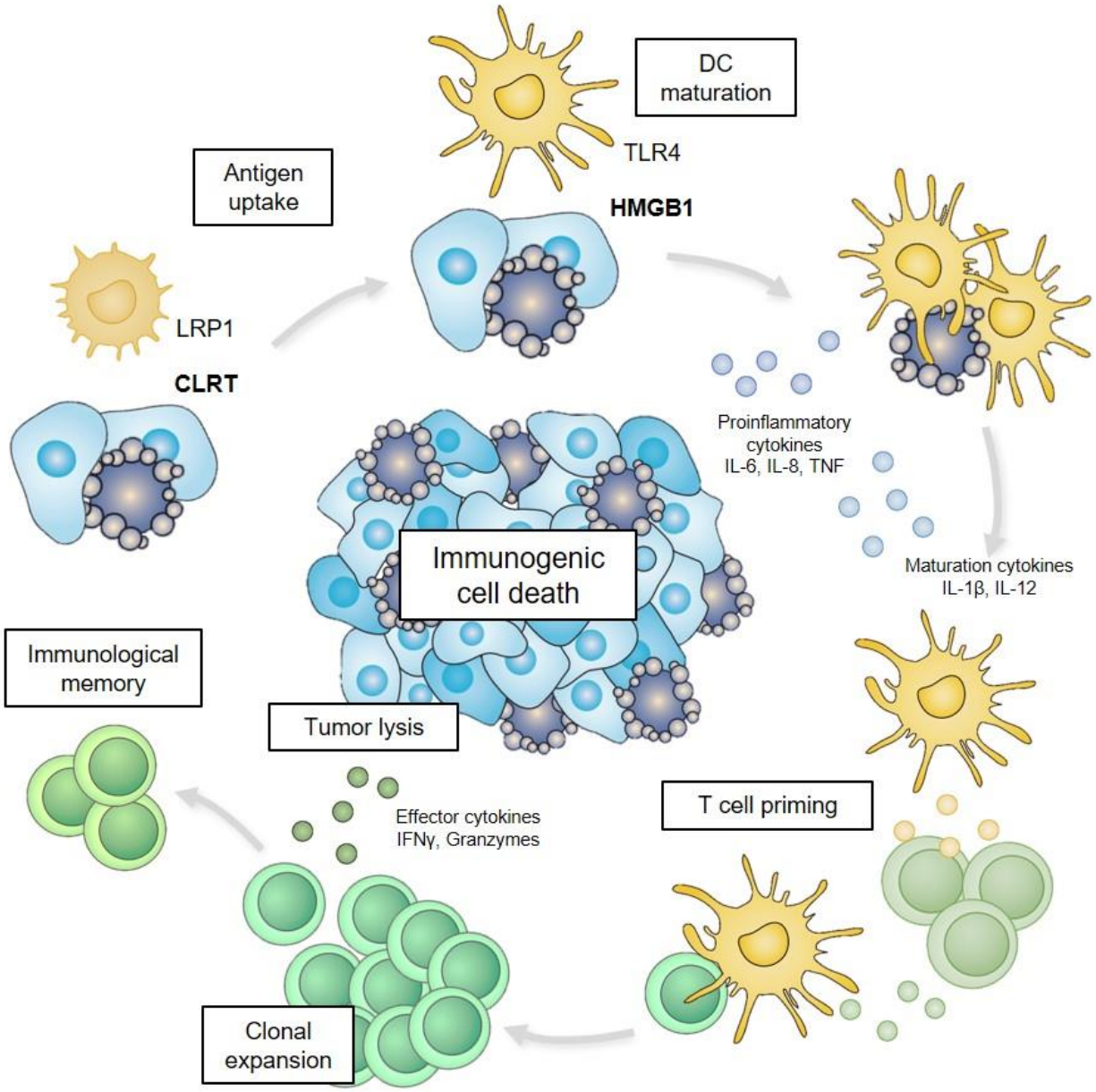

Figure 1.2. Mechanisms of ICD. In response to ICD inducers, malignant cells expose calreticulin (CLRT) and other endoplasmic reticulum chaperones on their surface, and release high-mobility group box 1 (HMGB1). Upon binding to cognate receptors on the surface of antigen-presenting cells (LDL-related protein1; LRP1 and Toll like receptor 4; TLR4), including dendritic cells (DCs) in the context of robust immunostimulatory signals provided by cytokines, these damage-associated molecular patterns favor the uptake of tumor cells, leading to the priming of an adaptive immune response. Such T cell-mediated response has the potential to eradicate malignant cells that survive chemotherapy via activity of IFNγ and granzymes and is associated with the establishment of immunological memory. Adapted from Galluzzi et al., Nature Reviews Immunology (2017).

Loss of CLRT and HMGB1 expression correlates with failed accumulation of immune cells and worst prognosis in lung cancer and breast cancer[56,57]. Moreover, low expression of CLRT receptor LRP1 has been associated with slow progression in melanoma[58] and loss-of-function mutations in the HMGB1 receptor TLR4 in DCs has been associated with shorten time-to-metastasis in breast cancer patients treated with anthracycline-based chemotherapy and local irradiation[49]. Cancer cells with defects in the activation of ER stress through the unfolded protein response (UPR), which is responsible for CLRT translocation and cell fate decision, fail to die in an immunogenic manner in response to stimuli that will otherwise trigger ICD. In particular, based on the integration of different signals, the UPR can decide to favor adaptation to cell damage, leading to cell survival, instead of apoptotic pathways involved in ICD[59]. For example, activation of one arm of UPR that leads to increased slicing of X-box binding protein 1 (XBP1) has been shown to mediate ICD resistance in colon carcinoma (CRC) treated with the anti-epidermal growth factor receptor (EGFR) antibody Cetuximab and chemotherapy[35]. Spliced XBP1 promoted ER-associated degradation (ERAD) of unfolded proteins and its production in CRC cells was dependent on the constitutive activation of ERK pathway due to mutations in *BRAF*[35]. Resistance to cell death, mediated by mutations in *TP53* and overexpression of anti-apoptotic proteins of the BCL-2 family[60], is another mechanism that can impair ICD induction in multiple tumors.

However, a resistance mechanism common to all ICD inducers has not been described yet, suggesting that different compounds may rely on the activation of specific signaling pathways to trigger ICD in different tumor types.

2. Aim of the study

Intravesical chemotherapy with MMC after surgery has been the standard of care in NMIBC for the last 40 years. However, disease-free survival is often short (as short as 3 to 12 months) and a large proportion of NMIBCs recur[18], indicating that some tumors are inherently resistant or become resistant to MMC. We speculated that long-term treatment success might not only rely on MMC cytotoxic potential, but also on its ability to exert immunostimulatory activities by triggering ICD. Compared to *bona fide* ICD inducers, like doxorubicin, mitoxantrone and oxaliplatin, MMC and other DNA-damaging agents, such as etoposide and camptothecin, have been reported as inefficient in eliciting ICD[34,37,42]. However, MMC immunogenicity has only been tested *in vitro* and in vaccination assays after long continuous treatment (24- 48 h) on tumor cells[34,37,42]. This long treatment schedule does not resemble the one used for intravesical therapy in NMIBC, during which MMC is instilled in the bladder with a catheter, where is retained for only 1 to 2 hours[24]. Therefore, we decided to test MMC immunogenicity in a shorter and clinically relevant treatment schedule. In particular, the objectives of this study were:

- Test *in vivo* the immunogenicity of different MMC treatment schedules (short and long) using vaccination regimens in a syngeneic mouse model.
- Characterize ICD induction upon MMC treatment *in vitro* in a panel of bladder cancer cell lines and *ex vivo* in patient-derived bladder cancer specimens.
- Investigate gene expression differences in ICD-responsive *versus* non-responsive tumor cells in order to identify an 'ICD signature', i.e. a gene expression profile that is common to tumors that undergo MMC-induced ICD.
- Identify which mechanisms impair DAMPs release and consequent ICD induction in bladder cancer cells
- Identify a marker of therapeutic response to MMC in bladder cancer

3. Material & Methods

Cell lines and reagents

Human bladder cancer cell lines and mouse cell line CT26 were purchased from the American Type Culture Collection (ATCC). The mouse dendritic cell line DC1 was from the laboratory collection of Prof. M. Rescigno. All cell lines and culture conditions are listed in Table 3.1. All media were supplemented with penicillin/streptomycin to avoid bacterial contamination. All cell lines were tested to exclude mycoplasma contamination. MMC was obtained from the hospital pharmacy at Humanitas Clinical hospital (Rozzano, Italy). Treatment of tumor cell lines with MMC was performed in culture medium at 37°C, 5% CO_2 for 1 h (25 μg/mL; 75 μM) or for 48 h (10 μg/mL; 30 uM); the latter treatment has been described in previous publications not to induce ICD[34,42]. For the downstream experiments requiring the assessment of ICD, culture medium containing MMC was removed after 1 h of treatment, cells were washed twice in PBS, and MMC-free fresh medium was added. In order to obtain mtDNA depleted cells (Rho 0, ρ^0), T24 cell line was cultured for 14 days in media supplemented with 100 ng/ml Ethidium Bromide (EtBr) (Sigma), as previously described[61].

Designation	Source	Culture medium
T24	Human urinary bladder, transitional cell carcinoma	90% McCoy, 10% FBS (NA), 2mM L-glutamine
5637	Human urinary bladder, carcinoma	90% RPMI 1640, 10% FBS (SA), 2mM L-glutamine, 1mM NaP, 10mM Hepes
HT-1376	Human urinary bladder, transitional cell carcinoma	90% MEM with Eagle's salt, 10% FBS (SA), 2mM L-glutamine, 0.1 mM NEAA
HB-CLS-2	Human urinary bladder, primary carcinoma	90% DMEM:Ham's F12K (1:1), 10% FBS (SA), 2mM L-glutamine
TCC-SUP	Human urinary bladder, transitional cell carcinoma	90% MEM with Eagle's salt, 10% FBS (SA), 2mM L-glutamine, 0.1 mM NEAA, 1mM NaP
CLS-439	Human urinary bladder, primary carcinoma	90% McCoy, 10% FBS (NA), 2mM L-glutamine
CT26	Mouse colon carcinoma	90% RPMI 1640, 10% FBS (SA), 2mM L-glutamine
D1	Mouse dendritic cell line	90% RPMI 1640, 10% FBS (NA), 2mM L-glutamine (+ R1 medium)

Table 3.1. List of cell lines and culture conditions.

Mice

Balb/c female mice (Charles River Laboratories) were maintained in our specific-pathogen free (SPF) animal facility and used at 6 weeks of age. The experimental procedures were carried out in agreement with Italian regulations (D.Lgs. 26/2014) and EU guidelines (2010/63/EU).

Assessment of proliferation

Cells were seeded into 96-well plates (2,000–3,000 cells per well). 24 h after seeding, cells were treated with MMC for 1h or untreated. After treatment the drug was removed and fresh medium was replaced in all wells. Cell proliferation was measured using the CyQUANT Cell Proliferation assay (Invitrogen), as described in the protocol. Briefly, medium was removed at different time points and plates were placed at -80 C for a minimum of 4 hours. The main component of the CyQUANT Cell Proliferation assay is a proprietary dye that exhibits fluorescence in the 488 channel when bound to nucleic acids. Sample's DNA content was measured by Clariostar plate reader.

Assessment of apoptosis

To analyze apoptosis, cells were seeded into 6-well plates (3×10^5 cells per well) or 96-well plates (2×10^3 cells per well) and treated the day after with MMC for 1 h or 48 h. Cell death was assessed at different time points by cytofluorimetric analysis using Annexin V and 7-aminoactinomycin (7-AAD) staining apoptosis kit (BD biosciences) or by Realtime-Glo Annexin V-necrosis assay (Promega). In apoptotic cells, PS is translocated from the inner to the outer leaflet of the plasma membrane, thereby exposing PS to the external cellular environment. Annexin V is a 35–36 kDa Ca2+-dependent phospholipid-binding protein with high affinity for PS, and binds to exposed apoptotic cell surface PS (Fig. 3.1). Annexin V can be conjugated to fluorochromes, including FITC, to be detected in flow cytometry. The vital dye 7-AAD is a fluorescent intercalator that undergoes a spectral shift upon association with DNA. 7-AAD/DNA complexes can be excited by the 488 nm laser and has an emission maxima of 647 nm Viable cells with

intact membranes exclude 7-AAD, whereas the membranes of dead and damaged cells are permeable to 7-AAD (Fig. 3.1). By flow cytometry analysis, we characterize cells that are viable as Annexin V negative and 7-AAD negative. Because externalization of PS occurs in the early stages of cell death, early apoptotic cells are Annexin V positive and 7-AAD negative. Whereas, cells that are in late apoptosis or that are already dead were characterized as Annexin V positive and 7-AAD positive. Samples were acquired with a FACSCanto and analyzed with FlowJo software. Detection of late apoptotic cells using Realtime-Glo Annexin V-necrosis assay was determined at different time points by the Glomax fluorescence reader (Promega).

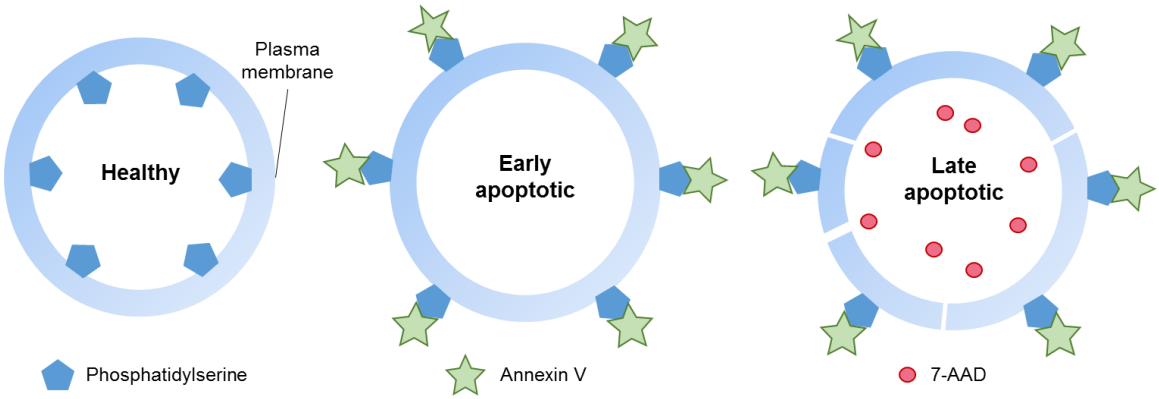

Figure 3.1. Detection of early and late apoptotic cells by Annexin V and 7-AAD staining.

Immunofluorescence

Tumor cells were seeded on coverslips in 12-well plates (5×10^4 cells per well) and treated the day after with MMC for 1 h or 48 h. After 48 h, cells were fixed with PFA 4% for 10 minutes, permeabilized with 0.3% Triton-X for 15 minutes, blocked in 2% FBS, 0.15% Triton-X and stained with Alexa 488-Phalloidin (Invitrogen) and DAPI. CLRT was visualized by staining with Alexa Fluor-647 goat anti-rabbit (1:1,000, Invitrogen). Samples were mounted with Mowiol (Sigma) on a microscope slide, acquired with DMi8 live cell microscope (Leica), and analyzed with ImageJ software.

CLRT translocation

Cells were seeded in 6-well plates (from 3×10^5 to 5×10^5 cells per well) and treated the day after with MMC for 1 h. 2 days after treatment cells were stained with Alexa Fluor-488 mouse monoclonal antibody anti-CLRT (1:100, Enzo life sciences) or with the primary rabbit polyclonal antibody anti-CLRT (1:1,000, Abcam) and with the secondary antibody Alexa Fluor-647 goat anti-rabbit (1:1,000, Invitrogen). Each sample was then acquired with a FACSCanto and analyzed with FlowJo software to identify cell-surface CLRT of stained cells, gated on live cells.

HMGB1 and cytokine release

Supernatants of not-treated or MMC-treated tumor cells were collected 48 h after 1 h treatment. Supernatants of not-treated or MMC-treated tissues were collected 15 h after 1 h treatment. Samples were stored at -80°C and HMGB1 concentration was tested by HMGB1 ELISA (IBL International) according to the manufacturer's instructions. Cytokines in the supernatants were quantified using Cytometric Bead Array (CBA, BD bioscience) technique according to the manufacturer's instructions. Samples were acquired with a FACSCanto and analyzed with FCAP array software (BD bioscience).

Phagocytosis

Human monocyte-derived dendritic cells (moDCs) were obtained from $CD14^+$ peripheral blood monocytes isolated using magnetic beads (Miltenyi Biotec) after 6 days of differentiation in RPMI supplemented with 10% FBS, 2 mM L-glutamine, 0.1 mM, GM-CSF and IL-4 (BD Biosciences)[62]. To test phagocytosis of murine cells we adopted the D1 cell line, generated in our laboratory following an established methodology[63]. Tumor cells were treated or not with MMC, stained with 2.5 μM of CFSE dye (Invitrogen) and seeded in 48-well plates (5×10^4 or 1×10^5 cells per well). After 15 hours, moDCs or D1 cells were stained with 5 μM of DDAO (Invitrogen), added in 1:1 ratio to tumor cells and incubated for 2h at 37°C. Cells were recovered, and then acquired with a FACSCanto and

analyzed with FlowJo software. moDCs that phagocytosed tumor cells were DDAO and CFSE -double-positive.

Stimulation of DCs with cell's supernatant

moDCs were seeded in 96-well plates (0.25×10^5 cells per well) and incubated in supernatants previously retrieved from MMC-treated or not-treated tumor cells or tissues at different concentrations (75% for cell line-derived supernatant and 25% for tissue-derived supernatant). As positive control, moDCs were incubated in 100 ng/ml LPS. As negative control, moDCs were incubated in standard medium (UT). After 24 h, moDCs were recovered, incubated for 15 minutes in 10% human serum and stained with the following antibodies: PE-Cy7 anti-CD11c (eBioscience), PE anti-CD80 (BD bioscience), BV421 anti-CD86 (BD bioscience), FITC anti-HLA-DR (BD bioscience) and BV510 vitality dye (BD bioscience), according to the manufacturer's instructions. Samples were acquired with a FACSCanto and analyzed with FlowJo software.

Assessment of PD-L1 expression by flow cytometry

Cells were seeded in 6-well plates (from 3×10^5 to 5×10^5 cells per well) and treated the day after with MMC for 1 h. 2 days after treatment cells were stained collected, blocked for 15 minutes in 10% human serum and stained with PE-Cy7 mouse monoclonal antibody anti-PD-L1 (1:200, BD bioscience) and BV510 vitality dye (BD bioscience), according to the manufacturer's instructions. Samples were acquired with a FACSCanto and analyzed with FlowJo software.

ICD scoring

In order to score ICD responses we first calculated the average CLRT exposure, HMGB1 secretion, phagocytosis and DC's maturation upon MMC treatment for each analyzed cell line, in terms of % (CLRT exposure, phagocytosis and maturation measured by flow cytometry) or concentration (HMGB1 measured by ELISA) and the relative fold increase on NT values. The median for each ICD parameter was used as a cut-off. We assigned a

score of 0 for values under the cut-off and a score of 1 for values equal or above the cut-off, as shown in Supplementary Table 1.

RNA extraction, RT–PCR and qPCR

Cells were seeded in 6-well plates (from 3×10^5 to 5×10^5 cells per well) and treated the day after with MMC for 1 h. Total RNA was isolated 15 h after treatment using Directzol (Zymo) according to the manufacturer's instructions, adding a DNase digestion step to eliminate genomic DNA contamination. A maximum of 1 µg of RNA from each sample was reverse-transcribed using ImProm-II Reverse Transcriptase (Promega) and random primers (Invitrogen), according to the manufacturers' protocol. Quantitative real-time PCR (qPCR) was carried out with Fast SYBR Green PCR kit using QuantStudio 7 Flex Real-Time PCR System (Thermofisher) starting with of 10 ng of cDNA. The relative expression level was calculated with the 2[−ΔΔCt] method and expressed as a "fold change": data were normalized to housekeeping genes (GAPDH, c1orf43, 18S) expression and compared to the untreated control. The primer list is reported in Table 3.2.

Target	Forward 5'-3'	Reverse 5'-3'
NLRP3	GATCTTCGCTGCGATCAACAG	CGTGCATTATCTGAACCCCAC
HK2	ATCCTGCAACACTTAGGGCT	CCACACCCACTGTCACTTTG
CHOP	AGAACCAGGAAACGGAAACAGA	TCTCCTTCATGCGCTGCTTT
BBC3	ACCTCAACGCACAGTACGAG	CCCATGATGAGATTGTACAGGA
sXBP1	CTGAGTCCGAATCAGGTGCAG	ATCCATGGGGAGATGTTCTGG
c1orf43	GGATGAAAGCTCTGGATGCC	GCTTTGCGTACACCCTTGAA
GAPDH	GTGGAAGGGCTCATGACCA	GGATGCAGGGATGATGTTCT
Mt_1	TCCATGCATTTGGTATTTTCGTC	CGAAGGGTTGTAGTAGCCCGTAG
Mt_2	ACCTTCAAATTCCTCCCTGTACG	TGATGGCCCCTAAGATAGAGGAG
Mt_3	GGCAACCTTCTAGGTAACGACCA	GAGGAGCGTTATGGAGTGGAAGT
Mt_4	GTAAGCCTCTACCTGCACGACAA	GTGGATGCGACAATGGATTTTAC
Mt_5	GCTCACTCACCCACCACATTAAC	TGAAGGGCAAGATGAAGTGAAAG
Mt_6	TGAGGGGCCACAGTAATTACAAA	GAGTGGGAGGGGAAAATAATGTG

Table 3.2. List of primers used in the study.

RNA QC and library preparation

RNA quality was assessed on an Agilent Bioanalyzer using the RNA 6000 Nano Kit (Agilent, Santa Clara, CA, USA), and samples were considered suitable for processing if the RNA integrity number was greater than 7.5. Sequencing libraries were prepared using the TruSeq Stranded mRNA Library Prep kit (Illumina, San Diego, CA, USA) using 800 ng of total RNA. Final libraries were validated with the Agilent DNA1000 kit and sequenced on a NextSeq500 Illumina platform, producing 75 × 2-base paired-end reads.

Sequencing data analysis

High-quality paired-end reads were aligned to the human reference genome (GRCh38) using STAR[64] (version 2.5.3a), and only uniquely mapping reads were used. Post Alignment Quality control was performed with QoRTs software package[65]. Reads were assigned to genes with featureCounts[66] (version 1.6.2) using the gencode (version 28) primary assembly gene transfer file as a reference annotation file for genomic feature boundaries.

Differential expression analysis

Data preprocessing, exploratory data analysis, and analysis of differential gene expression were performed using DESeq2[67] package built-in functions. We studied gene expression differences induced by MMC treatment in Responder (T24 and 5637) and non Responder (TCC-SUP and CLS-439) cell lines, using a paired analysis. Genes with padj < 0.01—Benjamini–Hochberg multiple test correction (FDR)—were considered differentially expressed (DEGs).

Gene Set Enrichment Analysis

We performed Gene Set Enrichment Analysis (GSEA)[68] to investigate biological processes, molecular functions, cellular components and molecular pathways induced or repressed following the MMC treatment. The lists of genes detected in each cell-line were ranked for log2FC between MMC and NT conditions, filtered (basemean > 5) and used

as input for GSEA, together with the gene sets database c5.all.v6.2.symbols.gmt (Gene Ontologies) and c2.cp.v6.2.symbols.gmt (KEGG, BIOCARTA, PID, REACTOME). Significant GSEA terms (FDR < 0.25) in both T24 and 5637 cell-lines were selected and the statistically significant DEGs were extracted.

Measurement of mtDNA

Total DNA was isolated from the same number of cells in all conditions using Wizard DNA purification kit (Promega), adding an RNase digestion step to eliminate RNA contamination. According to the manufacturer's instruction. mtDNA was quantified by qPCR starting with of 10 ng of DNA using primers specific for the MT-CO1 mitochondrial gene (Quiagen). Nuclear DNA encoding 18S (Quiagen) was used for normalization. To verify the presence of the full mitochondrial (mt) DNA six overlapping PCR products, averaging 3.3 kb in length, representing the entire human mtDNA were used according to previous publication[69]. PCR reactions were performed with 100 ng total DNA and GoTaq hot start polymerase (Promega). The primers used for mtDNA quantification are reported in Table 3.2.

Reactive oxygen species (ROS) measurements

Cells were seeded in 12-well plates (from 0.5×10^5 to 0.8×10^5 cells per well) and treated the day after with MMC for 1 h. After 24 h and 48 h, cells were stained with the mitochondrial superoxide indicator MitoSOX (Invitrogen) as described in the manufacturer's protocol. Cells were loaded with 2.5 µM MitoSOX for 10 minutes at 37°C and washed three times in HBSS/Ca/Mg. MitoSOX fluorescence was acquired by FACSCanto and MFI analyzed with FlowJo software.

Measurement of mtDNA release

Cells were seeded in 6-well plates (from 3×10^5 to 5×10^5 cells per well) and treated the day after with MMC for 1 h. After 15 h, cytosolic mtDNA was isolated from the same number of untreated or MMC-treated cells as described[70], with the addition of a RNase

digestion step to eliminate RNA contamination. mtDNA levels were quantified by qPCR as described above.

In vivo immunization studies

For the prophylactic vaccination regimen, 3×10^6 CT26 tumor cells treated for 1 h or 48 h with MMC were inoculated subcutaneously in 200µl PBS into the lower flank. As a control, a group of mice was injected subcutaneously with 200µl PBS. After 7 days, 5×10^5 cells per mouse of live CT26 cells were injected in the contralateral flank of all mice. Rechallenge of tumor-free mice 30 days following the first inoculation was performed by subcutaneous injection of 5×10^5 cells per mouse of live CT26 cells. In the therapeutic vaccination regimen, 5×10^5 cells per mouse of live CT26 cells were injected in the lower flank. After 4 and 8 days, a group of mice was injected subcutaneously with 3×10^6 MMC-treated CT26 cells in 200 µl PBS and another group of mice, as control, was injected with 200 µl PBS in the contralateral flank. Tumor growth was followed over time by measuring the two dimensions with a caliper.

Assessment of specific T cell response

The cytotoxic T lymphocyte (CTL) response against the immunodominant CT26-specific AH1 H2Ld-restricted peptide (SPSYVYHQF) was determined by flow cytometry. Splenocytes were isolated from immunized and control mice 30 days after tumor inoculation and cells were incubated with anti-CD16/CD32 (BD Biosciences) to block nonspecific FcR binding, and with Live/Dead vitality dye (BD bioscience) to eliminate dead cells from the analysis. Antibodies used were anti-CD4, anti-CD3, anti-CD8 primary antibodies (all BD bioscience) and the MHC dextramer (Immudex), according to the manufacturer's instructions. Samples were acquired with a FACSCanto and analyzed with FlowJo software. Tumor-reactive CTLs were gated as CD8 and dextramer-double-positive.

Ex-vivo assessment of anti-tumor IgG generation

CT26 tumor cells were seeded into 96-well plates (3,000 cells per well). 24 h after seeding, cells were incubated for 1 h at room temperature in serial dilutions of sera isolated from mice that we either vaccinated with MMC-treated cells (1h) or unvaccinated. Sera from naïve mice was used as control. Cells were washed in PBS and incubated with FITC anti-mouse IgG for 1h at 4C. After staining, cells were washed, acquired with a FACSCanto and analyzed with FlowJo software.

Patients' recruitment and specimen collection

Tissue specimens were collected from male and female patients undergoing standard or *en-bloc* TURBT[71] for urothelial carcinoma, admitted to Humanitas research hospital. Patients ranged from 40 years old to 87 years old (mean age was 69 years old). Patients included in the study were tumor naïve or untreated tumor recurrence after a tumor-free time of at least 24 months. All tumors were histologically confirmed as urothelial papillary carcinoma and staged Ta, T1 or T2 bladder cancer, graded according to WHO 2016 criteria[72] by two expert uropathologists. Data collection followed the principles stated in the Declaration of Helsinki and was in accordance with the Good Clinical Practice Guidelines. All participants had signed a written informed consent to contribute their anonymous information to the study, approved by the ethical committee of Humanitas research hospital (code: ICH-MIM-01). A list with the clinical data of enrolled patient is available in Table 3.3. Fresh tumor samples were retrieved endoscopically by resectoscope loop during TURBT. After surgery, uropathologists selected a fragment of neoplastic tissue from the specimens to be assigned to the study, which were kept in Hank's Balanced Salt Solution (HBSS) on ice until the start of the procedure. Based on tumor stage and other clinical considerations some of the patients included in the study were treated intravesically with MMC (a solution of 40 mg MMC dissolved in 50 ml sterile water was prepared by the hospital pharmacists) according to Humanitas research hospital and the European Association of Urology (EAU) guidelines (a first cycle of one

instillation a week for 8 weeks and , in absence of tumor recurrence, a second cycle of one installation every moth for 11 months). The list of patients included in the study that also received MMC as treatment after TURBT is available in Table 3.4.

Clinical-pathological features	N°
Cohort size	51
Mean age (±SD)	69 (±10)
Sex	
•Female	7 (13,7%)
•Male	44 (86,3%)
Clinical stage at TURBT	
•pTa LG	21
•pTa HG	8
•pT1 HG	16
•pT2 HG	6

Table 3.3. Clinical-pathological features of patients enrolled in the study.

Patient	Age	Sex	Stage	grade WHO 2016	Recurrence	Tumor-free time (months)	HMGB1 fold change	HMGB1 scoring
15	49	M	pTa	LG	No	15	5,46	high
28	72	M	pTa	LG	No	14	1,16	low
29	68	M	pTa	LG	Yes	12	1,06	low
30	62	M	pTa	LG	No	14	1,07	low
32	40	M	pTa	LG	No	13	1,40	high
34	62	F	pTa	LG	No	12	2,22	high
39	71	M	pTa	LG	No	11	1,13	low
42	76	M	pTa	LG	No	11	1,18	low
62	70	M	pTa	LG	No	4	3,15	high
64	74	M	pTa	LG	No	4	1,43	high
67	76	M	pTa	LG	No	3	1,92	high
69	84	M	pTa	LG	No	2	1,30	high

Table 3.4. Clinical-pathological features of patients enrolled in the study that were treated with MMC in the clinic and relative fold change HMGB1 secretion.

Ex-vivo treatment of patient-derived neoplastic tissue

Samples were processed for *ex vivo* tissue culture[73]. Briefly, specimens were placed on sterile metal grids on top of the center well of the plate (Falcon, center-well organ culture dish). Tissues were treated or not with MMC (0.8 mg/mL, the same concentration as the one used for intravesical instillation in the clinic) for 1 hour at 37°C, 5% CO_2 in the incubator. After treatment, the tissues were incubated in DMEM supplemented with 10% FBS, 2 mM L-glutamine, penicillin/streptomycin, epidermal growth factor (200ng/ml, Peprotech) and Insulin-Transferrin-Selenium-X (10µl/ml, Gibco) at 37°C for 15h before processing (Fig 3.2). Supernatants were collected and stored at -80°C and tissues processed for downstream analysis.

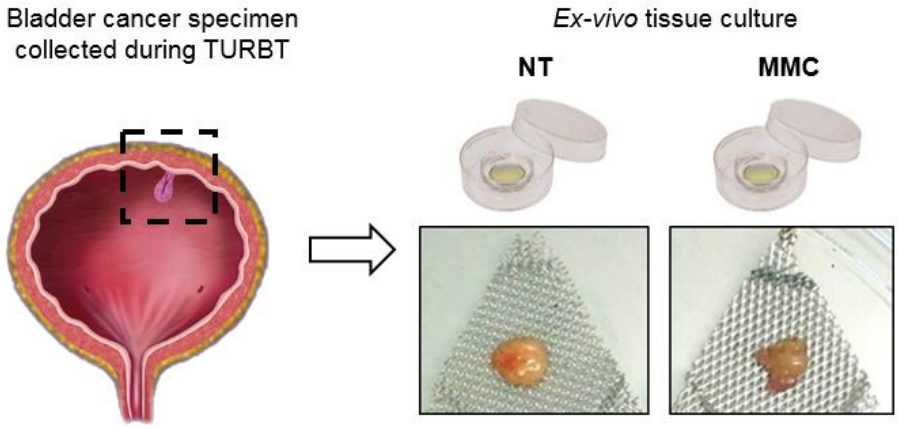

Figure 3.2. *Ex-vivo* treatment of bladder cancer specimens with MMC. Schematic of bladder tumor samples processing for *ex vivo* tissue culture and pictures of specimens untreated (NT) or after MMC-treatment, derived from the same patient.

Gene expression analysis

Gene expression analysis of available datasets was performed using the Kaplan Meier Scanner (Pro) function of R2, a web based genomics analysis and visualization application [74]. We analyzed human expression data of the bladder cancer Hoglund cohort [75] and Dyrskjot cohort [76], using "scan modus" to determine the cut-off for high and low gene expression.

Immunohistochemistry

Cell lines: Untreated cells were seeded on glass slides using cytospin microcentrifuge or on coverslips. For cytospin, a cell suspension of 5×10^5 cells/ml was prepared and a maximum of 500 µl/slide were loaded in the cuvette attached to the slide. Cell were centrifuged at 1200 rpm for 6 minutes (low brake). Cells on the slides were immediately fixed in 4% PFA for 10 minutes and permeabilized in 0,3% Triton X for 15 minutes. For staining of coveslips, were seeded on coverslips in 12-well plates (5×10^4 cells per well). After 16 h, cells were fixed with PFA 4% for 10 minutes, permeabilized with 0.3% Triton-X for 15 minutes. Cells were blocked for 15 minutes in Background Sniper (Biocare medical) and stained with NDUFB8 (Abcam, 1:100) or TOMM20 (SantaCruz, 1:200) in 0.1% BSA for 2 hours. Cells were washed in PBS, 0.05% Tween and incubated in MACH2 mouse horseradish peroxidase (HRP)-polymer detection (Biocare medical) and Universal HRP-polymer (Biocare medical) for 15 minutes and 30 minutes, respectively. Incubation with 3,3′-Diaminobenzidine (DAB) (Dako) was used for antibody detection. DAB is oxidized by hydrogen peroxide in a reaction typically catalyzed by HRP. The oxidized DAB forms a brown precipitate, at the location of the HRP, which can be visualized using light microscopy.

Formalin-fixed paraffin embedded (FFPE) tissues: FFPE slides of selected bladder cancer patients that received MMC treatment after TURBT were prepared in the Pathology department at Humanitas research hospital. We included primary tumors of MMC-responders patients, which were tumor-free for at least 36 month after treatment, and primary and recurrent tumors of MMC-non responders, which relapsed within 24 months after treatment. A list of the patients included in the retrospective analysis is included as Table 3.5. Deparaffination and rehydration was performed in xylene (2 times for 10 minutes) and in decreasing concentrations of ethanol. Antigen retrieval was performed in HIER Universal (Abcam) for 20 minutes at 98°C, followed by 20 minutes at RT. Incubation in H_2O_2 for 5 minutes was performed to suppress endogenous

peroxidase activity to reduce background staining. Blocking and staining with NDUFB8 and TOMM20 were performed as described for cells.

Samples were mounted with Eukitt (Sigma) on a microscope slide, acquired with BX51 light microscope (Olympus). For cell lines analysis at least 5 different images representing the entire section were captured using the same magnification (40X). For tumor samples at least 8 different images representing the entire section were captured using the same magnification (20X). For coverslip fixed cells, the number of DAB positive cells was determined counting manually a total number of 100 cells. Images were analyzed with ImageJ software, using the Immunoratio plug-in for quantification of DAB signal.

Patient code	Age	Sex	Stage (primary tumor)	grade WHO 2016	Recurrence	Tumor-free time (months)
R1	70	M	pTa	HG	No	56
R2	68	M	pTa	LG	No	59
R3	45	M	pTa	LG	No	40
R4	68	M	pTa/CIS	LG	No	66
R5	69	M	pTa	LG	No	54
NR1	73	F	pTa multifocal	LG	Yes	6
NR2	68	M	pTa	LG	Yes	24
NR3	70	M	pTa	LG	Yes	12
NR4	55	M	pTa	LG	Yes	12
NR5	56	M	pTa	LG	Yes	12

Table 3.5. Clinical-pathological features of patients included in the retrospective analysis. R patients responded to MMC and were tumor-free after treatment. NR patients are non-responders to MMC and experienced recurrence after MMC treatment.

Statistical analysis

Data were analyzed for normal distribution before any statistical analyses. Values are presented as mean ± standard deviation (s.d.) of individual experiments of multiple individual experiments, each of which was carried out at least in duplicate or as mean ± s.d. of replicates in a representative experiment. The statistical significance between two groups was determined with unpaired Student's t test, whereas the comparison of multiple

groups was carried out by one-way or two-way ANOVA, followed by Bonferroni's post-test. Kaplan–Meier curves showed the time line for tumor occurrence and survival and were analyzed by log-rank test. All statistical analyses were performed using GraphPad Prism software (San Diego, CA). Data display normal variance. A probability value of $*P<0.05$ was considered significant. In figures: *P<0.05 **P<0.01 ***P<0.001 ****P<0.0001. No statistical method was used to predetermine sample size. The experiments were not randomized. The investigators were not blinded to allocation during experiments and outcome assessments.

4. Results

Long treatment with MMC induces extensive cell death compared to short treatment

In order to investigate MMC immunogenicity we took advantage of the mouse CT26 colon carcinoma cells, since this cell line has been shown to undergo ICD in response to several chemotherapeutic agents, but not to MMC[34,42]. Moreover, the CT26 syngeneic model in mice provides an effective approach for studying how cancer therapies perform in the presence of a functional immune system[77].

First, we assessed MMC cytotoxic potential in CT26 cells treated *in vitro* for 1 h with MMC and then left in culture with fresh drug-free medium, or treated continuously for 48 h in MMC-containing medium, as performed in previous publications[34,42]. Proliferation and cell death were first analysed in a time course experiment (Fig. 4.1A). Treatment with MMC for 1 h drastically reduced cell proliferation (Fig. 4.1B), while slowly inducing cell death, detectable at 48 h compared to untreated cells (Fig. 4.1C). Continuous treatment with MMC for 48 h stopped cell proliferation (Fig. 4.1B) and rapidly induced cell death compared to both untreated and 1h treated cells (Fig. 4.1C).

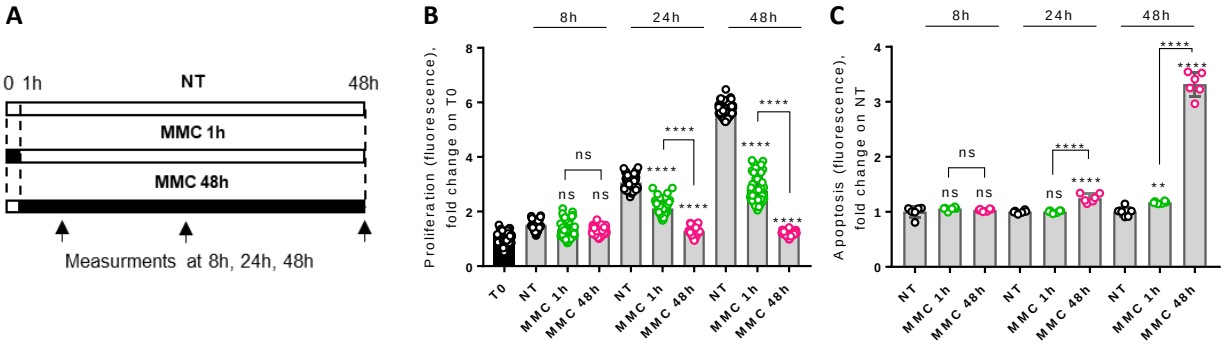

Figure 4.1. Proliferation and cell death upon MMC treatment in CT26 tumor cells. (A) Schematic of *in vitro* treatments with MMC. Arrows indicate the time points at which proliferation and cell death was assessed (8, 24, 48 h). (B) Proliferation as measured by CyQuant proliferation assay and (C) cell death as measured by Realtime-Glo assay of untreated cells (NT) or treated with MMC for 1 h or 48 h. Data are mean ± s.d. of six replicates in a representative experiment. One-way ANOVA using Bonferroni post test comparing the three conditions at each time point. *refers to NT. **P<0.01,****P<0.0001.

To confirm these data, we assessed cytotoxicity after 48 h by microscopy and AnnexinV/7-AAD staining (Fig. 4.2A). Morphologically, we observed that following 1 h of treatment with MMC, tumor cells displayed cell swelling and increased size, whereas upon 48h of treatment we detected mostly cell's debris and the remaining tumor cells were in suspension or shrinking (Fig. 4.2B). Indeed, AnnexinV/7-AAD staining revealed a significant increase in the amount of late apoptotic cells after 48 h of treatment when compared to 1 h of treatment, as measured by incorporation of 7-AAD (AnnexinV$^+$7-AAD$^+$ cells). On the contrary, around 50% of tumor cells treated for only 1 h and left in culture were still alive or in the early phases of apoptosis after 48 h, as measured by AnnexinV detection of PS derangement at the plasma membrane (Fig. 4.2C).

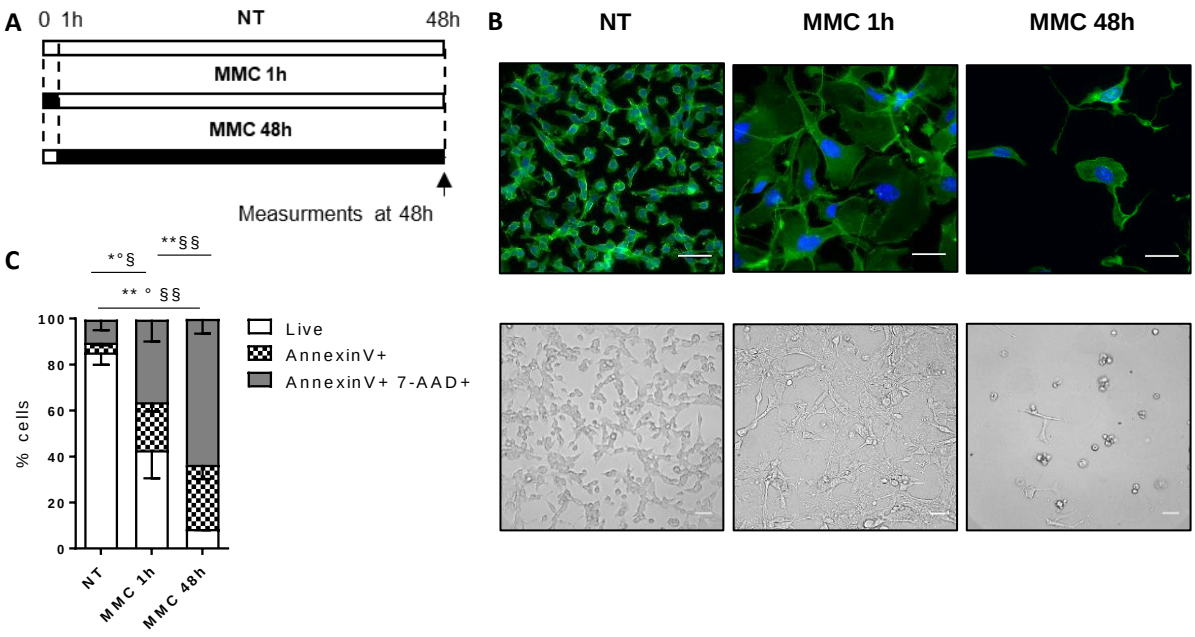

Figure 4.2. Cell death quantification in MMC short and long treated CT26 tumor cells. (A) Schematic of *in vitro* treatments with MMC. Arrows indicate the time point at which cell death was assessed by microscopy and AnnexinV/7-AAD staining (48 h). (B) Immunofluorescence (upper panel) and bright field imaging (bottom panel) of CT26 cells untreated (NT) or treated with MMC for 1 h or 48 h. Actin stained with phalloidin (green) and nuclei with DAPI (blue). Scale bars, 50µm. (C) Percentage of early apoptotic (AnnexinV+) and late apoptotic (AnnexinV$^+$7-AAD$^+$) cells MMC. Data are mean ± s.d. and represent the pool of two independent experiments. One-way ANOVA using Bonferroni post-test; * refers to live cells, ° refers to AnnexinV$^+$, § refers to AnnexinV$^+$7-AAD$^+$. *P<0.05, **P<0.01.

MMC short-treated tumor cells are immunogenic *in vivo*

To assess *in vivo* the immunogenicity of tumor cells following short and long exposure to MMC I adopted a well-established prophylactic vaccination regimen in a syngeneic mouse model[34]. Balb/c mice were first vaccinated subcutaneously with CT26 tumor cells either exposed to a short treatment of 1 h with MMC (MMC 1h) or to a long treatment of 48 h with MMC (MMC 48h). PBS was injected as a control in unvaccinated mice. Importantly, no tumor growth was found upon injection of tumor cells treated with MMC for 1 h or 48 h at vaccination site, confirming that both treatments efficiently induced a block in cell proliferation. Mice were challenged with live CT26 cells in the contralateral flank after 7 days from vaccination (Fig. 4.3A). Interestingly, immunization with MMC-short treated CT26 cells protected mice from tumor development at the challenge site resulting in a drastic reduction of tumor growth and about 80% survival rate of mice that were also tumor free (Fig. 4.3B, C, D). Conversely, confirming published data[34,42], mice vaccinated with MMC-long treated CT26 cells developed tumors concurrently with unvaccinated mice (control) and only 5% were alive at the end of the experiment (Fig. 4.3B, C, D). These data suggest that 1h treatment with MMC is able to induce a protective anti-tumor immune response.

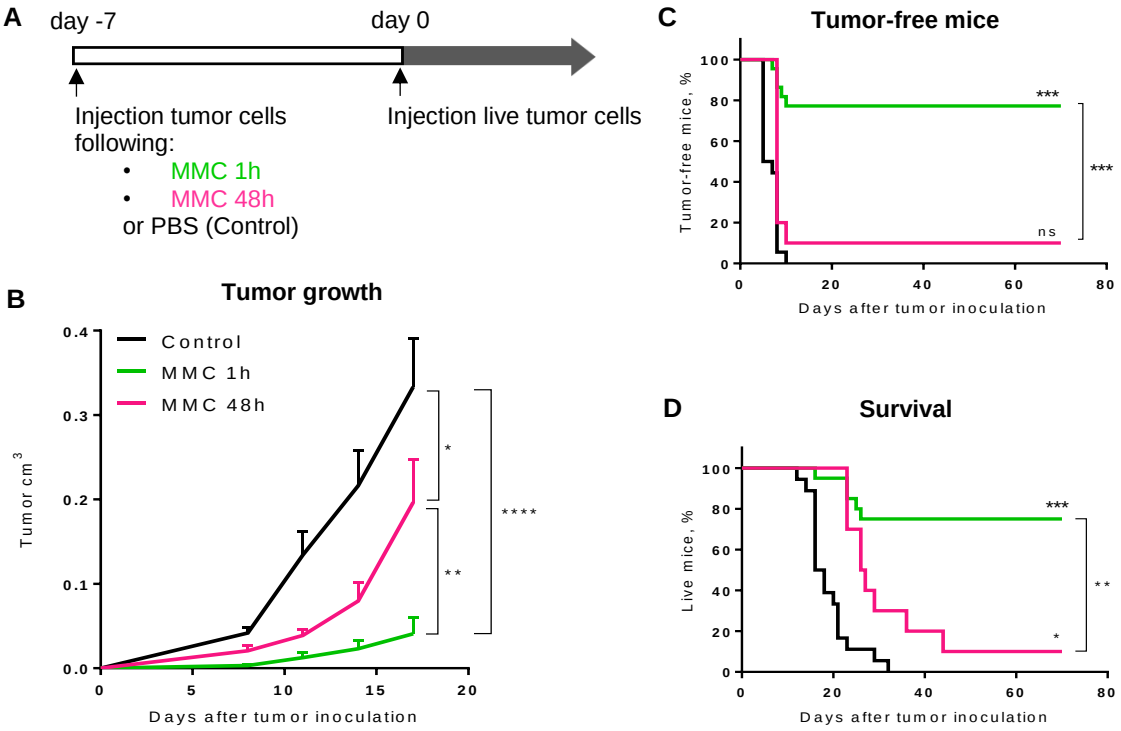

Figure 4.3. Prophylactic tumor vaccination regimen with MMC-short and long treated CT26 tumor cells. (A) Schematic of prophylactic tumor vaccination model. (B) Tumor growth of Balb/c mice vaccinated with MMC 1h or MMC 48h treated CT26 cells or unvaccinated (control). n= 10-22 per group. Data are mean ± s.d. and represent the pool of two independent experiments. Two-way ANOVA using Bonferroni post test. (C, D) Percentage of tumor free-mice (C) and Kaplan-Meier survival curves (D) upon vaccination. n= 10-22 per group; log rank test. *P<0.05, **P<0.01, ***P<0.001, ****P<0.0001.

In order to characterize the anti-tumor immune response occurring upon prophylactic vaccination, I analysed by flow cytometry the immune infiltrate in the spleen of tumor-bearing unvaccinated mice and tumor-free vaccinated mice (MMC 1h) 20 days after inoculation of live tumor cells. Unvaccinated mice exhibited enlarged spleen (Fig. 4.4A). On the contrary, vaccinated mice had normal size spleen that showed increased infiltration of $CD11c^+$ APCs expressing MHCII molecules and $CD3^+$ T cells compared to unvaccinated mice (Fig. 4.4B), suggesting increased ability to perform antigen presentation and T cell priming against tumor antigens following tumor inoculation.

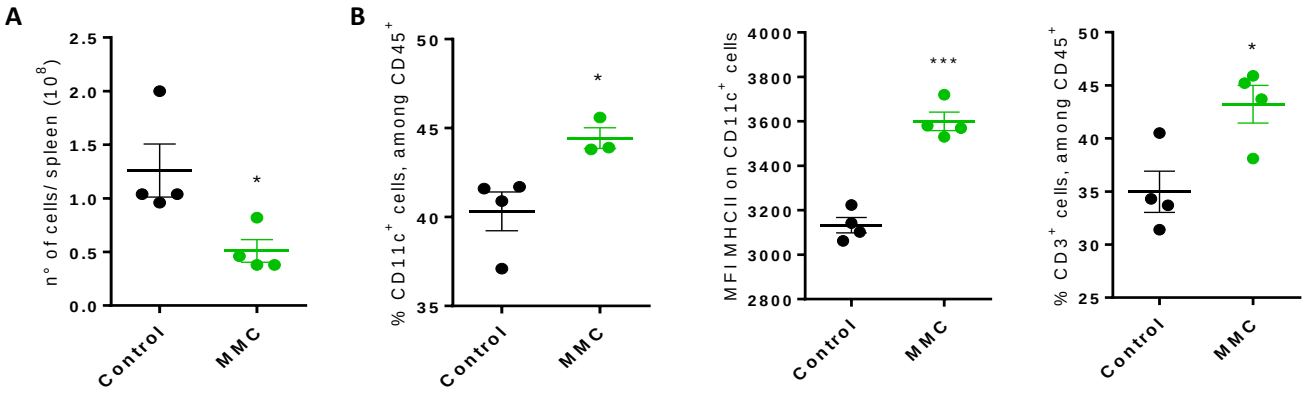

Figure 4.4. Characterization of immune populations in the spleen of vaccinated mice. (A) Total number of cells in the spleen of unvaccinated mice (controls) or mice vaccinated with tumor cells treated for 1h with MMC. (B) Flow cytometry analysis shows the percentage of $CD11c^+$ cells, MFI of MHCII, and percentage of $CD3^+$ T cells isolated from the spleen 20 days after inoculation of live tumor cells. Unpaired two-tailed *t*-test. *P<0.05, ***P<0.001.

Moreover, in the sera of vaccinated mice (MMC 1h) I detected an increased amount of immunoglobulin (Ig) G antibodies that were able to recognize and bind tumor cells *ex-vivo* compared to unvaccinated or naïve mice (Fig. 4.5A, B), indicating activation of B cell-mediated antitumor immunity upon vaccination.

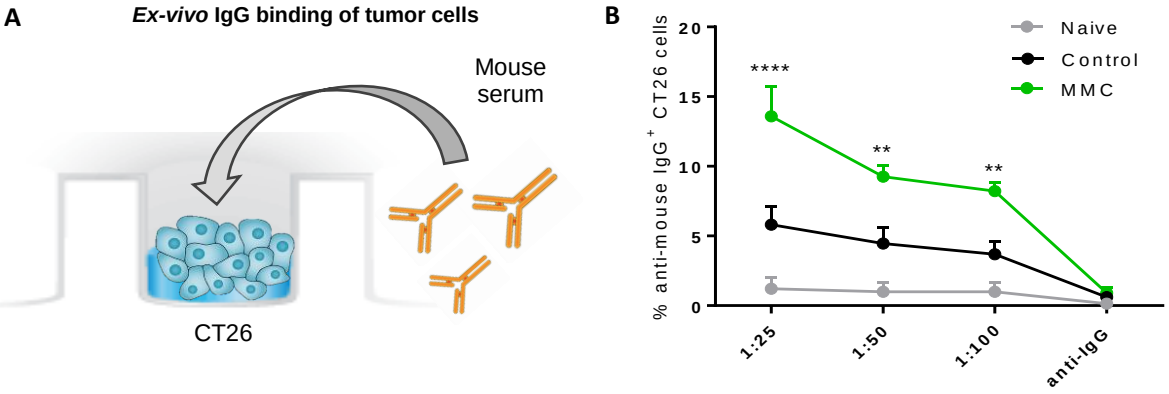

Figure 4.5. Characterization of B cell activation in vaccinated mice. (A) Schematic of *ex-vivo* assessment of the presence of anti-tumor IgGs in mouse serum. (B) Percentage of CT26 tumor cells bound by IgGs present in the sera of vaccinated (MMC 1h) or unvaccinated (NT) mice 20 days after inoculation of live tumor cells. Sera from naïve mice were used as negative control. Two-way ANOVA with Bonferroni post test. **P<0.01, ****P<0.0001

Consistent with the acquisition of immune protection, I observed higher frequencies of tumor-specific $CD8^+$ T cells, recognizing the CT26 antigen AH1, in mice vaccinated with MMC-short treated tumor cells compared to unvaccinated mice or mice vaccinated with MMC-long treated tumor cells (Fig. 4.6A). To test whether immunization with MMC-treated tumor cells was able to sustain long-lasting responsiveness, I challenged tumor-free mice again with viable CT26 cells 30 days after the first inoculation. Notably, 9 out of 10 mice were still completely protected from tumor engraftment (Fig. 4.6B).

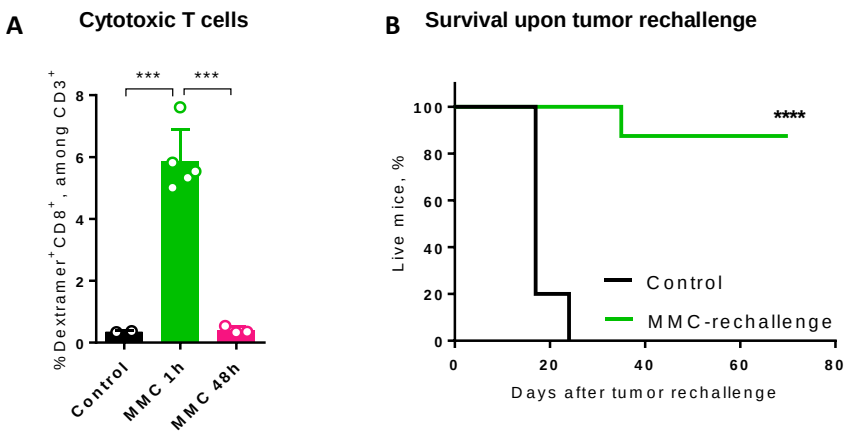

Figure 4.6.. Activation of antitumor T cells and immunological memory in mice vaccinated with MMC-treated tumor cells. (A) Percentage of tumor antigen-specific (dextramer-AH1) $CD8^+$ T cells derived from the spleen of Balb/c mice 30 days after tumor inoculation. Data are mean ± s.d. and represent the pool of two independent experiments. One-way ANOVA using Bonferroni post test. (B) Percentage of live mice (MMC 1h group from the prophylactic vaccination experiment) after re-challenge with live CT26 cells. n= 10 per group; log rank test. ***P<0.001 ****P<0.0001

I then tested the potential of MMC vaccination in a therapeutic regimen. Balb/c mice were first inoculated with live CT26 cells and after 4 and 8 days, when bearing measurable tumors, they were vaccinated subcutaneously with CT26 tumor cells treated for 1 h with MMC (MMC) or unvaccinated (Control) (Fig. 4.7A, B). Mice therapeutically vaccinated with MMC short-treated CT26 cells displayed a significant delay in tumor growth (Fig. 4.7C) and increased survival when compared to unvaccinated mice (Fig. 4.7D).

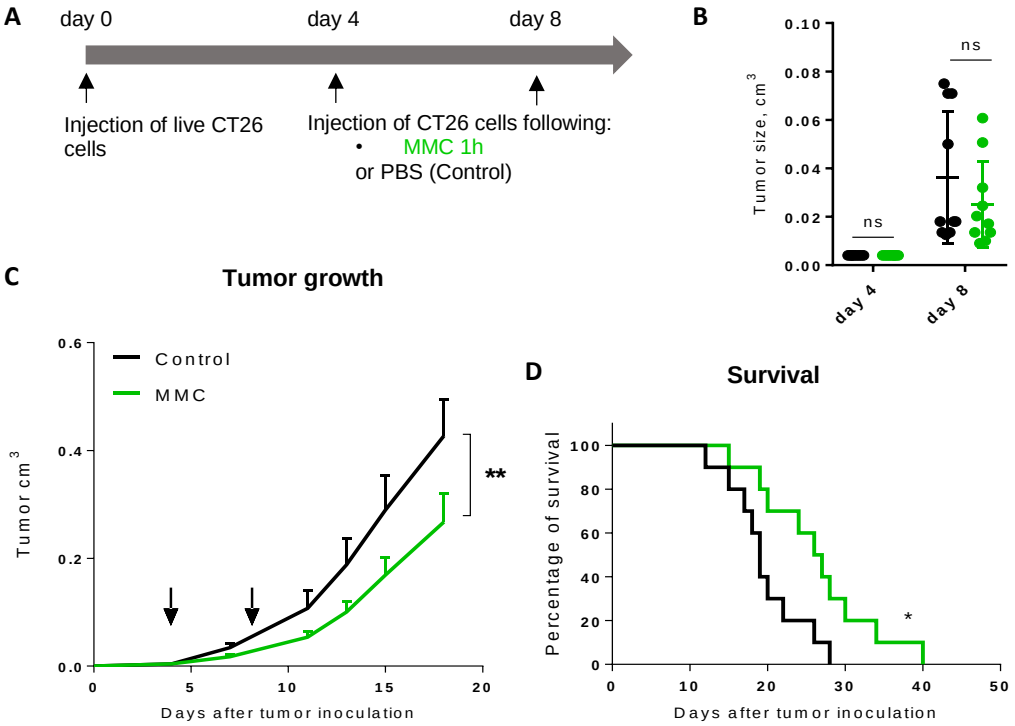

Figure 4.7. Therapeutic tumor vaccination regimen with MMC-treated CT26 tumor cells. (A) Schematic of therapeutic tumor vaccination model. (B) Tumor size at vaccination days 4 and 8. Data are mean ± s.d; unpaired two-tailed *t*-test at day 4 or day 8. (C) Tumor growth upon therapeutic vaccination regimen. Arrows indicate the days in which tumor-bearing mice received MMC 1h treated CT26 cells. n= 10 per group. Data are mean ± s.d; two-way ANOVA and Bonferroni post test. (D) Kaplan-Meier survival curves upon therapeutic vaccination. n= 10 per group. Log rank test. *P<0.05, **P<0.01.

Collectively, these data confirmed that a prolonged treatment with MMC does not induce the development of antitumor immunity *in vivo* in vaccination assays, suggesting that extensive cell death induced by long treatment with MMC rendered tumor cells non-

immunogenic. Conversely, a short treatment (1 h) with MMC was able to trigger ICD in dying tumor cells, eliciting a protective antitumor immune response.

Short treatment with MMC triggers ER stress response and promotes phagocytosis by dendritic cells

I speculated that protection from tumor growth observed *in vivo* upon vaccination was mediated by the ability of short-treated tumor cells to undergo a *premortem* stage that was essential for the display of ICD signals necessary to elicit protective immunity against tumor growth. The first described event of ICD is the early translocation of CLRT and ER-protein 57 (Erp57), a chaperone protein that binds to CLRT to facilitate its exposure, from the ER lumen to the plasma membrane of dying cells[78]. I found that 1h treatment with MMC induced the translocation of CLRT and Erp57 to the cell surface (Fig. 4.8 A, B). Moreover, dying cells undergoing ICD start to release damage-associated molecules including the chromatin protein HMGB1, which I detected in the supernatant of tumor cells after treatment with MMC (Fig. 4.8C).

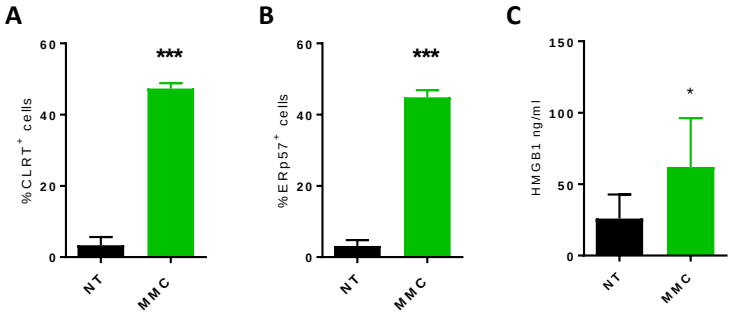

Figure 4.8. ICD markers expression in MMC-short treated CT26 tumor cells. (A) Quantification of CLRT (B) and ERp57 exposure by flow cytometry of CT26 cells untreated (NT) or treated with MMC for 1 h. (C) Quantification by ELISA of HMGB1 in the supernatants of MMC-treated and untreated CT26 cells. Data are mean ± s.d. and represent the pool of two independent experiments. Unpaired two-tailed *t*-test. ***P<0.001, ****P<0.0001.

To assess whether MMC was rendering treated tumor cells more susceptible to phagocytosis, I incubated CT26 tumor cells- either treated or not with MMC- with murine D1 DCs (Fig. 4.9A). Notably, I found that CT26 cells treated with MMC were phagocytosed better then untreated cells (Fig. 4.9B).

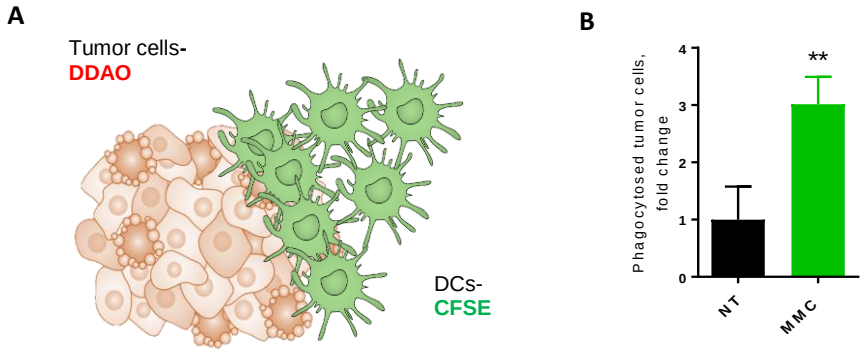

Figure 4.9. Phagocytosis of MMC-short treated CT26 tumor cells. (A) Schematic of phagocytosis assay. Tumor cells, untreated or MMC-treated, and DCs are stained with different fluorescence dyes (CFSE and DDAO respectively) and put in coculture. Phagocytosed tumor cells are quantified as double positive events ($CFSE^+$ $DDAO^+$). (B) Quantification of phagocytosis by DC1 dendritic cells of CT26 cells untreated (NT) or treated with MMC for 1 h, as measured by flow cytometry. Data are mean ± s.d. of five replicates in a representative experiment. Unpaired two-tailed *t*-test. **P<0.01.

Collectively, these results indicate that MMC can induce the first events of ICD: the translocation of ER proteins to the plasma membrane and the release of HMGB1, which in turn facilitate the engulfment of treated cells by DCs.

MMC can foster ICD in bladder cancer cells

MMC is mainly used in the treatment of NMIBC as intravesical chemotherapy administered through a catheter and left in the bladder for around 1-2 hours before elimination. Therefore, I tested the capacity of MMC to induce ICD in a panel of human bladder cancer cell lines (n=6) after 1 h treatment. MMC induced a reduction in tumor cell proliferation (Fig. 4.10A) and cell death (Fig. 4.10B) in all the analyzed cell lines.

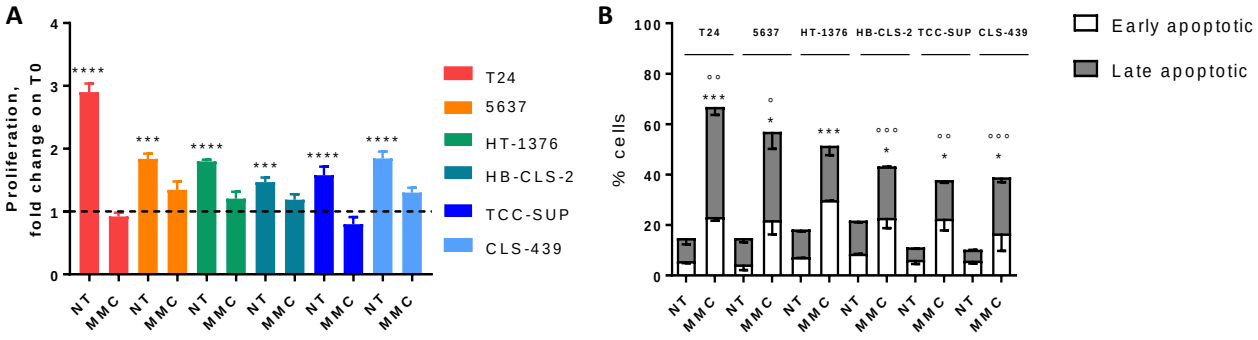

Figure 4.10. Proliferation and cell death upon MMC treatment in bladder cancer cells. (A) Proliferation of untreated cells (NT) or treated with MMC for 1 h (MMC), as detected 48 h after treatment with CyQuant proliferation assay. Data are mean ± s.d. of five replicates in a representative experiment. Unpaired two-tailed *t*-test comparing NT *vs* MMC in cell lines independently. (B) Percentage of early apoptotic (AnnexinV+) and late apoptotic (AnnexinV+7-AAD+) cells, as detected 48 h after treatment by flow cytometry. Data are mean ± s.d. and represent the pool of two independent experiments. Unpaired two-tailed *t*-test comparing NT *vs* MMC in cell lines independently.; * refers to AnnexinV+, ° refers to AnnexinV+7-AAD+. *P<0.05, **P<0.01, ***P<0.001, ****P<0.0001.

Aside from its cytotoxic activity, MMC increased CLRT translocation to the plasma membrane of bladder cancer cells, as detected by both flow cytometry (Fig. 4.11A) and immunofluorescence (Fig. 4.11B), and induced the release of the damage-associated molecule HMGB1 in the supernatant, with the exception of CLS-439 cells (Fig. 4.11C). Overall, I observed an heterogeneous expression of these molecules correlating with ICD among the different cells lines.

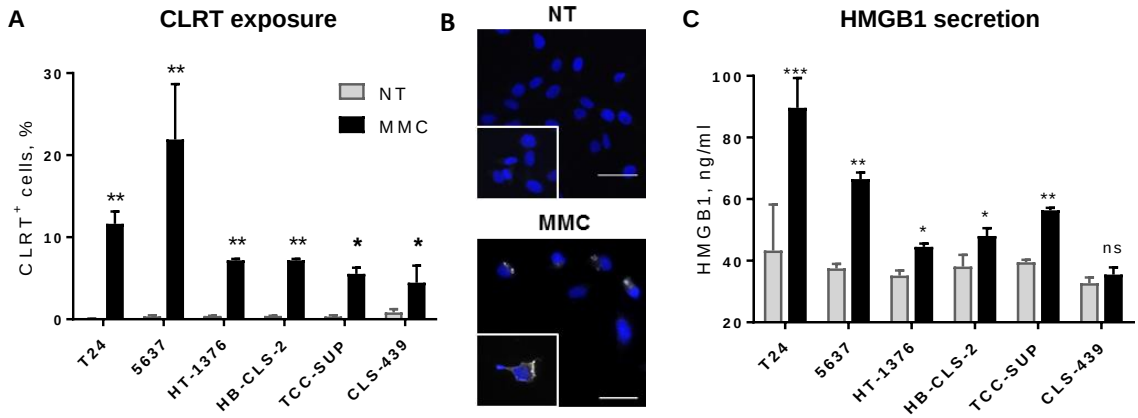

Figure 4.11. ICD marker expression in MMC-treated bladder cancer cells. (A) Quantification of CLRT exposure by flow cytometry. Data are mean ± s.d. and represent the pool of two independent experiments. Unpaired two-tailed *t*-test comparing NT *vs* MMC in cell lines independently. (B) Representative immunofluorescence images showing CLRT (white) and DAPI (blue). Scale bars, 50µm. (C) Quantification by ELISA of HMGB1 secreted in the

supernatants of MMC-treated and untreated bladder cancer cells. Data are mean ± s.d. and represent the pool of two independent experiments. Unpaired two-tailed *t*-test comparing NT *vs* MMC in cell lines independently. *P<0.05 **P<0.01, ***P<0.001.

Further, the majority of MMC-treated tumor cells were more susceptible to monocyte derived dendritic cells (moDC)–mediated phagocytic clearance compared to untreated cells (Fig. 4.12). However, HB-CLS-2 and CLS-439 treated tumor cells were not phagocytosed after MMC treatment.

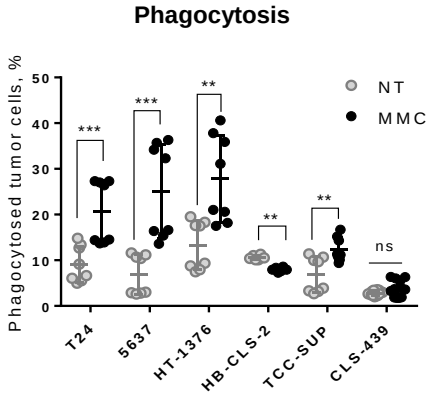

Figure 4.12. Phagocytosis of MMC-treated bladder cancer cells. Quantification of phagocytosis by mo-DCs of tumor cells exposed to MMC or untreated (NT), as measured by flow cytometry. Data are mean ± s.d. of four replicates in experiments using two different moDC donors. Unpaired two-tailed *t*-test comparing NT *vs* MMC in cell lines independently. **P<0.01, ***P<0.001.

Since secreted DAMPs, including the alarmin HMGB1, can activate DCs for efficient priming of adaptive immunity[32,50], I tested whether culturing moDCs in the supernatants collected from MMC-treated tumor cells was alone sufficient to induce their maturation. I found that moDCs upregulated the expression of the co-stimulatory ligands CD80 and CD86 when cultured in conditioned media from T24 or 5637 MMC-treated cells, but not from untreated cells. On the contrary, moDCs cultured in conditioned media from HT-1376, TCC-SUP and CLS-439 MMC-treated bladder cancer cell lines did not alter their maturation status (Fig. 4.13A, B, C). HB-CLS-2-treated supernatant midly induced CD80 expression on DCs (Fig. 4.13B).

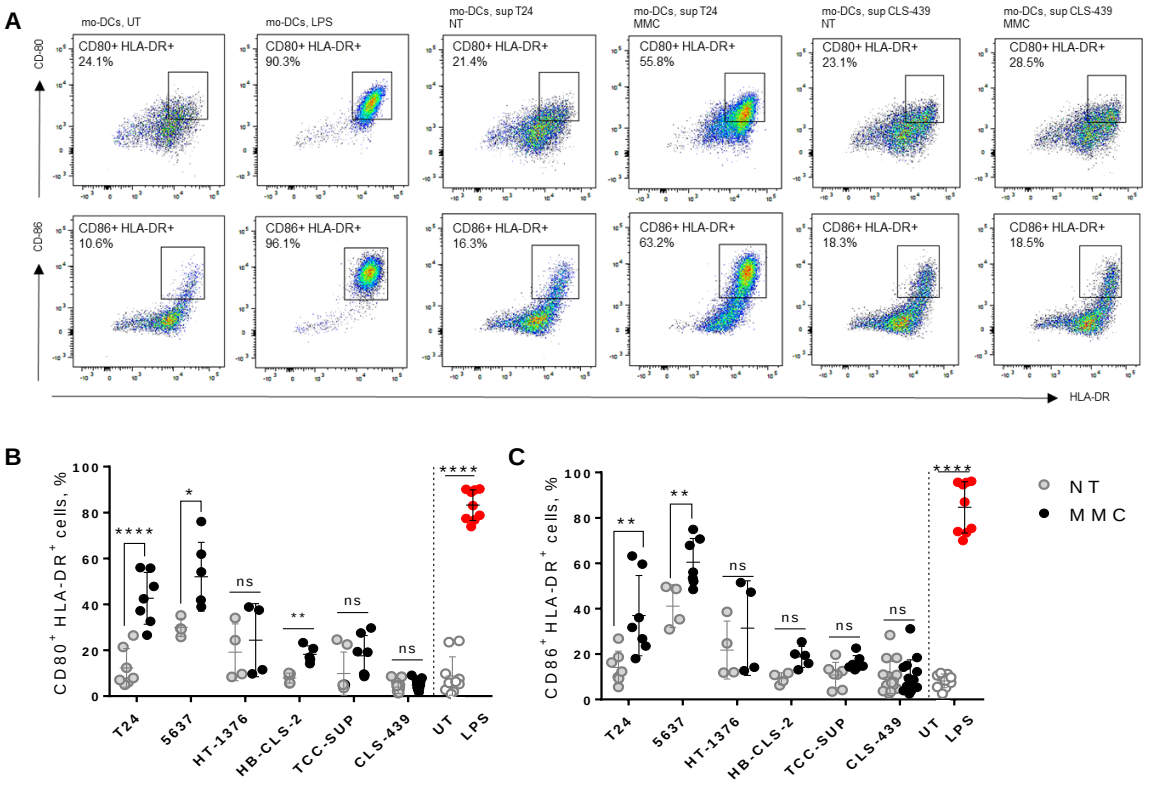

Figure 4.13. Dendritic cells activation in conditioned media of MMC-treated bladder cancer cells. (A) Representative flow cytometry dot plots showing the gating and percentage of $CD11c^+$ $CD80^+$ $HLA\text{-}DR^+$ moDCs (top panel) $CD11c^+$ $CD86^+$ $HLA\text{-}DR^+$ moDCs (bottom panel) upon co-culture with supernatants from MMC-treated or untreated (NT) bladder cancer cells. (B) Quantification of $CD80^+$ $HLA\text{-}DR^+$ (C) and $CD86^+$ $HLA\text{-}DR^+$ moDCs populations upon the different stimuli. Unstimulated (UT) moDCs served as negative control. Stimulation with LPS used as positive control. Data are mean ± s.d. of three to four replicates in experiments using two different moDC donors. Unpaired two-tailed *t*-test comparing NT *vs* MMC in cell lines independently or UT *vs* LPS. **P<0.01, ****P<0.0001.

Since I observed variability in ICD induction among bladder cancer cell lines, I developed a scoring system to evaluate MMC-induced responses combining the analyzed ICD parameters: CLRT exposure, HMGB1 secretion, phagocytosis and DC's maturation (Supplementary Table 1). This approach allowed us to identify ICD-responsive cell lines (T24 and 5637), which robustly expressed ICD markers upon MMC treatment, ICD-poorly responsive cell lines (HT-1376, HB-CLS-2, and TCC-SUP), which less potently

underwent ICD, and an ICD-resistant cell line (CLS-439), which did not undergo ICD upon MMC treatment (Fig. 4.14).

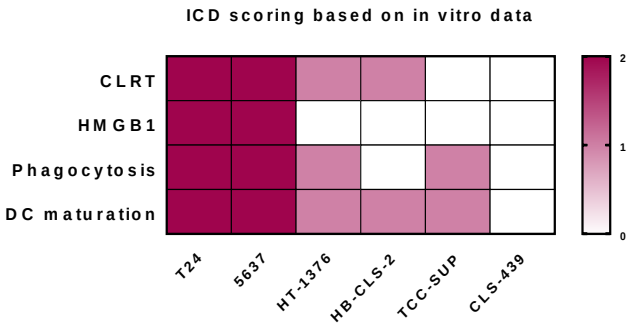

Figure 4.14. ICD scoring of bladder cancer cell lines. Graphic representation of ICD scoring upon MMC treatment. The median for each ICD parameter was used as a cut-off. I assigned a score of 0 for values under the cut-off and a score of 1 for values equal or above the cut-off, considering both percentage of positive cells or concentrations and fold change on untreated controls.

Ex-vivo MMC treatment of bladder tumor tissues can trigger HMGB1 secretion and moDC maturation

To investigate the clinical relevance of ICD induced by MMC, I designed a clinical trial in which ICD induction was assessed in neoplastic tissues derived from urinary bladder cancer patients treated *ex vivo* with MMC (n= 51; Table 3.3). Tumor tissues were collected after TURBT and processed for *ex-vivo* tissue culture. Tissues deriving from the same patient were divided into two parts: one was not treated, whereas the other one was treated with MMC for 1 hour. According to our scoring system, the discriminating parameter that characterized effective ICD induction was HMGB1 secretion (Fig. 4.14). Thus, I measured HMGB1 as an indicator of ICD in the supernatants collected after treatment. MMC increased the release of HMGB1 in about 45% of the treated tumor specimens, compared to their respective untreated controls (Fig. 4.15A). Relative amounts of HMGB1 were particularly increased in low grade non-invasive (pTa) urothelial carcinomas, the histological subtype for which MMC instillations are recommended according to the current clinical guidelines (Fig. 4.15B).

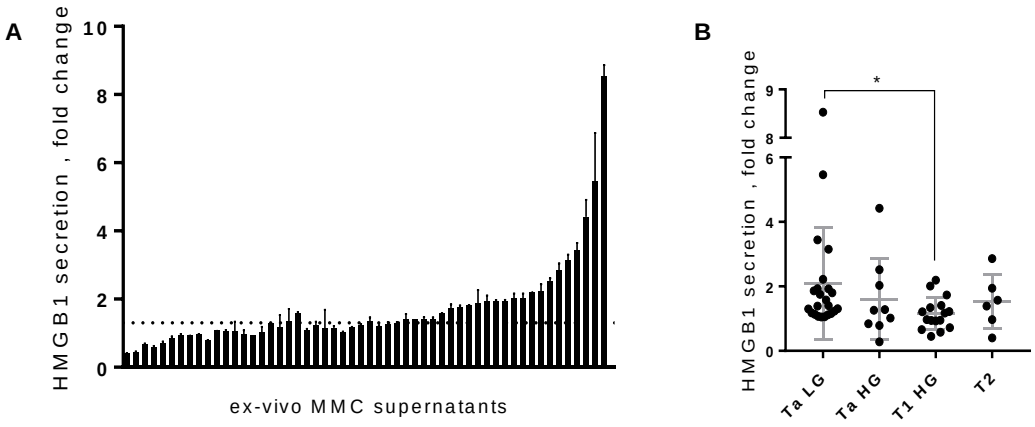

Figure 4.15. HMGB1 secretion in tumor specimens upon MMC treatment. (A) Fold change increase of HMGB1 secreted by tumor samples treated *ex-vivo* with MMC normalized on the respective untreated (NT) samples (n=51). Dotted line indicates the median cut-off of 1.28. (B) Fold change increase of secreted HMGB1 in the different bladder cancer histological grades. Each dot represents the mean fold change increase of secreted HMGB1 in a tumor specimen deriving from a single patient. Unpaired two-tailed *t*-test. *P<0.05.

Moreover, I observed a statistical significant increase in $CD80^+$ $HLA\text{-}DR^+$ and $CD86^+$ $HLA\text{-}DR^+$ mature populations upon culture of moDCs in conditioned media derived from MMC-treated tumor specimens, compared to moDCs cultured in conditioned media derived from untreated tumor specimens (Fig. 4.16A). Interestingly, when I divided the tumor specimens based on the increase of HMGB1 secretion, using the median fold change of 1.28 as cut-off value, as measured in Fig. 4.15A, I observed that tumor samples secreting more HMGB1 (HMGB1 high) induced higher expression of the activation marker CD80 compared to tumors that showed low levels of secreted HMGB1 (HMGB1 low) (Fig. 4.16B).

Overall, these data confirmed that MMC treatment can induce ICD in patient's surgical specimens treated *ex vivo* and that, consistent with the inability of MMC to always prevent recurrence in patients undergoing TURBT, there is variability among tumors in the propensity to release the damage signal HMGB1 that can drive the maturation of DCs, a crucial step for proper priming of adaptive immunity.

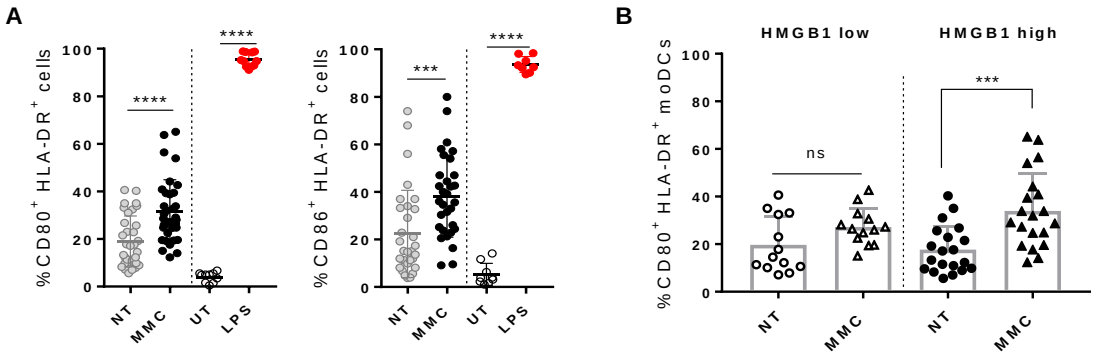

Figure 4.16. Dendritic cells activation in conditioned media of MMC-treated tumor specimens. (A) moDCs CD80$^+$ HLA-DR$^+$ and CD86$^+$ HLA-DR$^+$ populations upon stimulation with supernatants from MMC-treated or untreated (NT) tumor samples. Unstimulated (UT) moDCs were used as negative control. Stimulation with LPS was used as positive control. Unpaired two-tailed t- test NT *vs* MMC or UT *vs* LPS. (B) Percentages of CD80+ HLA-DR+ moDCs upon different stimuli scored as HMGB1 low and HMGB1 high based on the fold change increase in HMGB1 secretion (median cut-off= 1.28). Data are mean ± s.d. of duplicate measurements. One way ANOVA using Bonferroni post test. ***P<0.001, ****P<0.0001.

Gene expression profiling of ICD-responsive and ICD-non responsive cells

Having demonstrated that ICD can be triggered by MMC in some human bladder cancer cells and specimens, but not in others, I investigated the molecular changes occurring upon ICD induction by performing RNA sequencing of two ICD-responsive (T24 and 5637), one ICD-poorly responsive (TCC-SUP) and one ICD-resistant (CLS-439) cell lines, both untreated and MMC-treated. I found that ICD-responsive cells were characterized by the upregulated expression of several genes, which were not regulated or downregulated in ICD-poorly responsive and ICD-resistant cells (Fig. 4.17A). Gene set enrichment analysis (GSEA) revealed a gene signature specific for ICD-responsive cells characterized by the upregulation of genes involved in immune system functions. In particular, the upregulated gene sets in ICD-responsive cells belonged to processes like response to cytokines, inflammation and regulation of innate and adaptive immune response (Fig. 4.17B).

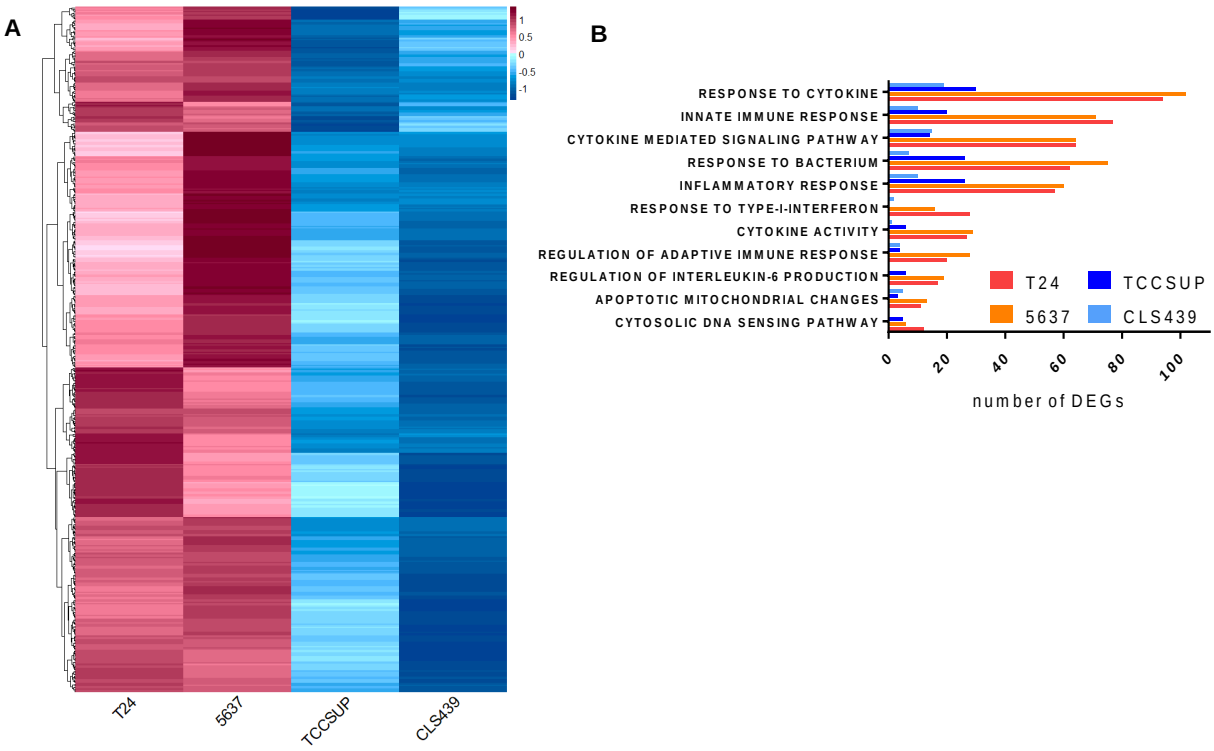

Figure 4.17. Upregulated gene sets in ICD-responsive bladder cancer cells. (A) Heatmap of 532 genes showing different fold-change expression (MMC vs NT) in ICD-responsive and not-responsive cells. Genes were selected by k-means clustering starting from the total of DEGs identified in the 4 cell lines. (B) Barplot of significantly upregulated gene sets in bladder cancer cell lines after MMC treatment (GSEA analysis - FDR < 0.25). Bars represent the number of differentially expressed genes (DEGs) in each cell line.

Among the most upregulated genes in the ICD signature I found proinflammatory cytokines (*IL1β*, *IL6*, *TNF*), chemotactic molecules that control the migration and adhesion of monocytes (*CXCL3*), neutrophils (*CXCL5*, *CXCL8*) and lymphocytes (*CCL20*), and growth factors (*CSF2*, *FGF*) (Table. 4.1).

Moreover, I observed multiple gene sets that were specifically downregulated in ICD-responsive cells. Many of these were related to the regulation of cell cycle, spindle formation, organelle fission, sister chromatid segregation, and protein processing, confirming that MMC treatment in these cells induced an early block in the replication machinery, stopped in cell cycle progression, leading to cytotoxicity (Fig. 4.18).

		LogFC MMC vs NT				
Gene Ontology	**Gene ID**	T24	5637	TCC-SUP	CLS-439	**padj**
CYTOKINE ACTIVITY	*IL6*	5.75	3.75	1.72	-	<0.01
	IL1B	2.08	0.74	-	-	<0.01
	FGF2	0.67	0.93	-	-	<0.01
	CSF2	4.48	1.78	-	-	<0.01
	CXCL5	0.91	0.98	-	-	<0.01
	EDN1	1.03	1.34	0.73	-	<0.01
	TNF	3.20	2.90	-	-	<0.01
	CCL20	3.75	1.38	-	-	<0.01
	CXCL2	2.69	2.66	-	-	<0.01
	CXCL3	3.07	2.75	-	-	<0.01
	CXCL6	0.99	1.36	-	-	<0.01
INNATE IMMUNE RESPONSE	*BMP2*	2.40	0.93	-	-	<0.01
	IRF5	1.17	1.19	-	-	<0.01
	NLRP3	0.86	1.25	-	-	<0.01
	MYD88	0.70	0.57	-	-	<0.01
	IRF1	1.74	0.55	-	-	<0.01
	IRF7	1.47	1.90	-	-	<0.01
INFLAMMATORY RESPONSE	*IL8*	2.42	2.31	1.94	-	<0.01
	ICAM1	30.10	1.91	0.68	-	<0.01
	FOS	3.34	2.40	-	-	<0.01
	NFKB2	2.76	0.93	1.14	-	<0.01
REGULATION OF ADAPTIVE IMMUNE RESPONSE	*IL1RL1*	1.26	2.65	-	-	<0.01
	HLA-B	1.17	0.56	-	-	<0.01
	HLA-A	0.79	0.53	-	-	<0.01

Table 4.1. Upregulated genes in ICD-responsive bladder cancer cells. Expression data of genes with cytokine activity depicted as log2FoldChange (logFC) expression (MMC vs NT comparison). Significant gene expression changes are shown (padj < 0.01).

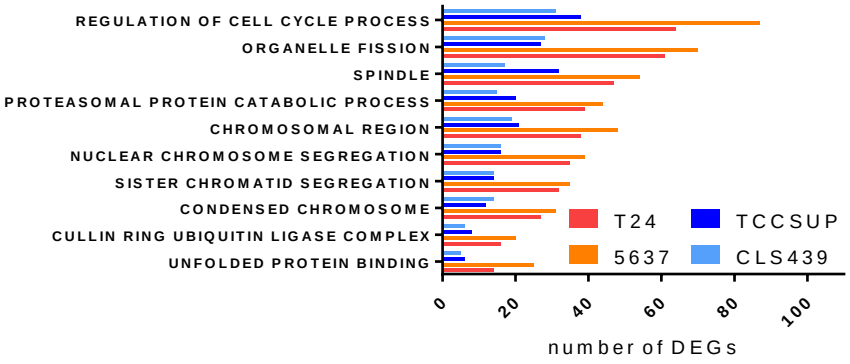

Figure 4.18. Downregulated gene sets in ICD-responsive bladder cancer cells. Barplot of significantly downregulated gene sets in bladder cancer cell lines after MMC treatment (GSEA analysis - FDR < 0.25). Bars represent the number of DEGs in each cell line.

Similarly to the expression of ICD markers, ICD-poorly responsive TCC-SUP cells showed a mild expression of some immune-related genes, but not to the same extent as ICD-responsive cells (Table. 4.1). Interestingly, the ICD-resistant CLS-439 cells did not upregulate the expression of inflammatory mediators or genes related to immune pathways (Table. 4.1) and showed fewer changes in gene expression upon MMC treatment compared to all the other cell lines (Fig. 4.19).

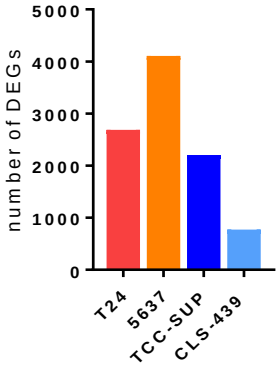

Figure 4.19. Overall changes in gene expression in bladder cancer cells. Number of DEGs upon MMC treatment in bladder cancer cells.

MMC induces ER-stress response

Since ER stress response is an early event necessary for ICD induction, I focused our attention on the activation of the UPR[59]. The UPR triggers three major pathways: (i) the activation of protein kinase RNA-like endoplasmic reticulum kinase (PERK) induces p-eIF2-α, which in turn suppresses global mRNA translation and favors apoptosis by increasing the translation of activating transcription factor (ATF) 4 that causes the upregulation of the proapoptotic proteins CCAAT-enhancer-binding protein homologous protein (CHOP) that transcribes p53-upregulated modulator of apoptosis (PUMA); (ii) the cleavage of ATF6, which leads to the transcription of genes required to restore ER homeostasis (for example, the molecular chaperone BiP); and (iii) the autophosphorylation of inositol-requiring kinase (IRE) 1-α (encoded by endoplasmic reticulum to nucleus signaling 1, ERN1), which leads to the splicing of XBP1 (to generate sXBP1), involved in ERAD, and the TNF receptor-associated factor 2 (TRAF2)-mediated

activation of Jun N-terminal kinases (JNK) and IkB kinase (IKK), involved in cell death induction and inflammation[79,80] (Fig. 4.20A).

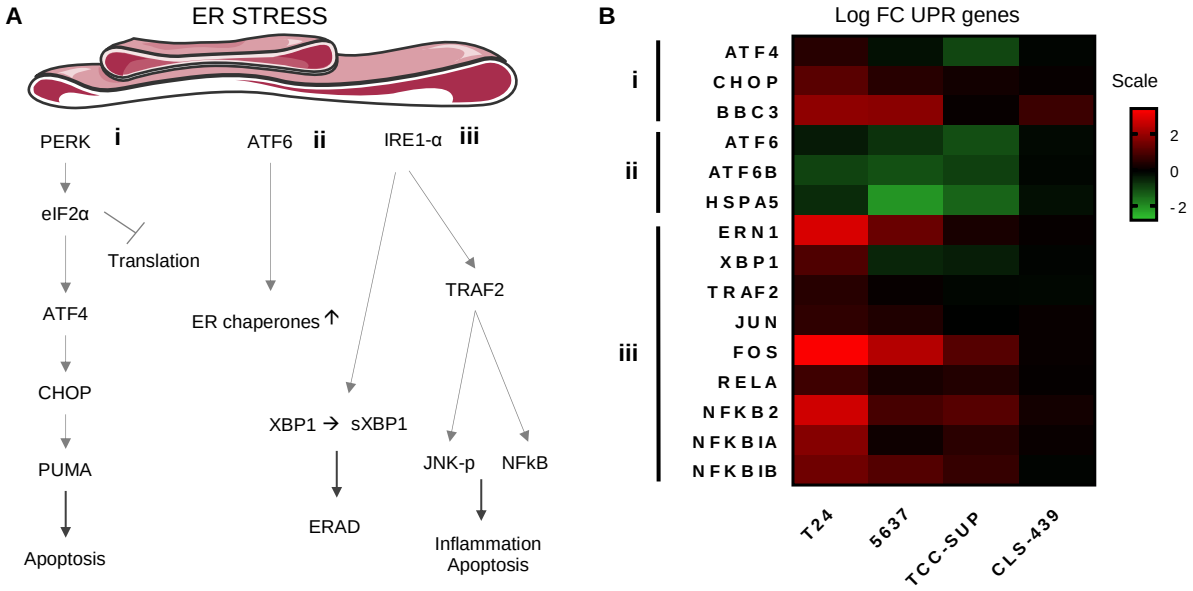

Figure 4.20. Analysis of the UPR pathways in bladder cancer cells treated with MMC. (A) Unfolded protein response pathways activated by endoplasmic reticulum (ER) stress. (B) Heatmap of genes involved in the UPR response showing fold-change expression (MMC vs NT) in T24, 5637, TCC-SUP, and CLS-439 cells.

RNA sequencing data revealed that upon MMC treatment ICD-responsive cells (T24, 5637) significantly upregulated the expression of *CHOP* and *BBC3*, which encodes PUMA (Fig. 4.20B). qPCR analysis of target genes confirmed that T24 and 5637 cells showed the highest levels of *CHOP* and *PUMA* in response to MMC treatment, but also the other cells lines upregulated the expression of these pro-apoptotic proteins, in line with observed cytotoxic activity of the drug, with the exception of HT-1376 cells (Fig. 4.21).

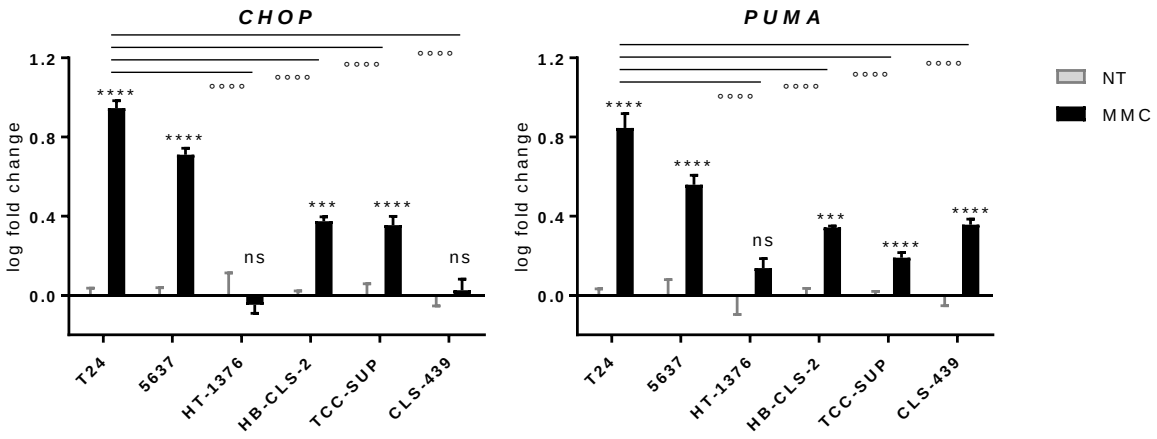

Figure 4.21. Expression of proapoptotic genes in bladder cancer cells treated with MMC. Quantification of *CHOP* and *BBC3* expression in MMC-treated cells. Data are mean ± s.d. and represent the pool of two independent experiments. * refers to unpaired two-tailed t-test comparing NT *vs* MMC cell lines independently. ° refers to one-way ANOVA using Bonferroni post test compared to T24. ***P<0.001, ****P<0.0001.

The UPR pathway initiated by ATF6 was attenuated in T24, 5637 and TCC-SUP cells, and not regulated in CLS-439 cells in response to MMC. Indeed, I observed decreased expression of *ATF6* and of heat-shock protein family A member 5 (*HSPA5*, which encodes BiP) in T24, 5637 and TCC-SUP cells, and no regulation of these genes in CLS-439 cells (Fig. 4.20B). Likely MMC-treated cells, independently from their ability to undergo ICD, do not try to adapt to cell damage by increasing the expression of ER chaperones to favor protein folding.

Interestingly, activation of the UPR arm initiated by IRE1-α was observed exclusively in ICD responsive cells (T24 and 5637), as detected by upregulated expression of *ERN1*, *c-JUN* and *c-FOS* subunits of AP-1 transcription factor, and p65 (*RELA* gene) and p50 (*NFKB1* gene) subunits of NFkB1 transcription factor (Fig. 4.20B). Moreover, IRE1-α activation upon MMC treatment favored the generation of sXBP1 in T24 and 5637 cells, as well as in HT-21376 and HB-CLS-2, but not in TCC-SUP and CLS-439 cells, as measured by qPCR (Fig. 4.22).

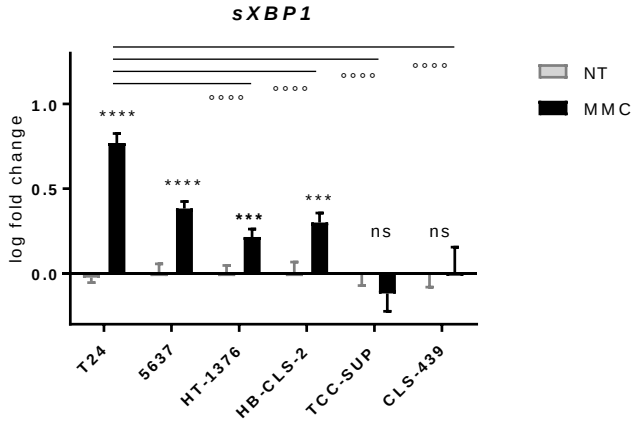

Figure 4.22. Expression of spliced XBP1 in bladder cancer cells treated with MMC. Quantification of spliced XBP1 expression in MMC-treated cells. Data are mean ± s.d. and represent the pool of two independent experiments. *refers to unpaired two-tailed t-test comparing NT *vs* MMC cell lines independently. °refers to one-way ANOVA using Bonferroni post test compared to T24. ***P<0.001, ****P<0.0001.

RNA sequencing data of bladder cancer cell lines revealed that MMC treatment triggers an ER stress signal that leads to apoptosis. ICD responsive cells highly upregulated the expression of genes involved in the UPR pathways initiated by PERK and IRE1-α, compared to ICD-poorly responsive or resistant cells.

ICD-responsive cells generate an immunogenic microenvironment through their inflammatory secretome

Proinflammatory cytokines released upon ICD induction orchestrate the activation of local and systemic immune responses[52]. Since response to cytokine was one of the biological processes related to MMC treatment in ICD responsive cells, I measured in the supernatant of treated and untreated cells the concentration of several cytokines and chemokines that are involved in the recruitment and activation of innate and adaptive immune cells. Our panel included the proinflammatory cytokines IL-1β, IL-1α, IL-6, IL-8, and TNF, interferons IFNα, IFNγ, and the anti-inflammatory cytokine IL-10. I found that only ICD-responsive T24 and 5637 cell lines secreted IL-1β, IL-6 and IL-8 upon treatment with MMC (Fig. 4.23). Concordantly, these cytokines were among the top

upregulated genes in RNA sequencing analysis (Table. 4.1). Also IL-1α and TNF were detected in the supernatant of treated ICD-responsive cells, but at different levels, suggesting that they might be involved in a cell-specific response to MMC (Fig. 4.23). On the contrary, IFNα, IFNγ and the anti-inflammatory IL-10 were either not detected or detected at low levels in the supernatants of all untreated or treated cells (Fig. 4.23).

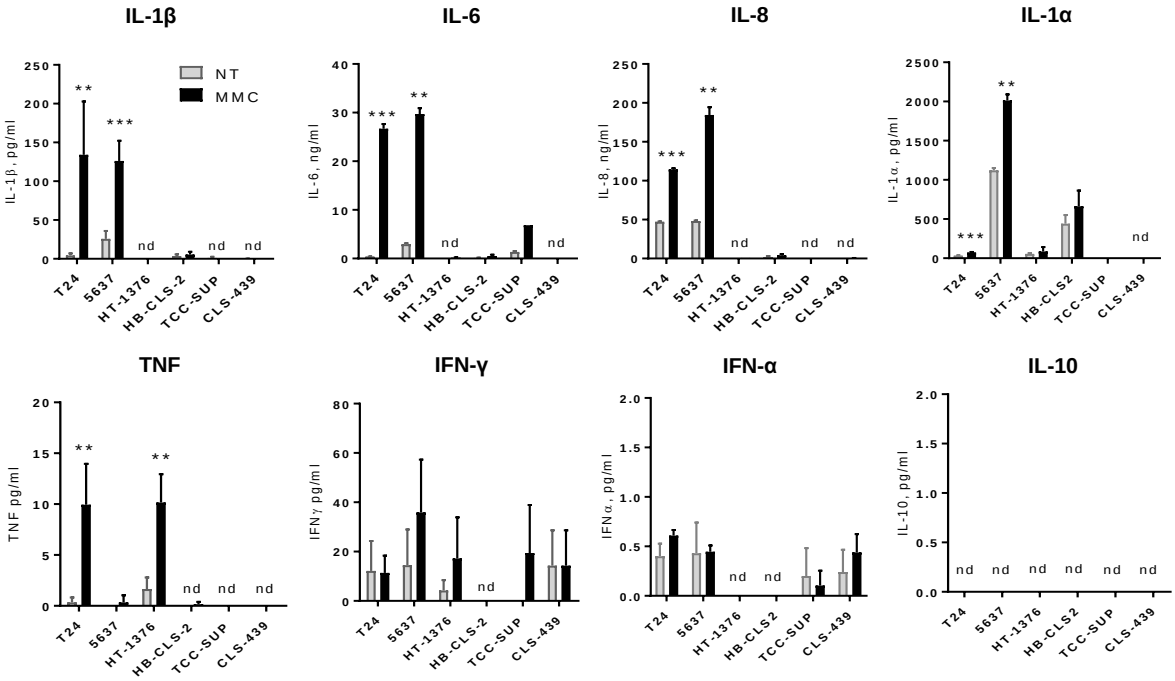

Figure 4.23. Cytokines secreted by bladder cancer cells treated with MMC. Cytokine quantification in the supernatants of MMC-treated and untreated (NT) bladder cancer cells, as assessed by cytometry bead assay. Data are mean ± s.d. of duplicates in representative experiment. nd stands for not detected. Unpaired two-tailed t-test comparing NT *vs* MMC cell lines independently. **P<0.01, ***P<0.001.

These data indicate that tumor cells that robustly undergo ICD upon MMC treatment are characterized by the generation of an inflammatory secretome, which favors an immunogenic microenvironment able to promote DC maturation, as seen in Fig. 4.13.

ICD-responsive cells secrete mtDNA upon MMC treatment to enable inflammasome activation

A crucial regulator of DC activation and T cell differentiation is IL-1β[81], which was among the genes that were significantly upregulated by MMC in ICD-responsive cells

(Table. 4.1). The maturation of IL-1β is tightly controlled by the inflammasome, a cytosolic complex whose assembly is initiated by engagement of the nucleotide binding domain and leucine-rich repeat pyrin domain containing 3 (NLRP3) pattern recognition receptor[82]. NLRP3 inflammasome triggers the self-cleavage and activation of caspase-1, converting pro-IL-1β to its mature form, which can be secreted[82]. Different stimuli, including pathogen- and danger-associated molecular patterns (PAMPs and DAMPs), can induce NLRP3 activation in APCs[82,83]. Mitochondrial DNA (mtDNA) has been described to be released by ROS-producing mitochondria into the cytosol, where it binds and activates the NLRP3 inflammasome[84,85]. Intrigued by the observation that the ICD-resistant CLS-439 cell line was found to be devoid of mtDNA-derived transcripts (Fig. 4.24A), I investigated whether MMC exposure in bladder cancer cells could induce cell damage leading to mtDNA release and mtDNA-mediated inflammasome activation. Firstly, I quantified total mtDNA in bladder cancer cell lines. All the analyzed cell lines had high mtDNA copy numbers except for the CLS-439 cell line that was totally devoid of mtDNA (Fig. 4.24B). Loss of the full mtDNA in CLS-439 cells was confirmed by the absence of PCR amplification of six overlapping products, representing the entire human mitochondrial genome (≈16.5 Kb) (Fig. 4.24C).

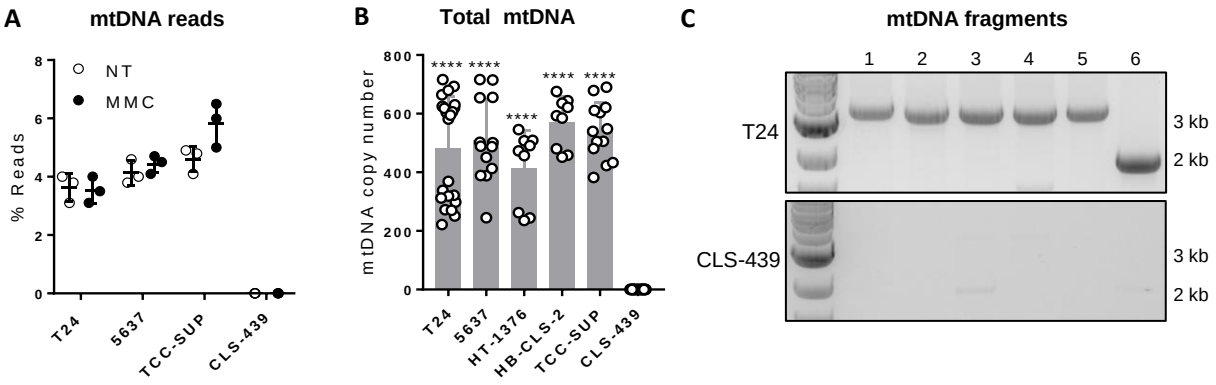

Figure 4.24. Quantification of mtDNA in bladder cancer cell lines. (A) Percentage of sequences corresponding to mtDNA reads found upon RNA sequencing of MMC treated and untreated cells. (B) Total mtDNA copy number in untreated bladder cancer cell lines as quantified by quantitative PCR (qPCR) with primers specific for the mitochondrial cytochrome c oxidase (CO) 1 gene and for nuclear 18S gene. Data are mean ± s.d. and represent the pool of two independent experiments. One-way ANOVA using Bonferroni post test compared to CLS-439. (C) PCR amplification of six mtDNA fragments, representing the entire human mtDNA, from total DNA isolated from untreated T24 or CLS-439 cells. ****P<0.0001.

Following MMC exposure, tumor cells experienced an accumulation of mitochondrial ROS (Fig. 4.25).

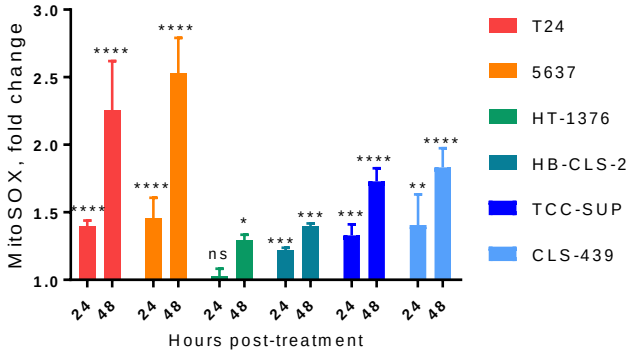

Figure 4.25. ROS quantification in bladder cancer cells treated with MMC. ROS accumulation quantified by MitoSOX staining in bladder cancer cells following MMC treatment. Data are mean ± s.d. and represent the pool of two independent experiments. Unpaired two-tailed *t*-test comparing NT *vs* MMC cell lines independently at different time points. *P<0.05, **P<0.01, ***P<0.001, ****P<0.0001.

Moreover, treatment with MMC resulted in increased mtDNA release in the cytosol of the ICD-responsive cells T24 and 5637, compared to HT-1376, HB-CLS-2, TCC-SUP and CLS-439 (Fig. 4.26A), and was accompanied by secretion of mature IL-1β (Fig. 4.26B).

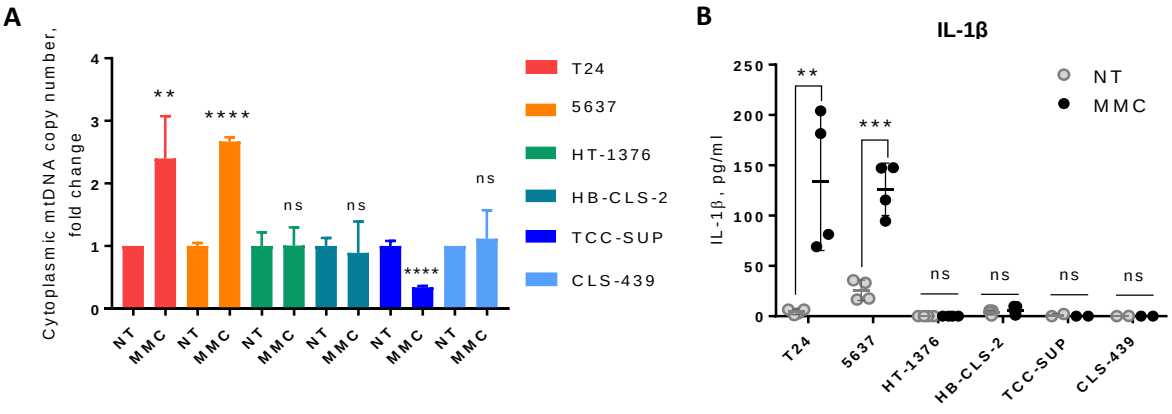

Figure 4.26. Cytoplasmic mtDNA triggers IL-1β secretion in bladder cancer cells treated with MMC. (A) Cytoplasmic mtDNA amounts in MMC-treated cells relative to NT cells. Data are mean ± s.d. and represent the pool of two to four independent experiments. Unpaired two-tailed *t*-test comparing NT *vs* MMC cell lines independently. (B) IL-1β concentration in culture supernatants of MMC-treated and untreated cells. Data are mean ± s.d. and represent the pool of two independent experiments. Unpaired two-tailed *t*-test comparing NT *vs* MMC cell lines independently.

MMC also increased the expression of *NLRP3* in ICD-responsive and poorly responsive cells, but not in ICD-resistant cells (Fig. 4.27A). Under oxidative stress, mtDNA can be released into the cytosol through the mitochondrial permeability transition pore (mPTP)[86,87], a non-specific channel that connects the inner and outer membrane of mitochondria[88]. Interestingly, upon MMC treatment, only ICD-responsive cells decreased the expression of hexokinase 2 (*HK2*) (Fig. 4.27B), a protein associated to the mitochondria outer membrane that is known to prevent mPTP opening[89].

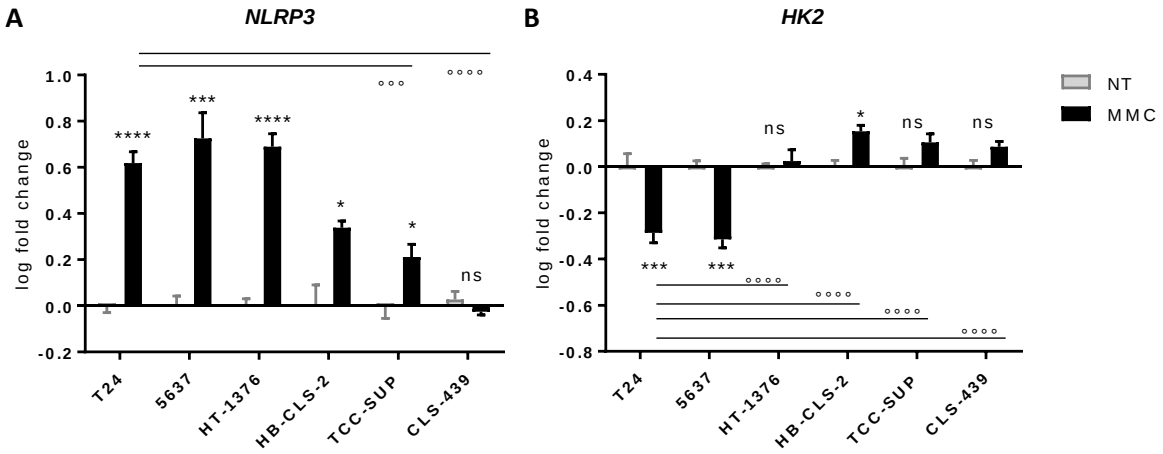

Figure 4.27. Expression of *NLRP3* and *HK2* in bladder cancer cells treated with MMC. (A) Quantification of *NLRP3* and (B) *HK2* expression in MMC-treated or untreated cells. Data are mean ± s.d. and represent the pool of two independent experiments. *refers to unpaired two-tailed *t*-test.comparing NT *vs* MMC cell lines independently. °refers to one-way ANOVA using Bonferroni post test compared to T24. *P<0.05, ***P<0.001, ****P<0.0001.

Hence, I have identified a sequence of events promoting MMC-induced ICD. Our data indicate that MMC induces a cell-damage response leading to mitochondrial ROS production and release of mtDNA in the cytosol, where it acts as an intracellular DAMP for efficient inflammasome activation and mature IL-1β production (Fig. 4.28). Failure of this process may lead to reduced inflammation and impaired DC maturation, as occurs following treatment of ICD poorly responsive and resistant cells.

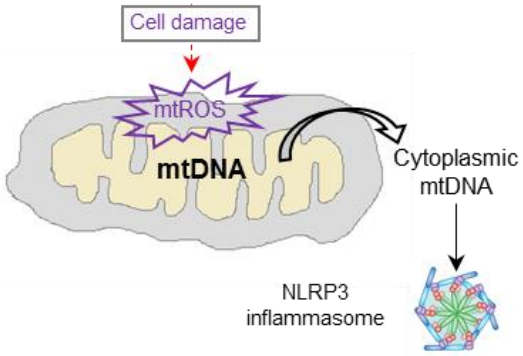

Figure 4.28. MMC favors the release of mtDNA to promote inflammasome activation. Working model to illustrate how MMC-mediated cell damage mediates mtDNA release from mitochondria and NLRP3 inflammasome activation.

ICD induction is impaired in mtDNA depleted cells

In order to confirm the key role of mtDNA in triggering inflammasome activation, I generated, starting from the ICD-responsive T24 cells, T24 mtDNA depleted cells (T24 ρ^0) by chronic treatment with low dose ethidium bromide (EtBr)[61] and tested the ability of these cells to secrete IL-1β and undergo ICD. Chronic treatment with EtBr-supplemented medium resulted in a dramatic reduction of mtDNA in T24 cells (Fig. 4.29A) and consequent absence of cytoplasmic mtDNA upon MMC treatment similarly to CLS-439 cells (Fig. 4.29B). Consistently, T24 ρ^0 cells, like CLS-439 cells, failed to secrete IL-1β upon MMC treatment (Fig. 4.29C).

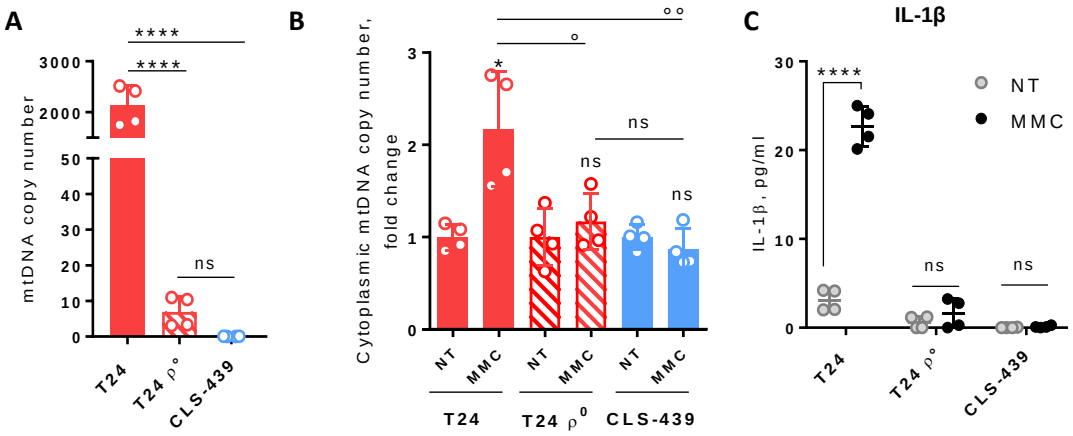

Figure 4.29. mtDNA-depleted cells fail to secrete IL-1β upon treatment with MMC. (A) Total mtDNA copy number in untreated T24, T24 mtDNA-depleted (ρ^0) and CLS-439 cells. Data are mean ± s.d. and represent the pool of two independent experiments. One-way ANOVA using Bonferroni post test. (B) Cytoplasmic mtDNA amounts upon MMC treatment relative to NT. Data are mean ± s.d. and represent the pool of two independent experiments. *refers to unpaired

two-tailed *t*-test comparing NT *vs* MMC cell lines independently. °refers to one-way ANOVA and Bonferroni post test. (C) Amounts of IL-1β in culture supernatants of MMC-treated and untreated cells. Data are mean ± s.d. and represent the pool of two independent experiments. Unpaired two-tailed *t*-test comparing NT *vs* MMC cell lines independently. *P<0.05, **P<0.01, ****P<0.0001.

Compared to T24 control cells, which upregulated *NLRP3* expression and downregulated *HK2* expression upon MMC treatment, the transcription of these genes was not affected in T24 ρ^0 cells, suggesting that inflammasome assembly did not occur and mPTP permeability was not perturbed (Fig. 4.30).

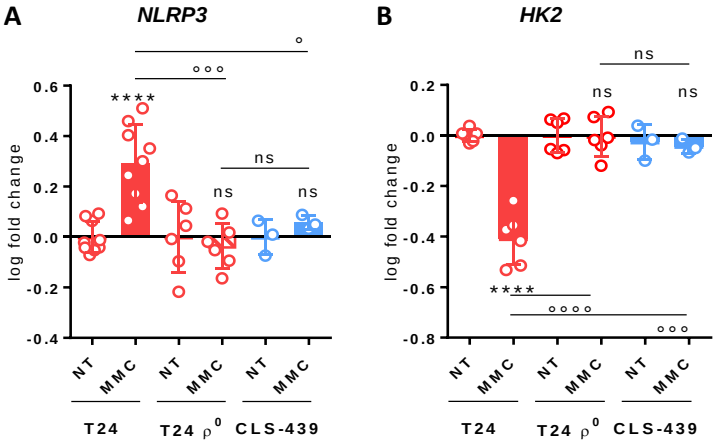

Figure 4.30. Regulation of *NLRP3* and *HK2* in mtDNA-depleted cells treated with MMC. (A) Quantification of *NLRP3* and (B) *HK2* expression. Data are mean ± s.d. and represent the pool of two independent experiments. *refers to unpaired two-tailed *t*-test comparing cell lines independently NT vs MMC. °refers to one-way ANOVA using Bonferroni post test. *P<0.05, ***P<0.001, ****P<0.0001.

The molecular changes triggered by mtDNA depletion in T24 ρ^0 cells also impaired the secretion of the proinflammatory cytokines IL-6 and IL-8, which instead characterized the response to MMC of ICD-proficient cells (Fig. 4.31).

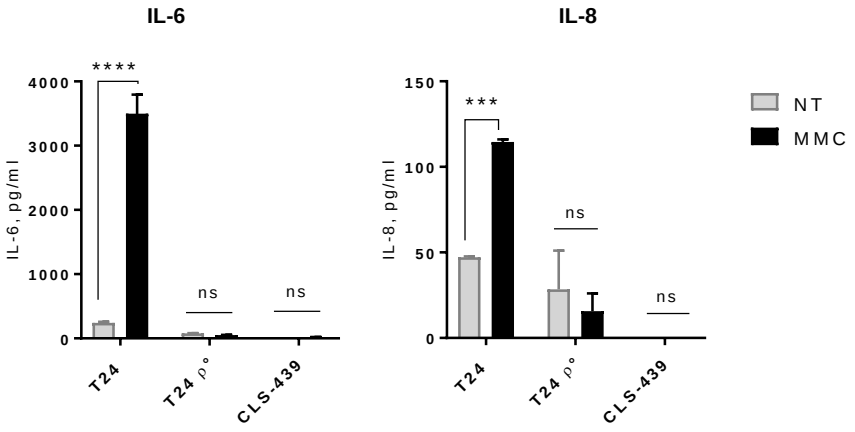

Figure 4.31. Cytokine secretion by mtDNA-depleted cells treated with MMC. Amounts of IL-6 and IL-8 in the supernatants of MMC-treated and untreated cells. Data are mean ± s.d. and represent the pool of two independent experiments. Unpaired two-tailed *t*-test comparing NT *vs* MMC cell lines independently. ***P<0.001, ****P<0.0001.

I next assessed whether mtDNA depletion, besides impairing inflammasome activation and cytokine release, could render ICD-responsive T24 cells resistant to MMC-induced ICD. MMC significantly induced HMGB1 secretion in T24 control cells, but not in mtDNA-depleted T24 ρ^0 cells similarly to CLS-439 cells (Fig. 4.32A). Additionally, treated T24 cells were readily engulfed upon co-culture with moDCs, whereas both T24 ρ^0 cells and CLS-439 cells were resistant to phagocytosis (Fig. 4.32B).

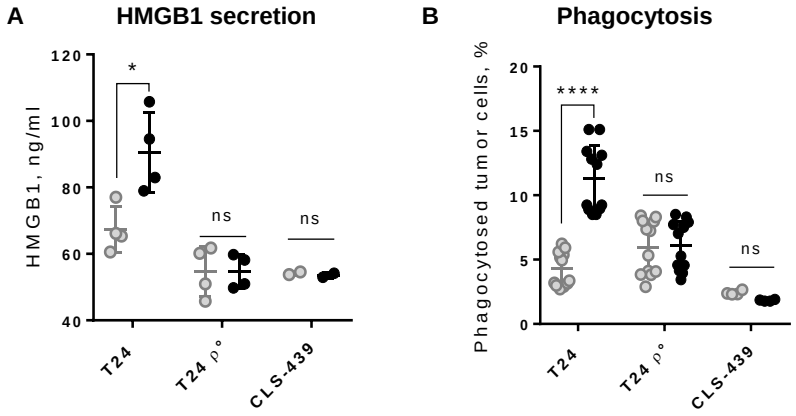

Figure 4.32. mtDNA-depleted cells do not secrete HMGB1 and are not phagocytosed upon treatment with MMC. (A) Amount of HMGB1 in culture supernatants of MMC-treated and untreated cells. Data are mean ± s.d. and represent the pool of two independent experiments. Unpaired two-tailed *t*-test comparing NT *vs* MMC cell lines independently. (B) Quantification of

phagocytosis of tumor cells exposed to MMC by moDCs, as measured by flow cytometry. Data are mean ± s.d. of six replicates in experiments using two different moDC donors. Unpaired two-tailed *t*-test comparing NT *vs* MMC cell lines independently. *P<0.05, ****P<0.0001.

Consistent with ICD induction, moDC maturation was significantly triggered by MMC-treated T24 control cells, but not by MMC-treated T24 ρ^0 cells or CLS-439 cells (Fig. 4.33). The slight increase of CD80 expression upon culturing in T24 ρ^0 supernatants is likely due to the presence of EtBr, as I observed CD80 expression also when DCs were cultured in media supplemented with EtBr.

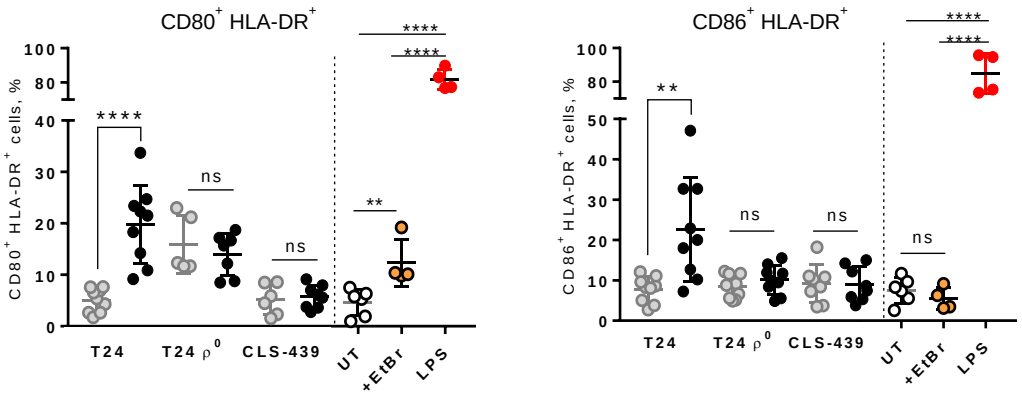

Figure 4.33. Dendritic cells activation in conditioned media of mtDNA-depleted cells. Quantification of $CD80^+$ $HLA\text{-}DR^+$ and $CD86^+$ $HLA\text{-}DR^+$ moDCs populations upon the different stimuli. UT=unstimulated moDCs (negative control). +EtBr= moDCs incubated in ρ^0 cells medium. LPS= moDCs incubated in LPS supplemented medium (positive control). Data are mean ± s.d. of three to four replicates in experiments using two different moDC donors. Unpaired two-tailed *t*-test comparing NT *vs* MMC cell lines independently or one-way Anova and Bonferroni post test to compare UT, +EtBr, and LPS. **P<0.01, ****P<0.0001.

In summary, these data suggest that the chemically-induced depletion of mtDNA induces a profound mitochondrial dysfunction that inhibits inflammasome activation and strongly suppresses ICD induction upon MMC treatment.

Low expression of mitochondrial Complex I is associated to reduced MMC-induced ICD in bladder cancer cells and tissues

I identified mitochondrial permeability upon MMC treatment to be a crucial event for mtDNA translocation into the cytosol and activation of the inflammasome. mPTP opening is regulated by oxidative stress, elevated matrix Ca^{2+}, adenine nucleotide

depletion, and drastic changes in pH[88]. Moreover, an increased probability of pore opening is observed when electron flux increases through mitochondrial Complex I of the respiratory chain. On the contrary, inhibition of Complex I with rotenone or metformin decreases mPTP opening in healthy and malignant cells, preventing cell death induction by Ca^{2+} overload or oxidative stress[90–93]. Several Complex I subunits are encoded by mtDNA, together with other components of complex III, IV and V of the oxidative phosphorylation (OXPHOS) (Fig. 4.34A). The nuclear genome encodes the additional structural and functional subunits of the respiratory chain[94].

Concordantly with mtDNA depletion, the ICD-resistant CLS-439 cell line did not express mitochondrial-transcribed genes compared to the ICD-responsive T24 cell line, (Fig. 4.34.B), suggesting that in these cells mitochondria homeostasis, including mPTP regulation, may be impaired.

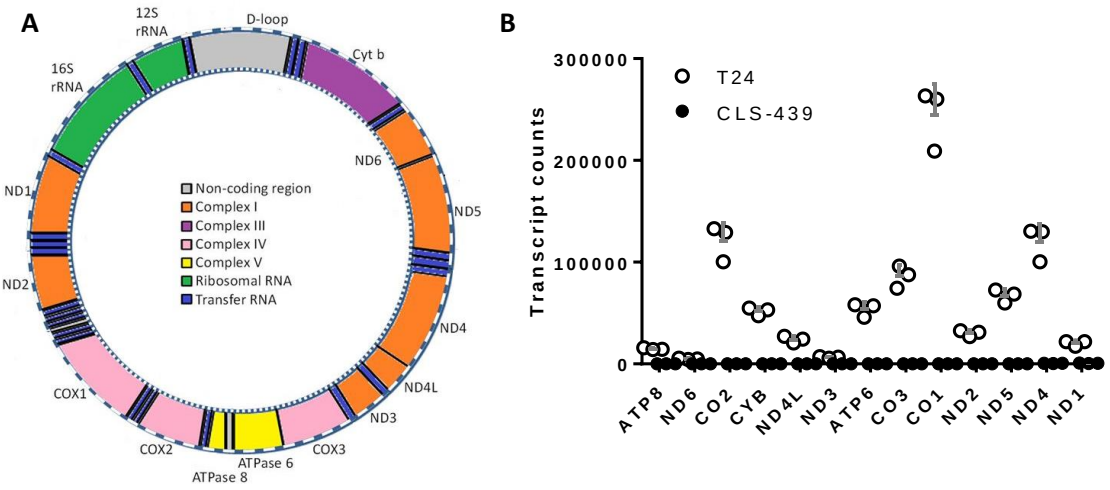

Figure 4.34. Expression of mitochondrial protein-coding genes in ICD-responsive and ICD-resistant cells. (A) The mtDNA encodes 37 genes, including 2 ribosomal and 22 transport RNAs required for protein synthesis. Mitochondrial encoded proteins constitute essential parts of the respiratory chain by contributing seven subunits to complex I (NADH dehydrogenase, ND), one subunit to complex III (cytochrome b, CYB), three subunits to complex IV (Cytochrome C Oxidase, COX), and two subunits to complex V (ATP synthase, ATP). The D-loop acts a non/coding promoter region (Adapted from Scientific Reports, Article number: 177; 2017). (B) Number of normalized counts of mtDNA transcribed protein-coding genes in untreated T24 and CLS-439 cells lines, as detected by RNA sequencing analysis. Data are mean ± s.d. of triplicates.

Since impaired mPTP opening was observed in ICD-poorly responsive and resistant cells, I wondered whether mitochondrial dysfunction related to low Complex I expression could be associated to the inability to undergo ICD in these cells. I analyzed by IHC the expression of Complex I (NADH dehydrogenase 1 beta subcomplex subunit 8, NDUFB8) and the mitochondrial mass, as determined by staining of the mitochondrial membrane (Translocase of Outer Mitochondrial Membrane 20, TOMM20) in bladder cancer cell lines. IHC analysis revealed that Complex I expression was heterogeneous among tumor cells. T24 and 5637 ICD-responsive cells showed high levels of Complex I, compared to HT-1376 and TCC-SUP cells that showed a milder expression. Lastly, very few HB-CLS-2 and CLS-439 cells expressed Complex I (Fig. 4.35A, B). Interestingly, mtDNA-depleted and ICD-resistant T24 ρ^0 cells lost NDUFB8 expression, compared to their ICD-responsive counterpart. I found that all tumor cells displayed similar mitochondrial mass, as detected by TOMM20 staining, also CLS-439 and T24 ρ^0 cells (Fig. 4.35A), suggesting that mtDNA depletion does not affect the number of mitochondria in the cell. Overall, decreased Complex I expression was found more frequently in ICD-non responsive or resistant cells, compared to ICD-responsive cells.

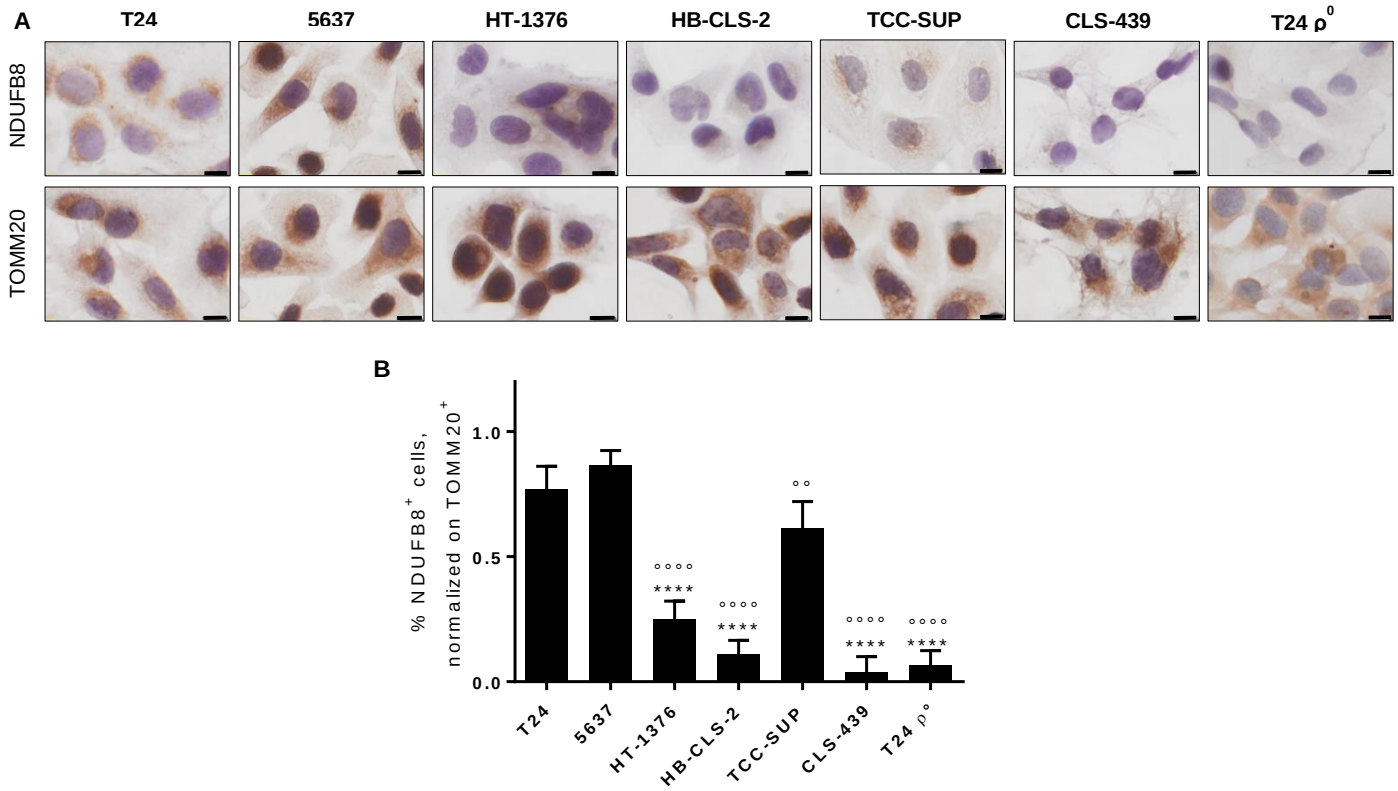

Figure 4.35. NDUF8 Complex I subunit and TOMM20 expression in bladder cancer cells. (A) IHC analysis of NDUFB8 subunit of mitochondrial Complex I and TOMM20 mitochondrial membrane protein expression in untreated bladder cancer cells. Scale bar, 10µm. (B) Percentage of NDUFB8$^+$ bladder cancer cells, normalized on TOMM20$^+$ cells, as detected by IHC analysis. Data are mean± s.d.. *refers to one-way ANOVA using Bonferroni post test compared to T24. °refers to one-way ANOVA using Bonferroni post test compared to 5637. **P<0.01, ****P<0.0001.

I then performed the same IHC analysis on bladder cancer cell lines T24 and CLS-439 using cytospin staining and quantification with Immunoratio plugin, in order to understand whether an automated method of quantitation could produce comparable values to the manual counting of DAB$^+$ cells and whether it could be used for scoring pathological specimens. Using Immunoratio plug in, I confirmed that there was a statistically significant decrease in the expression of NDUFB8 Complex I subunit in CLS-439 cells, compared to T24 cells, but a comparable mitochondrial mass between the two cell lines (Fig. 4.36), indicating that this automated method produced results that were comparable with the manual quantification method.

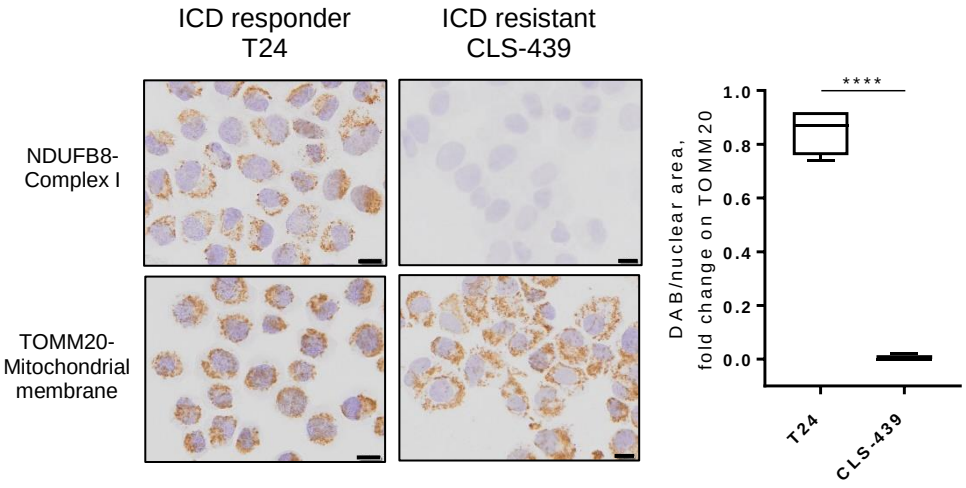

Figure 4.36. Quantification using Immunoratio of NDUF8 Complex I subunit. IHC analysis of NDUFB8 subunit of mitochondrial Complex I and TOMM20 mitochondrial membrane protein expression in T24 and CLS-439 bladder cancer cells. NDUFB8 staining was quantified using Immunoratio plug in and normalized on TOMM20 staining intensity. Scale bars, 10µm. Box plots show the interquartile range, median value and whiskers min to max. Unpaired two-tailed *t*-test. ****P<0.0001.

Next, I wondered whether differential expression of Complex I was associated with ICD sensibility in human bladder cancer specimens treated *ex-vivo* with MMC. From our cohort, I selected the 12 patients that were also treated in the clinic with MMC. Of these, 7 patients were considered more likely to respond to MMC by activation of ICD, based on the *ex-vivo* analysis of HMGB1 release that induced DC activation (HMGB1 high), and 5 patients were considered ICD-non responsive (HMGB1 low) (Table 3.4). The human healthy bladder mucosa was used as a positive control, since it expressed high levels of Complex I, indicating that in physiological conditions this protein is important for correct tissue homeostasis. Interestingly, I found that Complex I NDUFB8 expression was strongly reduced in HMGB1 low tumors compared to HMGB1 high, suggesting that mitochondrial dysfunction is associated with impaired ICD response in human bladder cancer (Fig. 4.37). Interestingly, one patient included in this analysis, whose tumor was classified as HMGB1 low and expressed low levels of Complex I, experienced recurrence 12 months after TURBT and MMC treatment.

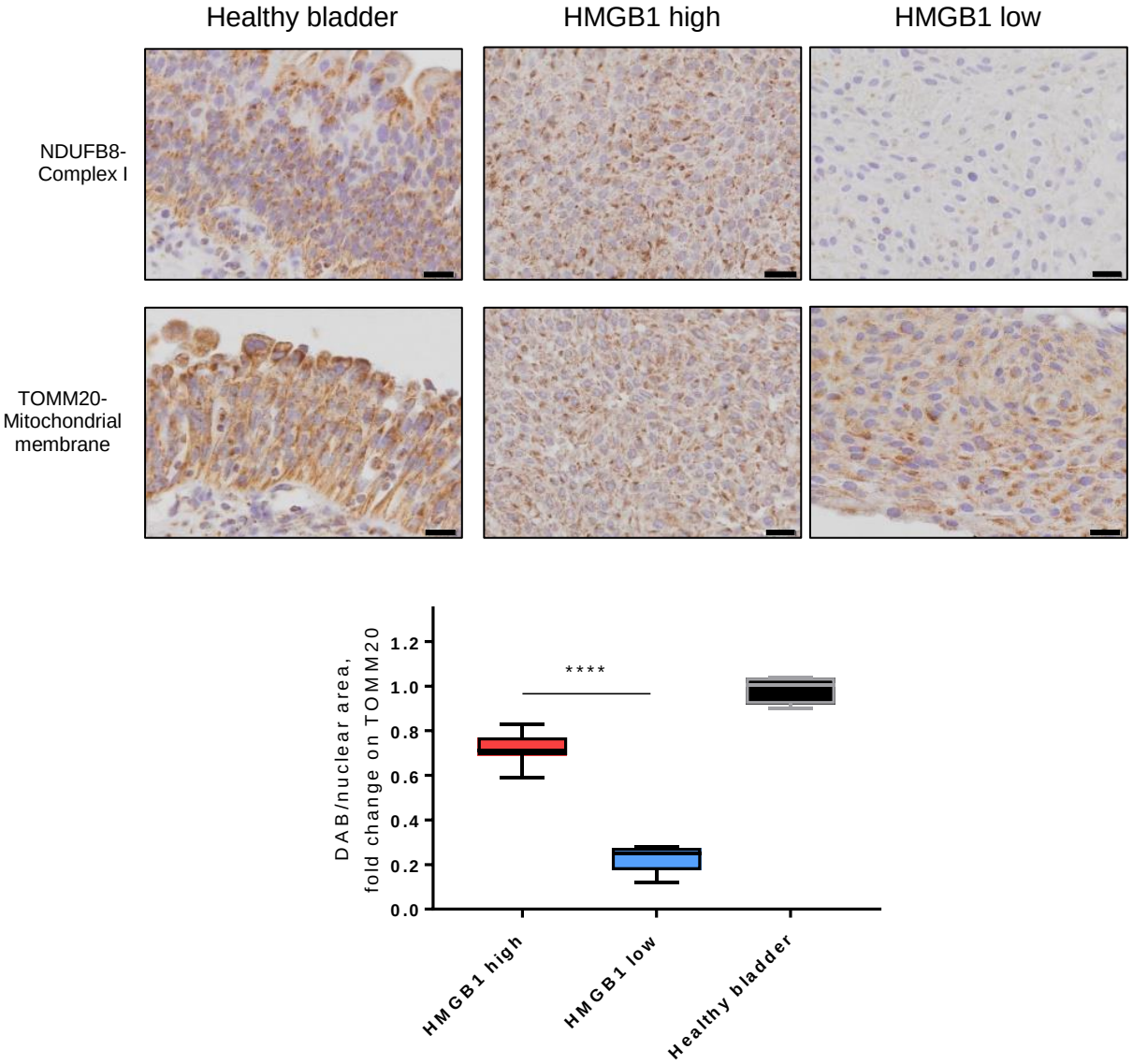

Figure 4.37. NDUF8 Complex I subunit and TOMM20 expression in the healthy bladder mucosa and tumor specimens. IHC analysis of NDUFB8 and TOMM20 expression in healthy urothelium and tumors of our cohort of patients that were treated in the clinic with MMC. Patients were classified as HMGB1 high (n=7) or HMGB1 low (n=5) based on the amount of HMGB1 secreted upon *ex-vivo* treatment with MMC. NDUFB8 staining was quantified using Immunoratio plug in and normalized on TOMM20 staining intensity. Scale bars, 20µm. Box plots show the interquartile range, median value and whiskers min to max. Unpaired two-tailed *t*-test. ****P<0.0001.

Low expression of Complex I characterizes NMIBC prone to recurrence

Since only one patient included in our study experienced recurrence up to now, I investigated in a retrospective analysis whether mitochondrial dysfunction is associated with recurrence after MMC treatment in bladder cancer. I selected patients that experienced recurrence after MMC adjuvant treatment, which I considered MMC non-

responders, and patients that did not experienced recurrence after MMC, which I considered responders (Table 3.5). Similar to the healthy bladder mucosa, Complex I was expressed in the majority of the tumors of MMC-responder patients (Fig. 4.38). On the contrary, Complex I was poorly expressed in the primary tumors of MMC non-responders patients and in the recurrences following treatment (Fig. 4.38). The expression levels of Complex I were comparable in matched primary tumors and recurrences. However, in the recurrences I observed a reduction of the variability in Complex I expression compared to primary tumors, which in general displayed a more heterogeneous staining.

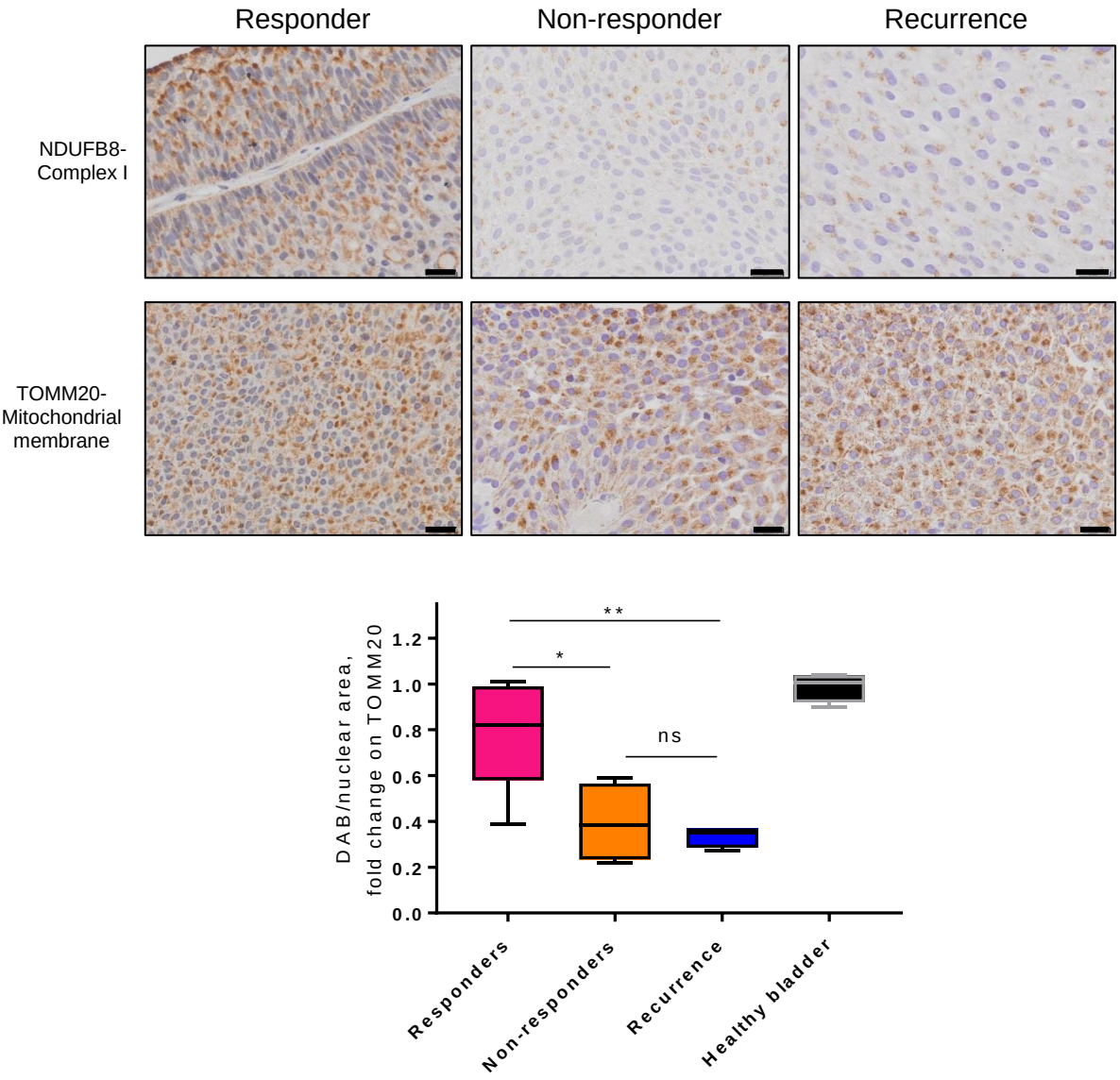

Figure 4.38. NDUF8 Complex I subunit and TOMM20 expression in primary tumors and recurrences of responding patients and relapsing patients. IHC analysis of NDUFB8 and TOMM20 expression in tumor specimens from patients that remained tumor-free after MMC (responders, n=5) and patients that experienced recurrence after MMC (non-responders and

recurrence, n=4 matched). NDUFB8 staining was quantified using Immunoratio plug in and normalized on TOMM20 staining intensity. Scale bars, 20µm. Box plots show the interquartile range, median value and whiskers min to max *P<0.05, **P<0.01.

Interestingly, patients that I defined HMGB1 high in our cohort and MMC-responder patients in the retrospective analysis expressed comparable amounts of Complex I (Fig. 4.39). Instead, a comparable reduction of Complex I expression, indicating mitochondrial dysfunction, was observed in HMGB1 low as well as MMC-non responder patients (Fig. 4.39). These data suggest that MMC-induced ICD may dependent on mitochondria functionality and that the expression levels of Complex I, as well as HMGB1 secretion following *ex-vivo* treatment, may be predictors of treatment efficacy.

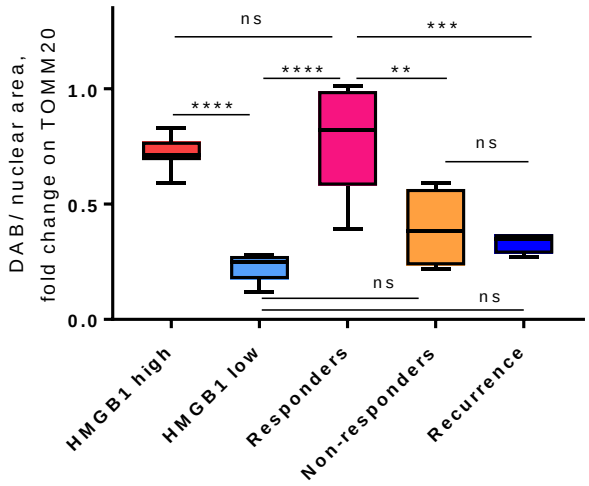

Figure 4.39. NDUF8 Complex I subunit across the different patient's groups. NDUFB8 quantification normalized on TOMM20 staining intensity across the different groups of samples. Box plots show the interquartile range, median value and whiskers min to max. One way ANOVA and Bonferroni post-test. **P<0.01, ***P<0.001, ****P<0.0001.

Mitochondrial dysfunction characterizes bladder tumors with a poor prognosis

Recent data highlighted a critical role of mitochondrial Complex I in the progression of other tumors of the urinary tract. In renal oncocytoma mtDNA mutations leading to loss of Complex I of the respiratory chain were found to be an early driving event of tumor formation[95]. In chromophobe renal cell carcinoma loss-of-function mutations in Complex I were found to be essential in the disease biology and low tumor mtDNA content was

associated with poor survival[96]. Genomic alterations in mtDNA have been reported also in prostate cancer and appear to work together with nuclear mutations to drive tumor aggressiveness[97]. In particular, lower Complex I expression was shown to correlate with increased prostate cancer risk features and poor overall survival[98].

To understand whether mitochondrial dysfunction could define bladder tumors with a worst prognosis, I investigated the expression of several genes related to mitochondrial functions, like OXPHOS, tricarboxylic acid cycle (TCA) cycle, mtDNA transcription and maintenance, in publicly available datasets including both NMIBC and MIBC patients[74–76]. I found that decreased expression of several mitochondria-related transcripts correlated with reduced overall survival (Table 4.2A) and tumor progression from NMIBC to MIBC (Table 4.2B). Many of these downregulated genes were subunits of Complex I (e.g. NDUFB8, NDUFB10, NDUFAF1, NDUFS1, NDUFB3), suggesting that, beyond response to MMC, defects in this structure may characterize aggressive bladder tumors with a poor prognosis.

Interestingly, also low expression of DNA Polymerase Gamma (*POLG*), the polymerase which is responsible for the replication of the entire mitochondrial genome, was associated with reduced overall survival and progression, suggesting that reduced mtDNA content in tumor cells may characterize a subset of bladder cancers with a poor prognosis.

A

Gene	p value	Function
NDUFAF1	1.30E-06	Complex I assembly
NDUFAF2	3.30E-03	Complex I assembly
NDUFS1	2.40E-05	Complex I iron protein fraction
NDUFB3	7.60E-06	Complex I subcomplex
NDUFB5	6.60E-07	Complex I subcomplex
NDUFB8	1.10E-02	Complex I subcomplex
NDUFA1	1.00E-03	Complex I subcomplex
NDUFA10	8.50E-09	Complex I subcomplex
BCS1L	3.20E-05	Complex III assembly
UQCRC2	2.10E-07	Complex III
LRPPRC	1.70E-03	Complex IV assembly
COX4I1	1.40E-05	Complex IV
ATP5A1	3.10E-03	Complex V ATPase activity
POLG	8.00E-03	Polymerase (mtDNA directed), gamma
HSPD1	1.60E-04	Mitochondrial chaperone
SPG7	5.00E-05	Mitochondrial chaperone
ABAT	4.10E-08	Alanine aspartate and glutamate metabolism
SDHD	5.80E-06	TCA cycle

B

Gene	p value	Function
NDUFB8	5.20E-06	Complex I subcomplex
NDUFB10	7.20E-06	Complex I subcomplex
NDUFS4	4.30E-06	Complex I subcomplex
NDUFAF1	1.80E-05	Complex I assembly
NDUFAF2	3.60E-03	Complex I assembly
NDUFS1	5.30E-04	Complex I iron protein fraction
NDUFB3	1.10E-04	Complex I subcomplex
NDUFB5	1.80E-03	Complex I subcomplex
NDUFA1	1.60E-03	Complex I subcomplex
COX5B	6.30E-06	Cytochrome c oxidase subunit
COX7C	2.70E-06	Cytochrome c oxidase subunit
POLG	6.50E-06	Polymerase (mtDNA directed), gamma
TFAM	6.90E-05	Mitochondrial transcription factor A
ATP5G2	7.70E-07	Complex V ATP synthase subunit
TCIRG1	1.80E-06	Complex V ATP synthase subunit
SDHD	2.10E-03	Succinate dehydrogenase subunit

Table 4.2. Low expression of mitochondria-related genes correlating with poor prognosis in bladder cancer. List of genes related to mitochondrial function whose low expression correlates with decreased overall survival in the bladder cancer Hoglund cohort (n=308) (A) and with decreased progression-free survival in the bladder cancer Dyrskjot cohort (n=476) (B).

MMC treatment induces the expression of immune checkpoint molecules

The advent of immune checkpoint inhibitors in the clinic revolutionized cancer treatment. Immune checkpoint inhibitors are being tested in clinical trials for the treatments of aggressive MIBC, as well as recurrent NMIBC. Since I found that MMC treatment can exert immunostimulatory activities, I wondered whether it could also affect the expression of immune checkpoint molecules on the surface of cancer cells. I found that the majority of treated cells increased the membrane expression of Programmed cell Death ligand 1 (PD-L1) (Fig. 4.40), suggesting that tumor cells activate mechanisms to elude antitumor cytotoxic lymphocytes in response to MMC. However, the upregulation of such molecules may sensitize tumors to treatment with anti-PD-L1 and anti-Programmed cell Death protein 1 (PD1) checkpoint inhibitors. Interestingly, CLS-439

cell line did not show expression of PD-L1 at baseline, or after MMC treatment. It is tempting to speculate that these cells do not need to activate such immune evasion mechanism, given their ability to resist MMC-induced ICD.

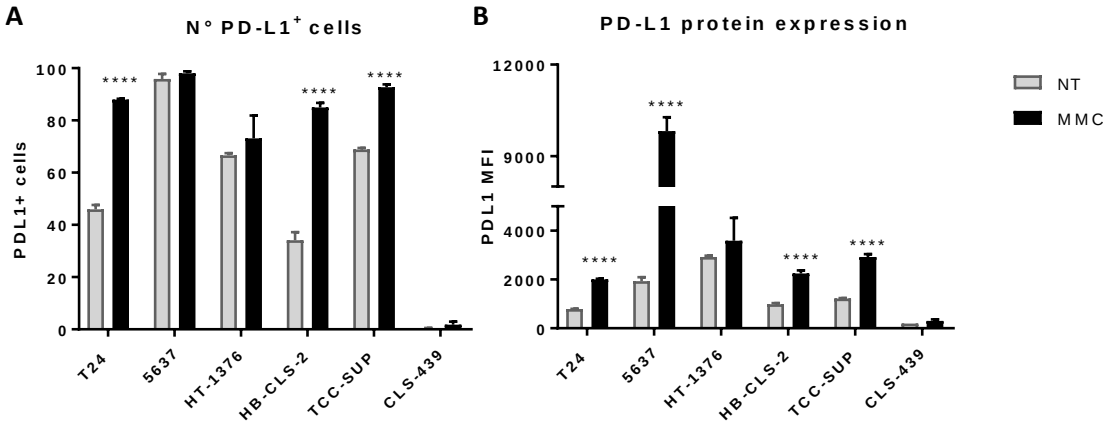

Figure 4.40. Immune checkpoint molecules expression upon MMC treatment. Percentage of PD-L1^{+} cells (A) and Mean Fluorescence Intensity (MFI) (B) of untreated cells (NT) and treated with MMC as detected by flow cytometry. Unpaired two-tailed *t*-test comparing NT *vs* MMC cell lines independently. ****P<0.0001.

5. Discussion

Nearly three-quarters of all newly diagnosed urothelial cancers are NMIBCs. Intravesical chemotherapy following surgery has been shown to reduce the rate of NMIBC recurrence, and MMC has become the most commonly used intravesical cytotoxic agent. Nevertheless, a large proportion of NMIBCs still recur[18].

Conventional chemotherapeutics have been developed and implemented in the clinic based on their ability to limit cancer cell proliferation and cause their death. However, it is becoming clear that many of these drugs mediate therapeutic effects also by eliciting tumor-specific immune responses[99]. Understanding the exact mechanisms of action of anticancer agents is important to identify key pathways underlying drug sensitivity/resistance and may also reveal markers of responsiveness to therapy that could be used for patient's stratification.

In this work, I provide evidence that MMC triggers anti-tumor immune responses via ICD induction. I demonstrated that MMC-induced ICD is critically dependent on the secretion of DAMPs and inflammatory cytokines by dying tumor cells, and that drug efficacy is impaired by mitochondrial dysfunction, as detected by low expression of Complex I. These data give insight into the mechanism of action of MMC and provide a rationale for introducing markers of ICD response in the clinic to guide treatment decision for bladder cancer patients.

MMC has previously been considered unable to induce ICD[34,37,42]. However, MMC immunogenicity has always been tested, both *in vitro* and *ex vivo*, following long continuous treatment of murine CT26 (colon), TC-1 (B cell lymphoma) or MCA205 (sarcoma) cell lines[34,37,42]. Therefore, we decided to assess whether a shorter treatment, which resembles the one used for bladder cancer intravesical therapy, could induce ICD *in vivo*, adopting the same mouse model in which MMC was proved not to induce tumor protection[34,42]. Here, we show that the ability of MMC to induce protective immunity

depends on the capacity of the adopted treatment to progressively elicit specific *premortem* ICD responses. Using the CT26 syngeneic model in mice, which provides an effective approach for studying how cancer therapies perform in the presence of a functional immune system, we showed that immunization with MMC-short treated CT26 cells (MMC 1h) protected mice from tumor development in a prophylactic vaccination regimen and delayed tumor growth in a therapeutic vaccination regimen. Conversely, mice vaccinated with MMC-long treated CT26 cells (MMC 48h) developed fast growing tumors, concurrently with unvaccinated mice. Vaccination with tumor cells treated for 1 hour with MMC was sufficient to trigger a potent immune response, mediated by antitumor T cells and antibodies, and stimulated long term memory responsiveness. Importantly, the ability of MMC-treated cells to induce a strong immune response was observed without adding an external adjuvant, suggesting that DAMPs expressed by MMC-treated tumor cells are sufficient to recruit immune cells *in vivo* and orchestrate antigen-specific immune responses. We showed that compared to a short treatment with MMC, which progressively induced cell death, a long treatment induces extensive cell death, resulting in few intact cells and mostly debris. We suggest that such material is not sufficient to trigger an anti-tumor immune response upon inoculation into mice and that intact dying cells are required for optimal ICD induction. Despite the fact that cell death has been shown not to correlate with the ability of a drug to induce ICD[42], cell integrity has been suggested as a crucial determinant for efficient immunostimulation[34]. Indeed, it has been reported that killing of tumor cells by freeze-thaw cycles, which result in disruption of the cells into fragments, fails to induce tumor protection in mice, even when tumor cells are pre-treated with an ICD inducer, like doxorubicin, meaning that disruption of membrane integrity is sufficient to abolish their immunogenic properties[34]. Similarly, the remaining tumor cells after 48 h of treatment with MMC were not sufficient to trigger anti-tumor immunity. Therefore, it appears that, beyond the selection of specific anticancer agents, also the particular protocol of apoptosis induction determines the

immunogenicity of cell death. It will be important to understand whether shortening the treatment length of other anticancer drugs that are now considered non-ICD inducers could facilitate the display of ICD signals and reveal their immunogenic potential.

Short treatment with MMC, similar to the one that is performed for intravesical chemotherapy instillation in NMIBC, triggered ICD of bladder cancer cells, as measured by increased CLRT translocation and HMGB1 secretion, which enabled the phagocytosis of dying tumor cells by DCs upon co-culture. However, we observed variability in ICD induction, with some tumor cell lines showing upon treatment a greater increase in DAMPs expression and phagocytosis compared to others. Consistently, we found that only tumor cells that displayed ICD markers could trigger DC maturation, as measured by increased expression of the costimulatory molecules CD80 and CD86 on DCs upon culture in conditioned medium of MMC-treated tumor cells. In order to understand whether the observations we made on *in vitro* were true also in urinary bladder cancer patients, we performed a clinical study in which ICD was assessed upon *ex vivo* treatment with MMC on bladder neoplastic tissues. In this setting we found that HMGB1 secretion, associated with increased DC maturation, was observed also in a proportion of treated tumor tissues. Importantly, consistent with the inability of MMC to always prevent tumor recurrence in patients, we observed variability among bladder cancer cell lines and tissues in the predisposition to undergo ICD.

In order to categorize the propensity of bladder cancer cell lines to undergo MMC-induced ICD we developed a scoring system based on the evaluation of the analyzed parameters: the induction of ICD-related DAMPs (CLRT translocation at the plasma membrane and HMGB1 secretion), predisposition to phagocytosis and ability to favor DC maturation. This approach allowed to us to distinguish between ICD-responsive cells, which robustly undergo ICD upon MMC treatment, and ICD-poorly responsive or

resistant cells, which less potently undergo ICD and may be resistant to MMC treatment. The degree of immunogenicity displayed by bladder cancer cells fluctuates to a significant extent, probably as a result of genetic predisposition and activation of alternative signaling pathways, reflecting the elevated heterogeneity that is observed even across cancers of the same type. These analyzed parameters appear to be sufficient to make accurate predictions about the susceptibility to MMC-induced ICD of a specific cell line. Considering that human cancer cell sensibility to ICD cannot be directly investigated in *in vivo* vaccination assays owing to cross-species-specific immunological incompatibility, *in vitro* scoring of multiple ICD parameters may be used in research settings to partially circumvent this obstacle and determine the likelihood of a drug to trigger ICD.

Next, we sought to characterize the transcriptional changes occurring upon MMC treatment. We performed RNAseq analysis of untreated and MMC-treated bladder cancer cells characterized by different degrees of sensitivity to ICD, as determined by scoring of *in vitro* analysis. We found that in response to MMC, tumor cells activated UPR processes responsible for cell fate decision. In particular, we observed upregulation of the UPR pathway that leads to ATF-4 activation and transcription of the proapoptotic mediators CHOP and PUMA. In response to MMC, ICD-responsive cells also showed increased activation of the UPR pathway initiated by IRE1-α, as we saw increased levels of *ERN1* expression (the gene coding for IRE1-α) in these cell lines. IRE1-α promoted the splicing of XBP1, a transcriptional regulator of ERAD pathway, and the activation of proinflammatory circuits initiated by AP-1 and NFkB transcription factors. In CRC cells, upregulation of sXBP1 was associated with cell adaptation and resistance to Cetuximab-induced ICD and was favored by the constitutive activation of ERK pathway in *BRAF* mutated cells[35]. However, sXBP1 expression did not correlate with ICD resistance in bladder cancer cell lines. On the contrary, the ICD-responsive cells T24 and 5637 showed

increased sXBP1 expression compared to ICD resistant cells, despite not being mutated in *BRAF* or *KRAS* genes. We suggest that in these tumor cells sXBP1-mediated adaptation to cell damage may be counteracted by the strong activation of proapoptotic proteins CHOP and PUMA, which favor cell death.

In addition to increased UPR activation in response to ER stress, ICD-responsive cells were characterized by the upregulation of genes related to apoptosis and immune system functions. In particular, the ICD signature included genes belonging to processes like cytokine-mediated signaling, regulation of innate and adaptive responses, inflammation and cytoplasmic DNA sensing. The observation that MMC increased the transcription of cytokine-related genes prompted us to investigate which secreted factors, together with HMGB1 alarmin, were crucial for DC maturation upon culture *in vitro*. We found that after MMC treatment the proinflammatory cytokines IL-6, IL-8 and IL-1β were secreted by ICD-responsive tumor cells, but not by ICD-poorly responsive or resistant cells. These data suggest that, before induction of apoptosis, MMC treatment of ICD-responsive cells triggers ER stress, display of DAMPs, and an inflammatory gene network, which promotes the production of proinflammatory cytokines. Overall, these processes result in the establishment of an immunogenic microenvironment that favors the recruitment of innate immune cells, the uptake of dying tumor cells and the activation of DCs for efficient priming of adaptive immunity. On the contrary, consistent with their inability to trigger DC maturation, ICD-poorly responsive and resistant cells did not express immune-related genes, and failed to release inflammatory cytokines upon MMC treatment compared to ICD-responsive cells.

Mature IL-1β, a critical regulator of the inflammatory response, is produced via inflammasome-mediated cleavage of pro-IL-1β, a process that is initiated by the interaction of PAMPs and DAMPs with the NLRP3 PRR[82]. In the context of ICD, we elucidated a crucial role of mtDNA as inflammasome activator. Upon MMC-induced damage and increased mitochondria permeability, mtDNA translocated into the

cytoplasm of ICD-responsive cells to induce inflammasome activation and secretion of mature IL-1β. Failure of this process, as seen in ICD-non responsive cells, blunted DC activation and may result in impaired ICD induction and unresponsiveness to MMC.

ATP has been described as the main trigger of inflammasome activation in APCs following ICD induced by mitoxantrone and oxaliplatin[100]. However, ATP secretion was not detected upon MMC treatment of bladder cancer cell (data not shown), but tumor cells themselves activated the inflammasome to secrete IL-1β, which is normally produced only by immune cells[52]. We suggest that ATP secretion might be dispensable for immune activation during MMC-induced ICD, which is instead supported by tumor cell-mediated IL-1β production.

Cytoplasmic mtDNA has been shown to also induce type I IFN production via cGAS/stimulator of interferon genes (STING) in the context of antiviral responses and caspases-independent cell death of tumor cells[101,102]. However, the presence of cytoplasmic mtDNA did not result in the activation of this pathway in MMC-treated cells, as we did not observed increased expression of IFN α/β transcripts by RNA sequencing analysis, nor secretion of IFN-α protein in the supernatants. We speculate that inhibition of this specific cytoplasmic DNA-sensing mechanism could be mediated by MMC-dependent activation of apoptotic caspases, which have been previously shown to suppress mtDNA-induced STING[34,103,104].

Loss of mtDNA, spontaneously occurring in the ICD-resistant cell line CLS-439 and experimentally induced in ICD-responsive T24 cells by EtBr treatment, was sufficient to impair mtDNA-mediated inflammasome activation and to abolish MMC-induced ICD. Indeed, compared to their ICD-proficient counterpart, MMC-treated T24 ρ^0 cells, did not secrete HMGB1 nor inflammatory cytokines, were not phagocytosed by DCs, and their death did not induce DC maturation. The mechanism by which mtDNA depletion impairs not only IL-1β secretion, but also ICD, remains elusive. Data in the literature indicate that

HMGB1 release can be dependent on inflammasome activation[105]. Indeed, caspase-1 and its upstream activators were required for secretion of HMGB1 in a mouse model of endotoxemia[105]. Apart from the crucial role of mtDNA in the activation of the inflammasome, we suggest that mtDNA depletion or genetic mutations that result in defects in mitochondria-related mechanisms can impair signaling pathways required for death-associated DAMP release and activation of anticancer immune responses.

Complete depletion of mtDNA is not a frequent characteristic of bladder tumors, but low mtDNA content and mtDNA mutations have been reported[106–109], suggesting that consequent impairment of mitochondria–related function could play an important role in carcinogenesis and response to treatment. We found that low expression of several proteins involved in mitochondrial functions correlate with a worst prognosis in bladder cancer patients. Of interest, several components of NADH dehydrogenase Complex I of the respiratory chain were associated with reduced overall survival in a cohort including both NMIBC and MIBC patients, and with progression from Ta/T1 stages to T2. Moreover, we found that decreased expression of Complex I NDUFB8 subunit associated with resistance to MMC-induced ICD in bladder cancer cell lines and patients, suggesting that ICD is impaired by mitochondrial dysfunction related to Complex I and that the propensity of tumor cells to undergo ICD is associated with response to MMC treatment and protection from tumor recurrence.

Respiratory chain complex I is a large protein complex composed of 45 subunits transcribed by both mtDNA and nuclear DNA genes. It includes an hydrophobic part embedded in the inner mitochondrial membrane, involved in proton transfer, and a hydrophilic part protruding into the matrix, in which electrons pass from NADH to ubiquinone via a succession of redox reactions[110]. Increased electron flux through Complex I has been shown to regulate mPTP opening[111]. Despite mPTP structure and regulations are still not completely understood, it is known that mPTP is normally closed

in order to maintain a high membrane potential required for OXPHOS. Once permanently opened, the membrane potential collapses, leading to a drastic inhibition of ATP synthesis and release of mitochondrial internal content[112]. Beyond this uncoupling effect, in physiological conditions mPTP opening allows the thermodynamic equilibrium of the mitochondrial and cytosolic redox potentials, leading to an increase in cytosolic NAD(P)H concentration[113], and it partially reallocates the electron flux for the production of ROS[114]. We found that mitochondria permeability is a critical determinant of MMC-induced ICD, since it allows mtDNA transfer into the cytosol for efficient inflammasome activation. We speculate that Complex I expression may influence MMC-induced ICD by regulating mitochondrial permeability. Low Complex I expression in MMC-resistant tumors may impair mPTP opening upon treatment, preventing mtDNA translocation into the cytoplasm and inflammasome activation. Failure of this process may lead to a reduction in the release of proinflammatory cytokines, resulting in ICD failure and drug resistance.

Complex I absence may not only impair mPTP, but also comprise deep changes in tumor metabolism and the activation of alternative signaling pathways that promote immune evasion and resistance to treatments that would otherwise trigger ICD. A crosstalk between altered mitochondrial processes in tumor cells and shaping of an immune-resistant tumor microenvironment has been suggested in some cancers. For example, reduced OXPHOS has been shown to drive M2-like polarization of tumor-associated macrophages in pre-clinical models of melanoma, colon and lung cancer[115]. Recently, proteomics of melanoma tumors showed that response to immunotherapies (anti-PD1 and adoptive T cell transfer) is associated with increased mitochondrial metabolism, including TCA cycle and OXPHOS. Functionally, mitochondrial metabolism, and in particular OXPHOS inhibition, was responsible for decreased MHCI and PD-L1 expression in tumor cells[116].

Our findings allow for a reinterpretation of several pre-clinical and clinical reports in the context of bladder cancer treatment. For example, augmented MMC efficacy, in terms of lower recurrence rates, and increased infiltration of immune cells in the tumor bed, has been reported upon combination of MMC with other bladder cancer treatments, such as BCG instillations[117–120] or radiotherapy[121]. In light of our findings, we can speculate that the reported outcomes could have been mediated by an additive effect in combination therapies that unleashed potent antitumor immune responses. Reduced recurrence rates have also been observed when MMC is instilled before TURBT as neoadjuvant treatment, compared to post-TURBT as adjuvant treatment (38% recurrence rate pre-TURBT *vs* 59% post-TURBT)[122], suggesting that in the neoadjuvant setting, the increased number of tumor cells undergoing ICD may boost the activation of anti-cancer immune responses and reach long term treatment success. Indeed, we suggest that the adjuvant regimen currently adopted in the clinic, as well as in this study, is not a favorable setting to assess the efficacy of MMC-mediated ICD induction, since the quality of the TURBT performed by the individual surgeons may cover the antitumor activity of MMC[123]. However, based on the *in vitro* ICD test and the lower expression of Complex I in tumor specimens, we could predict recurrence in at least one of the 'expected' non responders. The short follow up (2 to 15 months) of this study and the low number of enrolled patients that effectively underwent MMC treatment did not permit statistical power to confirm that ICD induction is indeed predictive of MMC efficacy. However, the retrospective analysis of MMC treated responders or non-responders patients confirmed that mitochondrial dysfunction, and particularly low expression of Complex I NDUFB8 subunit of the respiratory chain, is a potent biomarker of MMC efficacy. We therefore speculate that harnessing MMC immunogenic potential before surgery may be a more successful approach to bladder cancer treatment in general, because it may target all tumor clones, characterized by an heterogeneous expression of mitochondrial Complex I, as revealed by our study, and by different levels of antigenicity. Beyond bladder cancer, the effects of MMC on the

immune microenvironment have been shown to extend to other tumor types. In models of rectal cancer, MMC was found to suppress tumor growth by increasing the recruitment of cytotoxic T cells and NK cells into the tumor and reducing infiltration of regulatory T cells[124]. Moreover, MMC favored an immune-active tumor microenvironment in models of oropharyngeal carcinomas and cervical cancer[125,126].

In summary, we have identified ICD induction as a new mechanism of action of MMC that may be a critical determinant of therapeutic efficacy in bladder cancer. At the moment, bladder cancer management is based only on histological staging. We suggest that the identification of ICD-related biomarkers of treatment efficacy could improve personalized approaches to NMIBC therapy and patient's stratification. In particular, our data indicate that mitochondrial Complex I expression within the tumor may be a potential tool to predict responses to MMC. Moreover, our findings may prompt a modification of the dose, time of administration of the drug, and they may provide a rationale for combining MMC with other immunostimulatory agents. For example, MMC treatment in ICD-responsive NMIBC, as well as MIBC, expressing mitochondrial Complex I, may convert immunologically cold tumors into hot tumors to sensitize to immune checkpoint blockade. Extensive clinical research is on-going to test the efficacy of immune checkpoint inhibitors in bladder cancer, since these tumors are predicted to be highly immunogenic given the high mutational burden that increases the number of TTA and neoantigens[38]. Indeed, anti-PD1 and anti-PD-L1 have been associated with longer overall survival[127–129], but low PD-L1 expression on tumor cells has been associated with severe adverse events[130]. Based on our data, pre-treatment with intravesical MMC, which induces ICD and the upregulation of PD-L1 on tumor cells, may be safely combined with anti-PD-L1 treatment, increasing the likelihood to trigger *de novo* or pre-existing antitumor immune responses in patients. On the contrary, for ICD-poorly responsive and ICD-resistant tumors, where MMC effects are limited, a more aggressive treatment, such as intravesical BCG, may be preferred. By adopting new efficacious treatment options, it

may be possible to reach clinical efficacy and reduce recurrences in a higher proportion of urinary bladder cancer patients.

6. Bibliography

1. Siegel, R. L. & Miller, et al. Cancer Statistics, 2018. *Ca Cancer J Clin* **68,** 7–30 (2018).
2. Moch, H., Cubilla, A. L., Humphrey, P. A., Reuter, V. E. & Ulbright, T. M. The 2016 WHO Classification of Tumours of the Urinary System and Male Genital Organs—Part A: Renal, Penile, and Testicular Tumours. *Eur. Urol.* **70,** 93–105 (2016).
3. Bray F., Ferlay J., Soerjomataram I., Siegel R.L., Torre L.A., J. A. Global Cancer Statistics 2018: GLof Incidence and Mortality World in 185 Countries. *CA Cancer J ClinAnticancer Res.* **68,** 394–424 (2018).
4. Burger, M. *et al.* Epidemiology and risk factors of urothelial bladder cancer. *European Urology* **63,** 234–241 (2013).
5. Freedman, N. D., Silverman, D. T., Hollenbeck, A. R., Schatzkin, A. & Abnet, C. C. Association between smoking and risk of bladder cancer among men and women. *JAMA - J. Am. Med. Assoc.* **306,** 737–745 (2011).
6. Colt, J. S. *et al.* A case-control study of occupational exposure to metalworking fluids and bladder cancer risk among men. *Occup. Environ. Med.* **71,** 667–674 (2014).
7. Pesch, B. *et al.* Screening for bladder cancer with urinary tumor markers in chemical workers with exposure to aromatic amines. *Int. Arch. Occup. Environ. Health* **87,** 715–724 (2014).
8. Gouda, I., Mokhtar, N., Bilal, D., El-Bolkainy, T. & El-Bolkainy, N. M. Bilharziasis and bladder cancer: a time trend analysis of 9843 patients. *J. Egypt. Natl. Canc. Inst.* **19,** 158–162 (2007).
9. Pelucchi, C., Bosetti, C., Negri, E., Malvezzi, M. & La Vecchia, C. Mechanisms of disease: The epidemiology of bladder cancer. *Nature Clinical Practice Urology* **3,** 327–340 (2006).

10. Chrouser, K., Leibovich, B., Bergstralh, E., Zincke, H. & Blute, M. Bladder cancer risk following primary and adjuvant external beam radiation for prostate cancer. *J. Urol.* **174,** 107–110 (2005).

11. Ferlay, J., Steliarova-foucher, E., Lortet-tieulent, J. & Rosso, S. Cancer incidence and mortality patterns in Europe : Estimates for 40 countries in 2012. *Eur. J. Cancer* **49,** 1374–1403 (2013).

12. Dietrich, K. *et al.* Parity, early menopause and the incidence of bladder cancer in women: A case-control study and meta-analysis. *Eur. J. Cancer* **47,** 592–599 (2011).

13. Martin, C. *et al.* Familial Cancer Clustering in Urothelial Cancer: A Population-Based Case-Control Study. *J. Natl. Cancer Inst.* **110,** 527–533 (2018).

14. Figueroa, J. D. *et al.* Genome-wide association study identifies multiple loci associated with bladder cancer risk. *Hum. Mol. Genet.* **23,** (2014).

15. Estimated numbers of new cancer cases for 2017, excluding basal cell and squamous cell skin cancers and in situ carcinomas except urinary bladder.

16. Jimenez, R. E. *et al.* Grading the invasive component of urothelial carcinoma of the bladder and its relationship with progression-free survival. *Am. J. Surg. Pathol.* **24,** 980–987 (2000).

17. Stein, J. P. & Skinner, D. G. Radical cystectomy for invasive bladder cancer: Long-term results of a standard procedure. *World J. Urol.* **24,** 296–304 (2006).

18. Sylvester, R. J. *et al.* Predicting Recurrence and Progression in Individual Patients with Stage Ta T1 Bladder Cancer Using EORTC Risk Tables: A Combined Analysis of 2596 Patients from Seven EORTC Trials. doi:10.1016/j.eururo.2005.12.031

19. Sylvester, R. J. *et al.* Systematic Review and Individual Patient Data Meta-analysis of Randomized Trials Comparing a Single Immediate Instillation of Chemotherapy after Transurethral Resection with Transurethral Resection Alone

in Patients with Stage pTa-pT1 Urothelial Carcinoma. *Eur. Urol.* **69,** 231–244 (2016).

20. Shelley, M. D. *et al.* Intravesical bacillus Calmette-Guérin is superior to mitomycin C in reducing tumour recurrence in high-risk superficial bladder cancer: A meta-analysis of randomized trials. *BJU Int.* **93,** 485–490 (2004).
21. Kawai, K., Miyazaki, J., Joraku, A., Nishiyama, H. & Akaza, H. Bacillus Calmette-Guerin (BCG) immunotherapy for bladder cancer: Current understanding and perspectives on engineered BCG vaccine. *Cancer Science* **104,** 22–27 (2013).
22. Tomasz, M. Mitomycin C: small, fast and deadly (but very selective). *Chem. Biol.* **2,** 575–579 (1995).
23. Lee, Y. J., Park, S. J., Ciccone, S. L. M., Kim, C. R. & Lee, S. H. An in vivo analysis of MMC-induced DNA damage and its repair. *Carcinogenesis* **27,** 446–453 (2006).
24. Huncharek, M., McGarry, R. & Kupelnick, B. Impact of intravesical chemotherapy on recurrence rate of recurrent superficial transitional cell carcinoma of the bladder: Results of a meta-analysis. *Anticancer Res.* **21,** 765–769 (2001).
25. Burger, M. *et al.* ICUD-EAU International Consultation on Bladder Cancer 2012: Non–Muscle-Invasive Urothelial Carcinoma of the Bladder. **6,** 6–4
26. Sylvester, R. J., Oosterlinck, W. & Van Der Meijden, A. P. M. A single immediate postoperative instillation of chemotherapy decreases the risk of recurrence in patients with stage Ta T1 bladder cancer: A meta-analysis of published results of randomized clinical trials. *J. Urol.* **171,** 2186–2190 (2004).
27. Perlis, N. *et al.* Immediate post-transurethral resection of bladder tumor intravesical chemotherapy prevents non-muscle-invasive bladder cancer recurrences: An updated meta-analysis on 2548 patients and quality-of-evidence

review. *European Urology* **64,** 421–430 (2013).

28. Abern, M. R., Owusu, R. A., Anderson, M. R., Rampersaud, E. N. & Inman, B. A. Perioperative intravesical chemotherapy in non-muscle-invasive bladder cancer: A systematic review and meta-analysis. *JNCCN Journal of the National Comprehensive Cancer Network* **11,** 477–484 (2013).
29. Sylvester, R. J., Oosterlinck, W. & Witjes, J. A. The Schedule and Duration of Intravesical Chemotherapy in Patients with Non-Muscle-Invasive Bladder Cancer: A Systematic Review of the Published Results of Randomized Clinical Trials. *European Urology* **53,** 709–719 (2008).
30. Zargar, H., Aning, J., Ischia, J., So, A. & Black, P. Optimizing intravesical mitomycin C therapy in non-muscle-invasive bladder cancer. *Nat. Rev. Urol.* **11,** 220–230 (2014).
31. Green, D. R., Ferguson, T., Zitvogel, L. & Kroemer, G. Immunogenic and tolerogenic cell death. *Nature Reviews Immunology* **9,** 353–363 (2009).
32. Galluzzi, L., Buqué, A., Kepp, O., Zitvogel, L. & Kroemer, G. Immunogenic cell death in cancer and infectious disease. *Nature Reviews Immunology* **17,** 97–111 (2017).
33. Tesniere, A. *et al.* Immunogenic death of colon cancer cells treated with oxaliplatin. *Oncogene* **29,** 482–491 (2010).
34. Casares, N. *et al.* Caspase-dependent immunogenicity of doxorubicin-induced tumor cell death. *J. Exp. Med.* **202,** 1691–1701 (2005).
35. Pozzi, C. *et al.* The EGFR-specific antibody cetuximab combined with chemotherapy triggers immunogenic cell death. *Nat. Med.* **22,** 624–631 (2016).
36. Kleinovink, J. W. *et al.* Combination of photodynamic therapy and specific immunotherapy efficiently eradicates established tumors. *Clin. Cancer Res.* **22,** 1459–1468 (2016).
37. Liu, P. *et al.* Crizotinib-induced immunogenic cell death in non-small cell lung

cancer. *Nat. Commun.* **10,** (2019).

38. Schumacher, T. N. & Schreiber, R. D. Neoantigens in cancer immunotherapy. *Science (80-.).* **348,** 69–74 (2015).

39. Ghafouri-Fard, S. & Modarressi, M. H. Cancer-testis antigens: Potential targets for cancer immunotherapy. *Archives of Iranian Medicine* **12,** 395–404 (2009).

40. Fuchs, Y. & Steller, H. Live to die another way: Modes of programmed cell death and the signals emanating from dying cells. *Nature Reviews Molecular Cell Biology* **16,** 329–344 (2015).

41. Kroemer, G., Galluzzi, L., Kepp, O. & Zitvogel, L. Immunogenic Cell Death in Cancer Therapy. *Annu. Rev. Immunol.* **31,** 51–72 (2013).

42. Obeid, M. *et al.* Calreticulin exposure dictates the immunogenicity of cancer cell death. *Nat. Med.* **13,** 54–61 (2007).

43. Kepp, O. *et al.* eIF2α phosphorylation as a biomarker of immunogenic cell death. *Semin. Cancer Biol.* **33,** 86–92 (2015).

44. Gardai, S. J. *et al.* Cell-surface calreticulin initiates clearance of viable or apoptotic cells through trans-activation of LRP on the phagocyte. *Cell* **123,** 321–334 (2005).

45. Pawaria, S. & Binder, R. J. CD91-dependent programming of T-helper cell responses following heat shock protein immunization. *Nat. Commun.* **2,** (2011).

46. Li, M. O., Sarkisian, M. R., Mehal, W. Z., Rakic, P. & Flavell, R. A. Phosphatidylserine Receptor Is Required for Clearance of Apoptotic Cells. *Science (80-.).* **302,** 1560–1563 (2003).

47. Scaffidi, P., Misteli, T. & Bianchi, M. E. Release of chromatin protein HMGB1 by necrotic cells triggers inflammation. *Nature* **418,** 191–195 (2002).

48. Wang, H. *et al.* HMG-1 as a late mediator of endotoxin lethality in mice. *Science (80-.).* **285,** 248–251 (1999).

49. Apetoh, L. *et al.* Toll-like receptor 4-dependent contribution of the immune

system to anticancer chemotherapy and radiotherapy. *Nat. Med.* **13,** 1050–1059 (2007).

50. Apetoh, L. *et al.* Toll-like receptor 4–dependent contribution of the immune system to anticancer chemotherapy and radiotherapy. *Nat. Med.* **13,** 1050–1059 (2007).

51. Fang, H. *et al.* TLR4 is essential for dendritic cell activation and anti-tumor T-cell response enhancement by DAMPs released from chemically stressed cancer cells. *Cell. Mol. Immunol.* **11,** 150–159 (2014).

52. Showalter, A. *et al.* Cytokines in immunogenic cell death: Applications for cancer immunotherapy. *Cytokine* **97,** 123–132 (2017).

53. Michaud, M. *et al.* Autophagy-dependent anticancer immune responses induced by chemotherapeutic agents in mice. *Science (80-.).* **334,** 1573–1577 (2011).

54. Karmakar, M., Katsnelson, M. A., Dubyak, G. R. & Pearlman, E. Neutrophil P2X7 receptors mediate NLRP3 inflammasome-dependent IL-1β secretion in response to ATP. *Nat. Commun.* **7,** (2016).

55. Chen, D. S. & Mellman, I. Oncology meets immunology: The cancer-immunity cycle. *Immunity* **39,** 1–10 (2013).

56. Fucikova, J. *et al.* Calreticulin expression in human non-small cell lung cancers correlates with increased accumulation of antitumor immune cells and favorable prognosis. *Cancer Res.* **76,** 1746–1756 (2016).

57. Yamazaki, T. *et al.* Defective immunogenic cell death of HMGB1-deficient tumors: Compensatory therapy with TLR4 agonists. *Cell Death Differ.* **21,** 69–78 (2014).

58. Stebbing, J. *et al.* The common heat shock protein receptor CD91 is up-regulated on monocytes of advanced melanoma slow progressors. *Clin. Exp. Immunol.* **138,** 312–316 (2004).

59. Rufo, N., Garg, A. D. & Agostinis, P. The Unfolded Protein Response in

Immunogenic Cell Death and Cancer Immunotherapy. *Trends in Cancer* **3,** 643–658 (2017).

60. Hanahan, D. *et al.* Hallmarks of Cancer: The Next Generation. *Cell* **144,** 646–674 (2011).

61. Hashiguchi, K. & Zhang-Akiyama, Q. M. Establishment of human cell lines lacking mitochondrial DNA. *Methods Mol. Biol.* **554,** 383–391 (2009).

62. Rimoldi, M. *et al.* Monocyte-derived dendritic cells activated by bacteria or by bacteria-stimulated epithelial cells are functionally different. *Blood* **106,** 2818–2826 (2005).

63. Winzler, C., Rovere, P. & Rescigno…, M. Maturation stages of mouse dendritic cells in growth factor–dependent long-term cultures. *J. Exp. Med.* (1997).

64. Dobin, A. *et al.* STAR: Ultrafast universal RNA-seq aligner. *Bioinformatics* **29,** 15–21 (2013).

65. Hartley, S. W. & Mullikin, J. C. QoRTs: A comprehensive toolset for quality control and data processing of RNA-Seq experiments. *BMC Bioinformatics* **16,** (2015).

66. Liao, Y., Smyth, G. K. & Shi, W. FeatureCounts: An efficient general purpose program for assigning sequence reads to genomic features. *Bioinformatics* **30,** 923–930 (2014).

67. Love, M. I., Huber, W. & Anders, S. Moderated estimation of fold change and dispersion for RNA-seq data with DESeq2. *Genome Biol.* **15,** 550 (2014).

68. Subramanian, A. *et al.* Gene set enrichment analysis : A knowledge-based approach for interpreting genome-wide. *Proc Natl Acad Sci U S A* **102,** 15545–50 (2005).

69. Janes, M. S. *et al.* Rapid analysis of mitochondrial DNA depletion by fluorescence in situ hybridization and immunocytochemistry: Potential strategies for HIV therapeutic monitoring. *J. Histochem. Cytochem.* **52,** 1011–1018 (2004).

70. Bronner, D. & O'Riordan, M. Measurement of Mitochondrial DNA Release in Response to ER Stress. *BIO-PROTOCOL* **6,** (2016).

71. Hurle, R. *et al.* "En Bloc" Resection of Nonmuscle Invasive Bladder Cancer: A Prospective Single-center Study. *Urology* **90,** 126–130 (2016).

72. Humphrey, P. A., Moch, H., Cubilla, A. L., Ulbright, T. M. & Reuter, V. E. The 2016 WHO Classification of Tumours of the Urinary System and Male Genital Organs—Part B: Prostate and Bladder Tumours. *Eur. Urol.* **70,** 106–119 (2016).

73. Tsilingiri, K. *et al.* Probiotic and postbiotic activity in health and disease: comparison on a novel polarised ex-vivo organ culture model. *Gut* **61,** 1007–1015 (2012).

74. R2 database. Genomic Analysis and Visualization Platform. *The Department of Human Genetics in the Amsterdam Medical Centre (AMC)* (2019). Available at: http://hgserver1.amc.nl.cgi-bin/r2/main.cgi.

75. Sjödahl, G. *et al.* A molecular taxonomy for urothelial carcinoma. *Clin. Cancer Res.* **18,** 3377–3386 (2012).

76. Hedegaard, J. *et al.* Comprehensive Transcriptional Analysis of Early-Stage Urothelial Carcinoma. *Cancer Cell* **30,** 27–42 (2016).

77. Castle, J. C. *et al.* Immunomic, genomic and transcriptomic characterization of CT26 colorectal carcinoma. *BMC Genomics* **15,** (2014).

78. Obeid, M. ERP57 Membrane Translocation Dictates the Immunogenicity of Tumor Cell Death by Controlling the Membrane Translocation of Calreticulin. *J. Immunol.* **181,** 2533–2543 (2008).

79. Kato, H. & Nishitoh, H. Stress responses from the endoplasmic reticulum in cancer. *Frontiers in Oncology* **5,** (2015).

80. Zhang, K. & Kaufman, R. J. From endoplasmic-reticulum stress to the inflammatory response. *Nature* **454,** 455–462 (2008).

81. Ben-Sasson, S. Z. *et al.* IL-1 acts directly on CD4 T cells to enhance their

antigen-driven expansion and differentiation. *Proc. Natl. Acad. Sci.* **106,** 7119–7124 (2009).

82. Gross, O., Thomas, C. J., Guarda, G. & Tschopp, J. The inflammasome: An integrated view. *Immunol. Rev.* **243,** 136–151 (2011).

83. Zhong, Z., Sanchez-Lopez, E. & Karin, M. Autophagy, Inflammation, and Immunity: A Troika Governing Cancer and Its Treatment. *Cell* **166,** 288–298 (2016).

84. Shimada, K. *et al.* Oxidized mitochondrial DNA activates the NLRP3 inflammasome during apoptosis. *Immunity* **36,** 401–14 (2012).

85. Zhong, Z. *et al.* New mitochondrial DNA synthesis enables NLRP3 inflammasome activation. *Nature* **560,** 198–203 (2018).

86. García, N., García, J. J., Correa, F. & Chávez, E. The permeability transition pore as a pathway for the release of mitochondrial DNA. *Life Sci.* **76,** 2873–2880 (2005).

87. Patrushev, M. *et al.* Mitochondrial permeability transition triggers the release of mtDNA fragments. *Cell. Mol. Life Sci.* **61,** 3100–3103 (2004).

88. Halestrap, A. P. What is the mitochondrial permeability transition pore? *Journal of Molecular and Cellular Cardiology* **46,** 821–831 (2009).

89. Suh, D. H., Kim, M.-K., Kim, H. S., Chung, H. H. & Song, Y. S. Mitochondrial permeability transition pore as a selective target for anti-cancer therapy. *Front. Oncol.* **3,** (2013).

90. Chauvin, C. *et al.* Rotenone inhibits the mitochondrial permeability transition-induced cell death in U937 and KB cells. *J. Biol. Chem.* **276,** 41394–8 (2001).

91. Li, B. *et al.* Inhibition of complex I regulates the mitochondrial permeability transition through a phosphate-sensitive inhibitory site masked by cyclophilin D. *Biochim. Biophys. Acta - Bioenerg.* **1817,** 1628–1634 (2012).

92. Detaille, D. *et al.* Metformin prevents high-glucose-induced endothelial cell

death through a mitochondrial permeability transition-dependent process. *Diabetes* **54,** 2179–87 (2005).

93. Fontaine, E. Metformin-Induced Mitochondrial Complex I Inhibition: Facts, Uncertainties, and Consequences. *Front. Endocrinol. (Lausanne).* **9,** (2018).

94. Garcia, I., Jones, E., Ramos, M., Innis-Whitehouse, W. & Gilkerson, R. The little big genome: The organization of mitochondrial DNA. *Front. Biosci. - Landmark* **22,** 710–721 (2017).

95. Gopal, R. K. *et al.* Early loss of mitochondrial complex I and rewiring of glutathione metabolism in renal oncocytoma. *Proc. Natl. Acad. Sci. U. S. A.* **115,** E6283–E6290 (2018).

96. Davis, C. F. *et al.* The Somatic Genomic Landscape of Chromophobe Renal Cell Carcinoma. *Cancer Cell* **26,** 319–330 (2014).

97. Hopkins, J. F. *et al.* Mitochondrial mutations drive prostate cancer aggression. *Nat. Commun.* **8,** 656 (2017).

98. Sachdeva, A. *et al. Mitochondrial dysfunction correlates directly with progression and poor long-term prognosis in prostate cancer*. *European Urology Supplements* **18,** (2019).

99. Zitvogel, L., Galluzzi, L., Smyth, M. J. & Kroemer, G. Mechanism of Action of Conventional and Targeted Anticancer Therapies: Reinstating Immunosurveillance. *Immunity* **39,** 74–88 (2013).

100. Martins, I. *et al.* Molecular mechanisms of ATP secretion during immunogenic cell death. *Cell Death Differ.* **21,** 79–91 (2014).

101. Giampazolias, E. *et al.* Mitochondrial permeabilization engages NF-κB-dependent anti-tumour activity under caspase deficiency. *Nat. Cell Biol.* **19,** 1116–1129 (2017).

102. West, A. P. *et al.* Mitochondrial DNA stress primes the antiviral innate immune response. *Nature* **520,** 553–557 (2015).

103. Rongvaux, A. *et al.* Apoptotic Caspases Prevent the Induction of Type I Interferons by Mitochondrial DNA. *Cell* **159,** 1563–1577 (2014).

104. White, M. J. *et al.* Apoptotic caspases suppress mtDNA-induced STING-mediated type I IFN production. *Cell* **159,** 1549–62 (2014).

105. Lamkanfi, M. *et al.* Inflammasome-Dependent Release of the Alarmin HMGB1 in Endotoxemia. *J. Immunol.* **185,** 4385–4392 (2010).

106. Reznik, E. *et al.* Mitochondrial DNA copy number variation across human cancers. *Elife* **5,** (2016).

107. Williams, S. B. *et al.* Mitochondrial DNA content as risk factor for bladder cancer and its association with mitochondrial DNA polymorphisms. *Cancer Prev. Res.* **8,** 607–613 (2015).

108. Guney, A. I. *et al.* Detection of Mitochondrial DNA Mutations in Nonmuscle Invasive Bladder Cancer. *Genet. Test. Mol. Biomarkers* **16,** 672–678 (2012).

109. Cormio, A. *et al.* Mitochondrial dysfunctions in bladder cancer: Exploring their role as disease markers and potential therapeutic targets. *Critical Reviews in Oncology/Hematology* **117,** 67–72 (2017).

110. Wirth, C., Brandt, U., Hunte, C. & Zickermann, V. Structure and function of mitochondrial complex i. *Biochim. Biophys. Acta - Bioenerg.* **1857,** 902–914 (2016).

111. Fontaine, E., Eriksson, O., Ichas, F. & Bernardi, P. Regulation of the permeability transition pore in skeletal muscle mitochondria. Modulation By electron flow through the respiratory chain complex i. *J. Biol. Chem.* **273,** 12662–8 (1998).

112. Petronilli, V., Penzo, D., Scorrano, L., Bernardi, P. & Di Lisa, F. The mitochondrial permeability transition, release of cytochrome c and cell death. Correlation with the duration of pore openings in situ. *J. Biol. Chem.* **276,** 12030–12034 (2001).

113. Dumas, J. F. *et al.* Effect of transient and permanent permeability transition pore opening on NAD(P)H localization in intact cells. *J. Biol. Chem.* **284,** 15117–15125 (2009).

114. Batandier, C., Leverve, X. & Fontaine, E. Opening of the Mitochondrial Permeability Transition Pore Induces Reactive Oxygen Species Production at the Level of the Respiratory Chain Complex I. *J. Biol. Chem.* **279,** 17197–17204 (2004).

115. Colegio, O. R. *et al.* Functional polarization of tumour-associated macrophages by tumour-derived lactic acid. *Nature* **513,** 559–563 (2014).

116. Harel, M. *et al.* Proteomics of Melanoma Response to Immunotherapy Reveals Mitochondrial Dependence. *Cell* **179,** 236–250.e18 (2019).

117. Svatek, R. S. *et al.* Sequential intravesical mitomycin plus bacillus calmette-guérin for non-muscle-invasive urothelial bladder carcinoma: Translational and phase i clinical trial. *Clin. Cancer Res.* **21,** 303–311 (2015).

118. Di Stasi, S. M. *et al.* Sequential BCG and electromotive mitomycin versus BCG alone for high-risk superficial bladder cancer: A randomised controlled trial. *Lancet Oncol.* **7,** 43–51 (2006).

119. Deng, T. *et al.* Systematic Review and Cumulative Analysis of the Combination of Mitomycin C plus Bacillus Calmette-Guérin (BCG) for Non-Muscle-Invasive Bladder Cancer. *Scientific Reports* **7,** (2017).

120. Hori, S. *et al.* Intravesical treatment of chemotherapeutic agents sensitizes bacillus Calmette‐Guerin by the modulation of the tumor immune environment. *Oncol. Rep.* **41,** 1863–1874 (2019).

121. James, N. D. *et al.* Radiotherapy with or without chemotherapy in muscle-invasive bladder cancer. *N. Engl. J. Med.* **366,** 1477–88 (2012).

122. Di Stasi, S. M. *et al.* Electromotive instillation of mitomycin immediately before transurethral resection for patients with primary urothelial non-muscle invasive

bladder cancer: A randomised controlled trial. *Lancet Oncol.* **12,** 871–879 (2011).

123. Brausi, M. *et al.* Variability in the recurrence rate at first follow-up cystoscopy after TUR in stage Ta T1 transitional cell carcinoma of the bladder: A combined analysis of seven EORTC studies. *Eur. Urol.* **41,** 523–531 (2002).

124. Chen, Y. S. *et al.* Mitomycin C Enhances Radiation Effect against Rectal Cancer with Favorable Modulation of Tumor Microenvironment. *Int. J. Radiat. Oncol.* **102,** e162 (2018).

125. Hess, A. K. *et al.* Characterization of the tumor immune micromilieu and its interference with outcome after concurrent chemoradiation in patients with oropharyngeal carcinomas. *Oncoimmunology* (2019). doi:10.1080/2162402X.2019.1614858

126. Singh, S. V. *et al.* Proteasomal inhibition sensitizes cervical cancer cells to mitomycin C-induced bystander effect: the role of tumor microenvironment. *Cell Death Dis.* **6,** (2015).

127. Bellmunt, J. *et al.* Pembrolizumab as Second-Line Therapy for Advanced Urothelial Carcinoma. *N. Engl. J. Med.* **376,** 1015–1026 (2017).

128. Ning, Y.-M. *et al.* FDA Approval Summary: Atezolizumab for the Treatment of Patients with Progressive Advanced Urothelial Carcinoma after Platinum-Containing Chemotherapy. *Oncologist* **22,** 743–749 (2017).

129. Sharma, P. *et al.* Nivolumab in metastatic urothelial carcinoma after platinum therapy (CheckMate 275): a multicentre, single-arm, phase 2 trial. *Lancet. Oncol.* **18,** 312–322 (2017).

130. Powles, T. *et al.* Atezolizumab versus chemotherapy in patients with platinum-treated locally advanced or metastatic urothelial carcinoma (IMvigor211): a multicentre, open-label, phase 3 randomised controlled trial. *Lancet (London, England)* **391,** 748–757 (2018).

131. Viaud, S. *et al.* The intestinal microbiota modulates the anticancer immune effects of cyclophosphamide. *Science* **342,** 971–6 (2013).

132. Vétizou, M. *et al.* Anticancer immunotherapy by CTLA-4 blockade relies on the gut microbiota. *Science (80-.).* **350,** 1079–1084 (2015).

133. Matson, V. *et al.* The commensal microbiome is associated with anti-PD-1 efficacy in metastatic melanoma patients. *Science (80-.).* **359,** 104–108 (2018).

134. Wang, Y. J., Fletcher, R., Yu, J. & Zhang, L. Immunogenic effects of chemotherapy-induced tumor cell death. *Genes and Diseases* **5,** 194–203 (2018).

135. Thomas-White, K., Brady, M., Wolfe, A. J. & Mueller, E. R. The bladder is not sterile: History and current discoveries on the urinary microbiome. *Curr. Bladder Dysfunct. Rep.* **11,** 18–24 (2016).

136. Shrestha, E. *et al.* Profiling the Urinary Microbiome in Men with Positive versus Negative Biopsies for Prostate Cancer. *J. Urol.* **199,** 161–171 (2018).

137. Antunes-Lopes, T. *et al.* The Role of Urinary Microbiota in Lower Urinary Tract Dysfunction: A Systematic Review. *Eur. Urol. Focus* (2018). doi:10.1016/j.euf.2018.09.011

138. Burrello, C. *et al.* Therapeutic faecal microbiota transplantation controls intestinal inflammation through IL10 secretion by immune cells. *Nat. Commun.* **9,** (2018).

CLRT exposure		HMGB1 secretion		Phagocytosis		DC maturation	
%	fold change	ng/ml	fold change	%	fold change	%	fold change
Median cut-off= 7.2 Below =0 Above=1	Median cut-off= 38.6 Below =0 Above=1	Median cut-off= 59 Below =0 Above=1	Median cut-off= 1.6 Below =0 Above=1	Median cut-off= 10.5 Below =0 Above=1	Median cut-off= 1.8 Below =0 Above=1	Median cut-off= 21.3 CD80+ 25.1 CD86+ Below =0 Above=1	Median cut-off= 1.8 CD80+ 1.5 C86+ Below =0 Above=1

Supplementary Table 1. ICD scoring of bladder cancer cell lines.

ICD scoring method using the ICD parameters regarding CLRT exposure, HMGB1 secretion, phagocytosis and DC's maturation. The median calculated for each parameters was used as cut off value.

Appendix: Characterization of the urinary microbiota in bladder cancer

Background and objectives

Patient response to chemotherapeutic and immunotherapy is known to be modulated by environmental factors, including alterations in microbiota composition[131–133]. In particular, it has been reported that the efficacy of chemotherapeutics endowed with the ability to trigger ICD is modulated by commensal bacteria that can activate APCs and the subsequent anti-tumor immune response[131,134], suggesting a correlation between microbiota composition and ICD.

The dogma that urine is sterile has been overturned[135] and microbial imbalance (dysbiosis) of the urinary microbiota has been linked to urological disorders[136,137]. We propose that alteration in urinary microbial community composition may be associated to bladder cancer development, progression and response to therapies. Therefore, a additional aim of the clinical study we are conducting in collaboration with the Urology department at Humanitas hospital consists in the characterization of the urinary microbiota and dysbiosis present in bladder cancer patients. In particular, we plan to:

- Characterize the healthy urinary microbiota composition and the alterations that occur upon bladder carcinogenesis;
- Correlate the presence/ absence of specific bacteria with clinical parameters (tumor histological stages, response to treatments, and disease progression);
- Identify bacteria that can be used as predictive biomarkers of therapeutic response, focusing in particular on response to MMC.

Experimental design

Urines are collected using a catheter from NMIBC and MIBC patients before TURBT, according to the approved clinical protocol ICH-MIM-01. These procedure is performed

in the operating room before the administration of antibiotics. As control, urines are collected with the same modality from age and sex-matched subjects hospitalized at Humanitas hospital, which are not affected by urothelial carcinoma (healthy subjects). Subjects with prior history of sexually transmitted infection, chronic intestinal inflammation, urinary tract infection and recent usage of antibiotic or immunomodulatory agents are excluded. Bacterial DNA is extracted in sterile conditions and amplified for 16S rDNA sequencing. A list of the patients and healthy subjects included at the moment in the urinary microbiota analysis is displayed as Appendix Table 1. The preliminary analyses were done using custom scripts developed for the Qiime software suite and the Silva v. 128 database.

Clinical-pathological features	N°
Cohort size	39
Bladder cancer patients	27
Healthy subjects	12
Sex	
Female	0
Male	100% in both groups
Clinical stage bladder cancer	
pTa LG	11
pTa/T1 HG	8
CIS	4
pT2 HG	4

Appendix Table 1. Clinical-pathological features of patients and healthy subjects included in the analysis urinary microbiota.

Preliminary results

We isolated bacterial DNA from urine samples of 12 non-neoplastic control subjects and 27 bladder cancer patients. We found that bacterial richness and diversity, described by the Chao1 and Shannon community indexes, did not change between bladder cancer and healthy subjects groups (Appendix Figure 1.A). The most abundant phyla in both groups

were *Actinobacteria*, *Bacteroidetes*, *Firmicutes* and *Proteobacteria*, with *Bacteroidetes* being slightly more abundant in bladder cancer at the expense of *Proteobacteria* (Appendix Figure 1.B). Significant differences in the composition of urinary microbiota were visible at the family level, with *Sphingobacteriaceae*, *Bifidobacteriaceae* and *Enterobacteriaceae* being less abundant in bladder cancer patients compared to healthy subjects, whereas *Corynebacteriaceae* increased in bladder cancer patients (Appendix Figure 1.C). By dividing patients based on tumor histological stage we could observe specific alterations in urinary microbiota composition (genus level). In particular, pTa low grade tumors showed a decrease in *Sphingobacterium*, *Peptoniphilus*, *Mobiluncus*, Family XIII family (*Clostridiales* order), *Peptococcus*, *Diaphorobacter*, *Proteus* abundance, compared to healthy subjects. High grade Ta and T1 tumors not only displayed decrease of certain bacteria, like *Gardenerella*, *Ruminococcus* and *Diaphorobacter*, but also increased abundance of *Corynebacterium* and *Actinomyces*. MIBC were characterized by the increase abudance of many bacteria, including *Corynebacterium*, *Flavobacterium*, *Rikenellaceae*, *Staphylococcus*, *Romboutsia* and *Subdoligranulum*.

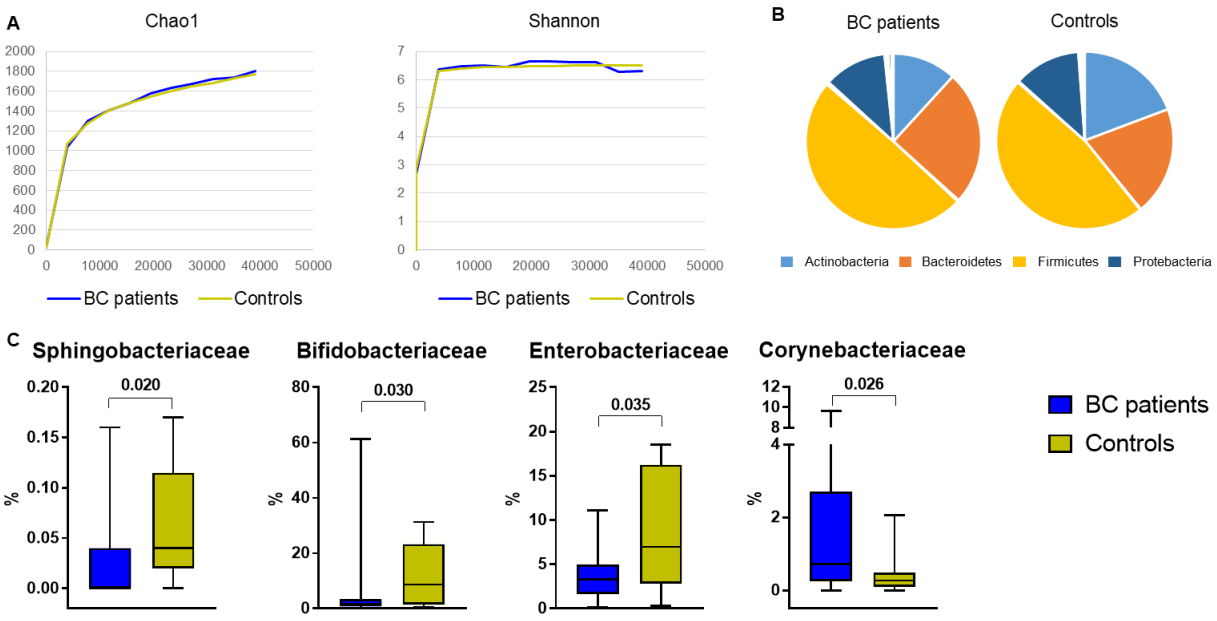

Appendix Figure 1. Urinary microbiota composition in bladder cancer patients. (A) Chao1 and Shannon indexes that describe community richness and diversity, respectively, in bladder cancer (BC) patients and healthy subjects (Controls). (B) Abundance of bacterial phyla in BC

patients and controls. (C) Abundance of bacterial families in BC patients and controls. Box plots show the interquartile range, median value and whiskers min to max. Unpaired two-tailed *t*-test.

Conclusions and future perspective

From these preliminary analyses we can conclude that the samples collected from bladder cancer patients displayed a significantly different pattern relative to those from the control group, suggesting that the tumor microenvironment can influence dysbiosis in the bladder. However, further research is needed to understand whether perturbations of the urinary microbiota composition are a consequence, or partially a cause of tumorigenesis. Interestingly, we found that different bladder cancer histological stages are characterized by distinct modifications in microbiota composition. Low grade, superficial tumors displayed a reduction in specific bacterial genera, whereas high grade and MIBC showed also increased presence of other bacteria. In particular, decreased *Bifidobacterium* and *Ruminococcus*, which in the intestine are known to protect from inflammation[138], were found in bladder cancer patients compared to control subjects, whereas *Corynebacterium* was more abundant and was found to associate with aggressive tumors.

We have now isolated around 60 additional DNA samples from bladder cancer patient's urine samples, which are being analyzed by 16S rDNA sequencing. By integrating these data, we expect to characterize the urinary microbiota in healthy and bladder cancer conditions. To our knowledge, this is the first study that analyzes the urinary microbiota starting from catheter-isolated urine samples, which more closely represent the bladder environment compared to midstream urine samples that have been commonly used to study the urinary microbiota until now, but that can be contaminated by genital microbes.

Next, we will associate the presence of specific bacteria with clinical parameters in order to use the urinary microbiota as a potential biomarker and/or therapeutic target for bladder cancer.

Appendix references

131. Viaud, S. *et al.* The intestinal microbiota modulates the anticancer immune effects of cyclophosphamide. *Science* **342,** 971–6 (2013).

132. Vétizou, M. *et al.* Anticancer immunotherapy by CTLA-4 blockade relies on the gut microbiota. *Science (80-.).* **350,** 1079–1084 (2015).

133. Matson, V. *et al.* The commensal microbiome is associated with anti-PD-1 efficacy in metastatic melanoma patients. *Science (80-.).* **359,** 104–108 (2018).

134. Wang, Y. J., Fletcher, R., Yu, J. & Zhang, L. Immunogenic effects of chemotherapy-induced tumor cell death. *Genes and Diseases* **5,** 194–203 (2018).

135. Thomas-White, K., Brady, M., Wolfe, A. J. & Mueller, E. R. The bladder is not sterile: History and current discoveries on the urinary microbiome. *Curr. Bladder Dysfunct. Rep.* **11,** 18–24 (2016).

136. Shrestha, E. *et al.* Profiling the Urinary Microbiome in Men with Positive versus Negative Biopsies for Prostate Cancer. *J. Urol.* **199,** 161–171 (2018).

137. Antunes-Lopes, T. *et al.* The Role of Urinary Microbiota in Lower Urinary Tract Dysfunction: A Systematic Review. *Eur. Urol. Focus* (2018). doi:10.1016/j.euf.2018.09.011

138. Burrello, C. *et al.* Therapeutic faecal microbiota transplantation controls intestinal inflammation through IL10 secretion by immune cells. *Nat. Commun.* **9,** (2018).

Funding

This work has been supported by grants of the Italian Association for Cancer Research (AIRC, AIRC- IG and AIRC 5x1000), the European Research council (HomeoGUT, ERC) to Maria Rescigno, and the Italian Ministry of Health (Ricerca Finalizzata giovani ricercatori) to Chiara Pozzi. Bianca Oresta was supported by a Marie Curie fellowship and is now a recipient of an Italian Foundation for Cancer Research (FIRC)-AIRC fellowship.

Acknowledgement

While a PhD thesis carries the name of only a single person on the cover, in order to put it together the help and support of many others is needed. Here I would like to acknowledge the people that helped me pursue and reach this point, through their direct involvement in my research or their support along the way.

Above all, I would like to express my deep gratitude to my supervisor: Maria Rescigno. Besides giving me the opportunity to work in your lab, you fueled my scientific imagination and thought me the importance of a critical thinking, especially in front of apparently negative unexpected results, which led us to this particular project. During these years I have grown as a researcher and as a person, not only thanks to the support and guidance you provided, but also thanks to the challenges you entrusted or confronted me with.

I would like to thank all my colleagues who contributed to the work and helped me along the way, inside and outside of the lab. Thank you for the constructive discussions and your sincere friendship. In particular, I am deeply grateful to Chiara Pozzi, for introducing me to ICD and for stepping in when I needed help, and Daniele Braga for the tremendous work on bioinformatics data.

Furthermore, I would like to acknowledge with much appreciation our collaborators of the Urology unit, directed by Prof. Giorgio Guazzoni, and the Pathology unit at IRCCS Humanitas hospital, Rozzano (Milan). In particular, Dr. Rodolfo Hurle and Dr. Massimo Lazzeri, who supported this project from the very beginning with enthusiasm and dedication, and Dr. Piergiuseppe Colombo, who helped in the selection and evaluation of tissue specimens. I also thank all the patients who participated in the observational and

retrospective clinical trials and the doctors, nurses and the data manager for the help during sample's collection.

Moreover, I would like to express gratitude to my PhD advisors: Dr. Karin de Visser (Netherlands Cancer Institute, Amsterdam) and Dr. Stefano Casola (FIRC Institute of Molecular Oncology, Milan). They really supported me during these years with useful insights and valuable comments.

Finally, a big thank you to my friends and family who walked beside me along the way of this tortuous journey. Thank you for your continuous support, your understanding and your love.